7

THE LUNAR REGOLITH

David S. McKay, Grant Heiken, Abhijit Basu, George Blanford, Steven Simon, Robert Reedy, Bevan M. French, and James Papike

Regolith is a terrestrial term, also used for the Moon. It has been defined as "a general term for the layer or mantle of fragmental and unconsolidated rock material, whether residual or transported and of highly varied character, that nearly everywhere forms the surface of the land and overlies or covers bedrock. It includes rock debris of all kinds, [including] volcanic ash . . ." (*Bates and Jackson,* 1980). All the lunar landings and all photographic investigations show that the entire lunar surface consists of a regolith layer that completely covers the underlying bedrock, except perhaps on some very steep-sided crater walls and lava channels, where there may be exposed bedrock.

The regoliths developed on the Earth are produced by processes that are uniquely terrestrial—the presence of oxygen, the influences of wind and water, and the activities of life. In contrast, on the airless, lifeless Moon, the lunar regolith results from uniquely different processes—the continuous impact of large and small meteoroids and the steady bombardment of the lunar surface by charged atomic particles from the sun and the stars.

Exposed rocks on the lunar surface are covered with impact craters whose diameters range from more than 1000 km to less than 1 μm. The corresponding impacting objects range from asteroids tens of kilometers in diameter to particles of cosmic dust a few hundred angstroms across, a range of more than 12 orders of magnitude. Despite the size disparity, the effects on bedrock are similar at both ends of the size spectrum—excavation of a crater, accompanied by shattering, pulverization, melting, mixing, and dispersal of the original coherent bedrock to new locations in and around the crater.

The moment that fresh bedrock is exposed on the Moon (e.g., by the eruption of a lava flow), meteoroid bombardment begins to destroy it. As the impacts continue, the original bedrock is covered by a fragmental layer of broken, melted, and otherwise altered debris from innumerable superimposed craters. This layer is the *lunar regolith.*

Studies of returned samples have shown that the bulk of this lunar regolith (informally called the lunar soil) consists of particles <1 cm in size although larger cobbles and boulders, some as much as several meters across, are commonly found at the surface. Because the impact cratering events produce shock overpressures and heat, much of the pulverized material is melted and welded together to produce *breccias* (fragmental rocks) and *impact melt rocks,* which make up a significant portion of the regolith and add to its complexity.

The processes of regolith formation can be divided roughly into two stages. During the early stage, shortly after bedrock is first exposed and the regolith is still relatively thin (less than a few centimeters), both large and small impacts can penetrate the regolith and excavate fresh bedrock. The regolith layer builds up rapidly. As time goes on and the thickness increases (to a meter or more), only the larger (and far less frequent) impacts penetrate the

regolith and bring up new bedrock. In this later stage, the smaller (and more numerous) impacts only disturb and mix (garden) the regolith layer already present, and the regolith thickness increases more slowly.

Since about 4 b.y. ago, the impact flux on the lunar surface has been relatively low, and a regolith only a few meters thick is adequate to shield the underlying bedrock almost indefinitely. For this reason, the regolith thickness rarely exceeds 10 to 20 m. Regolith thicknesses on the maria are typically only a few meters (*Langevin and Arnold,* 1977; *Taylor,* 1982). Astronauts have drilled to a depth of approximately 3 m in the regoliths at Apollo sites, and estimates based on grain-size distributions suggest that the maximum thickness of the regolith may not exceed 20 m, at least in these locations (*McKay et al.,* 1974). Early estimates of regolith thicknesses by *Oberbeck and Quaide* (1968), based on crater-shape models, ranged from 3.3 m on Oceanus Procellarum to 16 m for the inner wall of the crater Hipparchus. At the four Surveyor mare sites, apparent regolith thicknesses range from 1 to 10 m (*Shoemaker et al,* 1968).

The current consensus is that the regolith is generally about 4–5 m thick in the mare areas but may average about 10–15 m in older highland regions. Beneath this true regolith is a complex zone that probably consists of large-scale ejecta and impact-fractured, brecciated bedrock (based on orbital radar data and modeling; *Peeples et al.,* 1978; *Langevin,* 1982). This layer of fractured bedrock has been called the *megaregolith* and may consist of large (>1 m) blocks. Some of the inferred properties of this megaregolith are different from those of the unconsolidated surficial material that has been sampled (see Fig. 4.22). However, the detailed properties of the megaregolith are essentially unknown, and we shall not consider it further in this section.

The formation and evolution of the lunar regolith is a complex process. At any given spot, the nature and history of the regolith is determined by two completely random mechanisms. One is destructive—the excavation of existing regolith by impact craters. The other is constructive—the addition of layers of new material (either from bedrock or older regolith) that is excavated from either near (small) or distant (large) impact craters. Superimposed on these mechanical processes are the effects of solar and cosmic particles that strike the lunar surface. At the very surface, dust particles form microcraters, and solar-wind atomic particles are trapped in the outer layers of regolith grains, while high-energy particles produce distinctive nuclear reactions to depths of several meters.

These simultaneous processes combine to produce a regolith whose structure, stratigraphy, and history may vary widely, even between locations only a few meters apart. Surface layers can be buried and then reexposed. Single layers, or slabs containing multiple layers, can be transported, overturned, or buried. Deciphering these complications is a major challenge that requires the application of a wide range of analytical techniques—petrologic studies, gas analyses, measurements of radioactivity, stable isotope studies, trace element geochemistry, magnetic measurements, and statistical modeling—to have any hope of success.

Importance of the lunar regolith. The lunar regolith is the actual boundary layer between the solid Moon and the matter and energy that fill the solar system. It contains critical information about both of these regions, and the complexities of studying the regolith are exceeded only by its importance to understanding the Moon and the space environment around it.

The regolith is the source of virtually all our information about the Moon. All direct measurements of physical and chemical properties of lunar material have been made on samples, both rocks and soils, collected from the regolith. Experiments, whether conducted by astronauts on the Moon or remotely monitored from the Earth, were done on or in the regolith layer. For example, heat flow measurements were made with sensors that were emplaced in the regolith; estimates of heat flow from the rocks below were made only by inference from the regolith data. Even seismic data were obtained from seismometers that were implanted on or in the regolith and were not coupled to bedrock. Remotely sensed X-ray fluorescence, infrared spectra, and gamma-ray signals come from the very top of the lunar regolith; in fact, from depths of no more than 20 μm, 1 mm, and 10–20 cm respectively (*Morris,* 1985; *Pieters,* 1983; *Adler et al.,* 1973; *Metzger et al.,* 1973). At the resolution of these methods (>1 km^2), the lunar surface appears totally covered with regolith. Thus, all the remotely sensed chemical data, even on a regional scale, have also come from the regolith. Finally, because of its surficial, unconsolidated, and fine-grained nature, it is likely that the regolith will be the raw material used for lunar base construction, mining, road building, and resource extraction when permanent lunar bases are established in the twenty-first century (*Mendell,* 1985). In other words, the economic importance of the lunar regolith is far greater than that of the underlying bedrock, at least in the foreseeable future.

The lunar regolith also preserves information from beyond the Moon. Trapped in the solid fragments that make up the regolith are atoms from the sun

and cosmic-ray particles from beyond the solar system. In the regolith, data about the nature and evolution of the Moon are mixed with other records. These records include the composition and early history of the sun, and the nature and history of cosmic rays. The regolith also contains information about the rate at which meteoroids and cosmic dust have bombarded the Moon—and, by inference, the Earth. Unscrambling these intertwined histories is a major challenge—and a major reward—of lunar research.

Data sources. The principal source of data about the regolith is, of course, the samples returned by both manned and unmanned missions to the Moon. The relatively large (e.g., >1 cm) fragments of pebbles, cobbles, and boulders are treated as separate rock samples (see section 7.6 for a discussion of regolith breccias). On the other hand, all scoop samples and drill cores are true regolith samples (for cataloging purposes, an arbitrary definition of a lunar *soil* is the "unconsolidated portion of regolith with particle sizes of less than 1 cm"). Therefore, all the Soviet Luna samples, as well as the U.S. collections (Apollo samples) are actually regolith.

Regolith samples returned from the Moon during the Apollo missions were handled in many different ways, and the sample handling protocols evolved from mission to mission (*Morris et al.,* 1983). When evaluating grain-size studies of these samples, one must look carefully at the sample's history from the time it was collected on the lunar surface to the time when the research results were published. Nearly all regolith samples in the Apollo collection have been sieved into size fractions of >1 cm, 1 cm–4 mm, 4-2 mm, 2–1 mm, and <1 mm at the Johnson Space Center curatorial facilities (see section 2.3). Most of the detailed regolith studies have been performed on the <1-mm-sized fractions, also called the "fine fines." It is important to note that the >1-mm fractions (coarse fines) have not been studied in such a way that their data can be easily integrated with results from the fine fines. In addition, no data from the >1-mm fraction have been included in attempts to infer the bulk properties of the regolith. Most of the laboratory data on lunar regolith have been obtained from the <1-mm fractions; although these fractions make up the bulk of the regolith (>90% of most regolith samples), some caution should be used in applying the results to the regolith as a whole.

The regolith, being at the Moon's surface, has been continuously bombarded by meteoroid impacts for at least 3–4 b.y. Some of these impacts were large enough to reconsolidate and lithify parts of the regolith into coherent fragmental rocks, called *regolith breccias* (section 7.6). These breccias make up some of the large individual rocks picked up by astronauts. The ages of assembly or "closure" of some of these breccias, measured by radiometric age-dating techniques, may be more than 4 b.y. (*McKay et al.,* 1986), and many regolith breccias were lithified more than 1 b.y. ago. Studies of the regolith breccias provide critical data about the Moon's ancient regolith and also add to the general database for the modern regolith.

In addition to laboratory studies of returned soils, cores, and regolith breccias, data on the lunar regolith have been obtained from a variety of other sources. Many physical and mechanical properties were directly measured during experiments on the Moon itself. For example, the penetration depth of the landing gear of the lunar module provided an estimate of regolith compressibility. Such geotechnical properties, extremely important for any engineering venture, are discussed in detail in Chapter 9. Photogeology and other remote-sensing methods also reveal many large-scale regolith properties.

The underlying assumption in most lunar studies is that the regolith cover adequately represents local bedrock and, in general, represents the Moon's crust in a given region. To test this assumption, it is especially important to measure regolith properties that can be used to infer the extent of lateral transport and regolith mixing on the lunar surface. It now appears that lateral transport of primary ejecta from impact craters has been restricted to relatively short distances, i.e., a few crater radii, although a small fraction of primary ejecta may be present in crater rays that have traveled halfway round the Moon from large impacts such as the ones that formed larger craters like Copernicus and Tycho. Similarly, the sharp contrasts in color and chemical compositions at highland-mare contacts, inferred from optical observations and orbital X-ray fluorescence data on the regolith, imply that lateral transport and mixing could not have been extensive, even over more than 3 b.y.

7.1. LUNAR SOIL

The lunar science community has generally used the word "soil" in an engineering geology sense. Although "lunar soil" is lexicographically synonymous with "lunar regolith" (*Bates and Jackson,* 1980), "lunar soil" usually refers to the finer-grained fraction of the unconsolidated material (*regolith*) at the lunar surface. In this discussion *we define lunar soil as the subcentimeter fraction of the lunar regolith.*

7.1.1. General Description

The lunar soil is a somewhat cohesive, dark grey to light grey, very-fine-grained, loose, clastic material derived primarily from the mechanical disintegration

of basaltic and anorthositic rocks. The mean grain size of analyzed soils ranges from about 40 μm to about 800 μm and averages between 60 and 80 μm. Individual lunar soil particles are mostly glass-bonded aggregates (*agglutinates*), as well as various rock and mineral fragments. The soils range in composition from basaltic to anorthositic, and they include a small (<2%) meteoritic component. Although the chemical compositions of lunar soils show considerable variation, physical properties such as grain size, density, packing, and compressibility are rather uniform (see Chapter 9). One manifestation of such uniform physical properties is that seismic velocities in regolith materials at both mare and highland sites are quite similar, varying between 92 m/sec and 114 m/sec (*Cooper et al.,* 1974).

7.1.2. Petrography

Petrographic studies of regolith samples make it possible to characterize the material in two complementary ways: by the relative proportions of different kinds of fragments and by the chemical and mineral compositions of individual rock and mineral fragments. These studies are done by examining thin sections of regolith samples with an optical microscope or by studying individual regolith particles with a scanning electron microscope (SEM).

Optical studies of regolith samples make it possible to conduct a census of the relative amounts (by volume) of different particles—rocks, mineral and glass fragments, and other components—in each sample. This determination of relative volumes of components, a process called *modal analysis,* can be expanded to estimate the chemical composition of the soil as well if chemical data for individual mineral, rock, and glass components can be summed. (Usually, the chemical data for fragments are determined directly with an electron microprobe.) The bulk chemical composition, reconstructed in this way, can be compared with destructive "whole rock" chemical analyses. The chemical analyses can be used to interpret the sources for particles, origin, and evolution of the soil sample.

These studies show that five basic particle types make up the lunar soils: mineral fragments, pristine crystalline rock fragments, breccia fragments, glasses of various kinds, and the unique lunar constructional particles called *agglutinates.* These diverse particles can also be divided into two groups: regolith derived and bedrock derived. All agglutinates, fragments of regolith breccias, and heterogeneous glasses have been formed by the action of meteorite impacts (chiefly impact melting) on regolith targets. These particles are sometimes called the *fused soil component.* The remaining fragments are pieces of igneous rocks, monomict breccias, and polymict breccias, which make up the bedrock-derived component.

Except for a few igneous rock fragments, the average size of rock clasts in the regolith is <250 μm. In general, it is difficult to identify the rock type in particles <250 μm, and most rock fragments in lunar soils are even smaller. For this reason, the chemistry of individual mineral grains in the fragments has been used instead for identifying the parent rock.

A further complication in studying the bedrock-derived component is that the relative abundance of particle types depends on the particle size. Polymineralic and lithic (rock) fragments dominate the coarser size fractions. In contrast, the finer soil fractions are enriched in feldspars and glassy phases. The glasses come from two sources—the noncrystalline material in the groundmass of basaltic rocks and the glassy bonding material originally present in breccias and agglutinates (Table 7.1).

Modal analyses commonly provide an adequate picture of the relations between the composition of the local bedrock and that of the regolith developed on it. All lunar soils have a minor exotic component derived from some distance away, but most of these soils appear to have been derived largely from bedrock in their immediate vicinity. The modal compositions of a regolith reference suite (*Papike et al.,* 1982) illustrate the local influence well (Table 7.2; Fig. 7.1). The Apollo 11, Apollo 12, Luna 16, and Luna 24 missions landed well inside mare basalt regions. The soil samples from these sites contain abundant mare-derived basaltic rock fragments and their mafic minerals like pyroxene and olivine. The Apollo 16 and Luna 20 missions landed in highland regions, and Apollo 14 landed on a ridge apparently formed by material ejected from the Imbrium Basin. Soils from these missions show a preponderance of highland-derived lithic fragments (anorthositic rocks) and plagioclase feldspar. Apollo 15 and 17 landings were made in areas where highland hills meet the mare plains. Soil samples collected during these missions are intermediate in character between those from the mare and highland regions, and they contain rock and mineral fragments derived from both.

Even within a single landing site, there can be remarkable variation between sampling locations. For example, soil 15221 (Table 7.2), collected from the slopes of the Apennine Front (Fig. 7.1), contains significant amounts of both highland and mare material. On the other hand, soil 15601 (Table 7.3),

TABLE 7.1. Petrography of grain size fractions from 71061,1 (a typical Apollo 17 mare soil) and 72441,7 (a typical South Massif soil) (*Heiken,* 1975).

Components	Petrographic Description, vol.%							%, Visual Estimate in Lunar Receiving Laboratory			
	<20 μm	20–45 μm	45–75 μm	75–90 μm	90–150 μm	150–250 μm	250–500 μm	0.5–1 mm	1–2 mm	2–4 mm	4–10 mm
*Soil 71061,1**											
Agglutinates	17.0	17.3	13.0	17.3	9.3	11.8	10.0	10.0	—	—	—
Basalt, equigranular			9.0	15.0	30.9	—	—	—	—	—	—
Basalt, variolitic			0.6	1.6	19.6	3.4	51.5	65.0	100.0	100.0	100.0
Breccia											
Low grade, brown			1.0	4.0	3.6	5.1	6.9	—	—	—	—
Low grade, colorless			0.3	1.3	0.6	—	—	5.0	—	—	—
Medium, high grade			1.0	1.3	1.6	2.8	1.5	—	—	—	—
Anorthosite			—	—	0.3	—	—	—	—	—	—
Cataclastic anorthosite			1.0	—	—	—	—	—	—	—	—
Norite			—	—	—	—	—	—	—	—	—
Gabbro			—	—	—	—	0.5	5.0	—	—	—
Plagioclase			16.3	7.0	17.3	9.0	8.5	—	—	—	—
Clinopyroxene			21.3	26.3	21.0	17.4	10.8	—	—	—	—
Orthopyroxene			—	—	—	—	—	—	—	—	—
Olivine			—	—	—	0.6	—	—	—	—	—
Ilmenite			6.0	3.3	4.6	3.3	2.3	—	—	—	—
Glass											
Orange			7.6	5.0	6.3	4.5	0.8	—	—	—	—
"Black"			18.7	10.6	9.6	5.1	6.1	5.0	—	—	—
Colorless			1.0	1.0	1.3	—	1.5	—	—	—	—
Brown			0.3	5.2	4.6	3.3	—	—	—	—	—
Gray, ropy			0.7	0.6	—	1.7	—	10.0	—	—	—
Other			2.0	—	—	1.0	—	—	—	—	—
Total number of grains counted	300	161	300	300	300	178	130	20	100	?	?
Wt.% of total sample for each size fraction	17.98	12.21	8.39	3.0	8.66	7.04	7.08	3.44	6.15	6.74	10.16

TABLE 7.1. (continued)

Components	Petrographic Description, vol.%							%, Visual Estimate in Lunar Receiving Laboratory			
	<20 μm	20–45 μm	45–75 μm	75–90 μm	90–150 μm	150–250 μm	250–500 μm	0.5–1 mm	1–2 mm	2–4 mm	4–10 mm
Soil 72441,7†											
Agglutinates	21.0	50.0	39.3	45.5	41.7	54.6	30.5	x	20.0	25.0	25.0
Basalt, equigranular			0.6	1.5	1.3	1.3	—	x	—	—	—
Basalt, variolitic			0.3	—	1.3	—	1.0	x	—	—	—
Breccia											
Low grade, brown			9.3	6.6	9.3	10.7	9.4	x	—	—	—
Low grade, colorless			2.7	2.3	6.3	0.7	6.3		80.0	74.0	75.0
Medium high grade			22.7	29.0	19.3	20.0	30.5	x	—	—	—
Anorthosite			—	—	1.0	—	—	x	—	1.0	—
Cataclastic anorthosite			0.7	1.2	1.3	0.7	2.1	x	—	—	—
Norite			—	—	0.7	0.7	1.0	x	—	—	—
Gabbro			—	—	—	—	—	x	—	—	—
Plagioclase			10.7	1.2	6.7	3.3	7.3	x	—	—	—
Clinopyroxene			6.0	3.9	3.0	2.7	2.1	x	—	—	—
Orthopyroxene			1.0	—	3.3	—	—	x	—	—	—
Olivine			—	1.2	0.7	—	2.1	x	—	—	—
Ilmenite			—	—	0.3	—	—	x	—	—	—
Glass											
Orange			0.3	1.2	0.3	—	—	x	—	—	—
"Black"			1.3	1.5	0.3	—	1.0	x	—	—	—
Colorless			1.0	1.5	1.3	—	—	x	—	—	—
Brown			3.3	3.0	1.0	5.3	4.2	x	—	—	—
Gray, ropy			—	—	0.3	—	1.0	x	—	—	—
Other			—	—	0.3	0.7	1.0	x	—	—	—
Total number of grains counted	300	162	249	259	300	150	95	x	—	—	—
Wt.% of total sample for each size fraction	25.84	18.79	12.0	4.01	11.02	8.37	8.55	x	3.67	2.76	1.01

Sample 71061,1 was collected at Station 1 on the mare surface. Agglutinate vs. nonagglutinate grains were identified by using a scanning electron microscope in size ranges of <20 and 20–45 μm. The >10-mm fraction made up 9.42% of the sample. "Black" glass is partly crystalline orange glass. Sample 72441,7 was collected at the base of the South Massif, on the "light mantle" deposit (from *Heiken and McKay,* 1974). Agglutinate vs. nonagglutinate grains were identified by using a scanning electron microscope in size ranges of <20 and 20–45 μm. x = Data for the 0.5–1.0 mm fraction of 72441,7 were not available.

* The <20-μm fraction is 83% nonagglutinate; the 20- to 45-μm fraction is 82.7% nonagglutinate.
†The <20-μm fraction is 79.0% nonagglutinate; the 20- to 45-μm fraction is 50.0% nonagglutinate.

TABLE 7.2. Modal (vol.%) abundance data for particles in the 1000–90 μm size fraction of representative soils from each mission (*Simon et al.*, 1981).

	10084	12001	12033	14163	15221	15271	64501	67461	72501	76501	78221	21000	22001*	24999
Mineral Fragments														
Pyroxene + Olivine	4.2	18.3	26.3	2.6	16.1	13.5	1.0	0.5	5.2	17.3	9.8	6.4	8.9	40.2
Plagioclase	1.9	3.9	9.9	5.1	13.1	7.4	32.1	12.2	10.9	15.2	9.9	1.1	14.7	10.6
Opaque	1.1	0.2	1.3	—	0.1	0.3	—	1.1	0.1	2.8	0.4	—	0.1	0.2
Lithic Fragments														
Mare basalts	24.0	12.9	7.5	2.2	3.1	3.2	0.3	0.5	2.9	9.2	5.7	18.3	1.7	6.9
ANT†	0.4	1.0	1.3	2.9	2.6	2.2	5.0	21.7	5.2	0.5	2.2	0.8	9.7	3.5
LMB‡	0.8	0.1	0.3	0.3	0.6	0.4	2.1	30.7	2.4	6.3	2.3	0.3	2.8	0.5
Feldspathic Basalt (KREEPY)	1.1	0.5	—	0.6	0.4	1.9	1.6	1.6	0.2	0.2	0.2	1.4	0.8	1.4
RNB/POIK§	—	2.3	3.7	10.9	2.7	2.8	8.3	7.9	9.7	8.1	4.4	2.8	10.9	2.2
Fused Soil Component														
DMB	7.5	9.5	11.9	19.3	13.3	12.9	13.9	11.1	22.6	4.2	12.0	15.0	15.0	10.6
Agglutinate	52.0	40.1	17.0	45.7	36.9	37.0	29.1	8.5	37.6	29.2	46.6	42.8	28.7	16.6
Glass Fragments														
Orange/Black	2.7	0.5	1.5	—	0.4	1.6	0.7	0.5	1.7	1.6	1.6	1.4	0.2	—
Yellow/Green	0.8	2.8	0.2	2.9	4.5	7.0	1.2	—	0.1	1.3	1.3	1.7	0.7	0.9
Brown	—	1.5	7.8	—	0.3	0.3	—	—	0.2	—	—	—	—	0.2
Clear	1.3	1.0	—	1.3	1.5	3.8	1.4	—	0.2	0.8	1.0	2.5	1.1	0.6
Miscellaneous														
Devitrified Glass	1.8	5.0	10.8	6.1	4.1	5.6	3.4	3.2	0.4	2.2	1.9	4.4	4.6	5.4
Others	0.3	0.5	0.5	—	0.3	0.2	—	0.5	0.4	1.1	0.7	1.1	0.1	0.3
Total	99.9	100.1	100.0	99.9	100.0	100.1	100.1	100.0	99.8	100.0	100.0	100.0	100.0	100.1
Number of points	625	823	666	311	1000	1008	942	189	801	820	1266	360	1333	634

* 500–90 μm fraction.
† ANT = anorthosite, norite, troctolite.
‡ LMB = Light matrix breccia.
§ RNB/POIK = Recrystallized noritic breccia/poikilitic breccia.

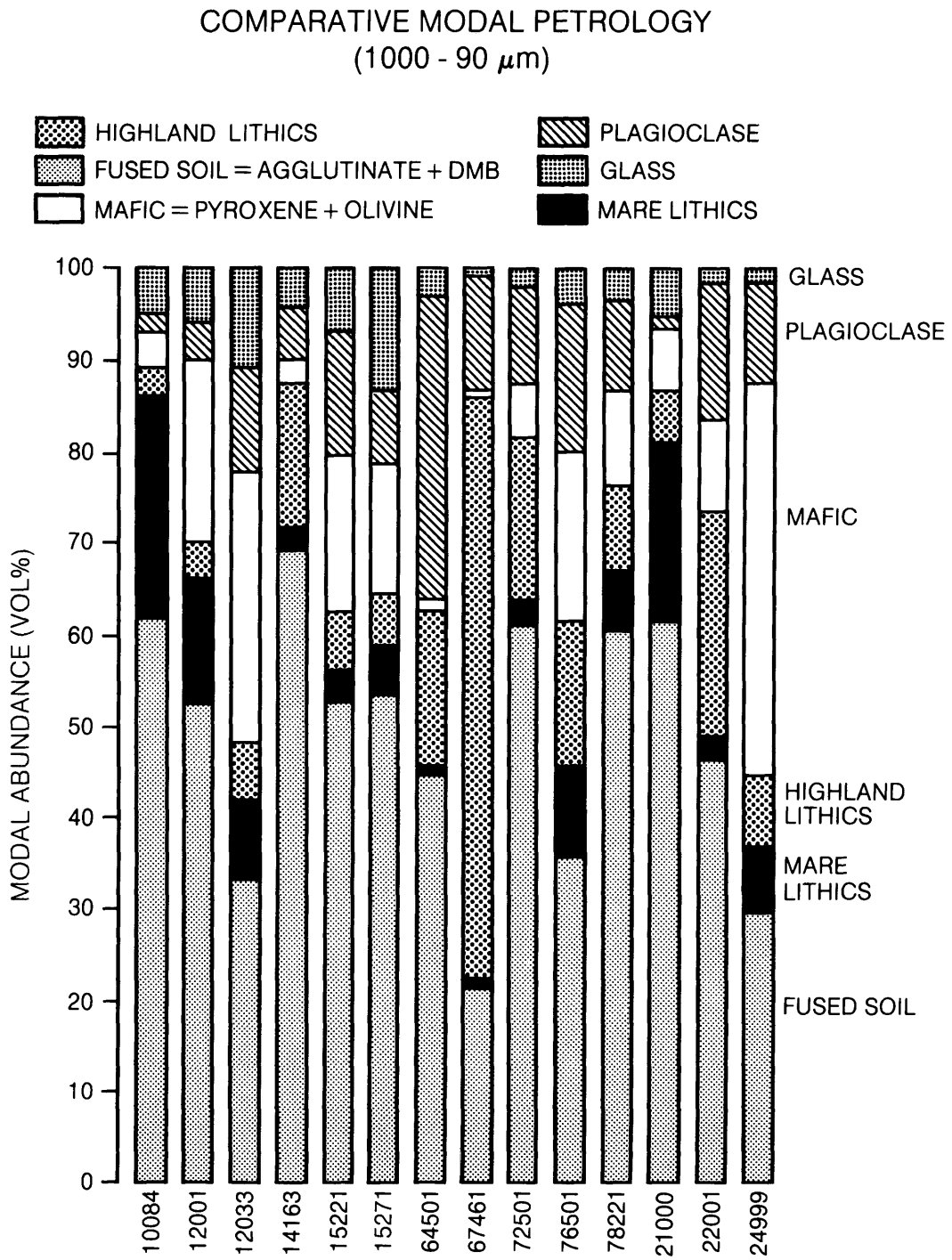

Fig. 7.1. Bar graphs showing modal (volume) abundances of principal particle types in 14 lunar soil samples (*Simon et al.,* 1981). This diagram distinguishes between rock fragments (mare lithics, highland lithics), single mineral and glass fragments (pyroxene and olivine, plagioclase, glass), and fused soil (agglutinates and dmb—Dark Matrix Breccia). Soil samples are from Apollo 11 (10084), Apollo 12 (12xxx), Apollo 14 (14163), Apollo 15 (15xxx), Apollo 16 (6xxxx), Apollo 17 (7xxxx), Luna 16 (21000 and 22001), and Luna 24 (24999).

TABLE 7.3. Modal (volume) abundances of particles in six size fractions of lunar soil 15601,96.

Size (μm)	250–500	150–250	90–150	75–90	45–75	20–45	15601,96 avg. (%)	Error
Wt.%	11.91	13.13	15.99	5.48	14.45	17.37	78.33	%
Monomineralic	21.4	35.4	39.7	53.3	47.6	52.5	41.5	1.2
Plagioclase	1.3	4.2	7.5	6.0	6.1	8.8	5.9	0.5
Pyroxene	17.6	28.3	27.2	43.9	37.4	37.8	31.3	1.1
Olivine	2.5	2.9	4.3	2.2	2.8	2.5	3.0	0.4
Opaque Minerals	—	—	(0.7)	(1.2)	(1.6)	(3.4)	(1.3)	
Oxides	—	—	0.7	1.2	1.6	2.2	1.0	
Metal, sulphide	—	—	—	—	—	1.2	0.3	
Silica phase	—	—	—	—	—	—	0.0	
Crystalline lithic clasts	34.0	24.1	15.7	14.6	11.4	11.7	18.1	0.9
ANT suite	(1.3)	(0.6)	(0.3)	(0.0)	(0.0)	(0.0)	(0.4)	
Anorthositic	1.3	0.6	—	—	—	—	0.3	
Gabbroic	—	—	0.3	—	—	—	0.1	
Mare basalt	(29.0)	(17.7)	(8.6)	(10.8)	(9.8)	(8.3)	(13.5)	1.2
Olivine-bearing	14.5	7.1	3.6	2.5	1.2	1.2	4.8	0.5
Olivine-free	(17.7)	(4.8)	(2.7)	(2.7)	(2.4)	(0.9)	(3.8)	0.4
Microgabbroic	1.9	1.0	0.7	0.9	0.6	0.6	0.9	
Porphyritic, etc.	6.9	2.9	1.3	0.3	0.3	0.3	2.0	
Ophitic, etc.	1.9	0.6	0.7	0.9	0.6	—	0.7	
Intersertal/granular	—	0.3	—	0.9	0.6	—	0.2	
Other	3.8	5.8	2.3	5.6	6.2	6.2	4.9	0.5
Nonmare basalt	(0.6)	(1.6)	(0.7)	(1.3)	(0.0)	(0.6)	(0.7)	
Feldspathic	—	—	—	—	—	—	0.0	
KREEPy	0.6	1.6	0.7	1.3	—	0.6	0.7	
Plagioclase-phyric	—	—	—	—	—	—	0.0	
Indeterminate	3.1	4.2	6.2	2.5	1.6	2.8	3.5	0.4
Breccias	5.7	6.1	4.9	5.6	6.2	4.7	5.5	0.6
Vitric	(4.4)	(5.8)	(4.6)	(3.4)	(5.6)	(4.4)	(4.8)	0.5
Dark matrix	4.4	5.5	4.3	3.4	4.7	4.1	4.5	0.5
Light matrix	—	0.3	0.3	—	0.9	0.3	0.3	
Crystalline	(1.3)	(0.3)	(0.3)	(2.2)	(0.6)	(0.3)	(0.6)	
Poikilitic	—	—	—	—	—	—	0.0	
Melt matrix	1.3	—	—	1.9	0.6	0.3	0.5	
Other	—	0.3	0.3	0.3	—	—	0.1	
Agglutinate	32.1	28.0	32.1	19.7	26.5	25.9	28.1	1.1
Glass	6.3	6.4	7.5	6.6	8.1	4.9	6.6	0.6
Ropy/Clast-laden	3.1	2.9	2.0	1.9	2.5	1.2	2.2	0.2
Quench-crystal (vitrophyres)	(0.6)	(1.6)	(1.6)	(0.6)	(0.9)	(0.0)	(0.9)	
Green glass	—	0.3	0.3	0.3	0.6	—	0.2	
Other	0.6	1.3	1.3	0.3	0.3	—	0.7	
Devitrified	1.3	1.3	2.3	1.6	1.9	0.9	1.5	
Homogeneous	(1.3)	(0.6)	(2.0)	(2.5)	(2.8)	(2.8)	(2.0)	0.2
Green	1.3	0.3	1.0	1.6	2.5	1.6	1.4	
Yellow	—	—	1.0	0.3	—	—	0.2	
Gray, colorless	—	—	—	0.3	—	0.3	0.1	
Brown, black, etc.	—	0.3	—	0.3	0.3	0.9	0.3	
Miscellaneous	0.6	—	—	—	—	—	0.1	
No. of particles	159	311	305	319	321	320	1735	

A weighted average is calculated for the bulk sample and is given in the far right column. The errors (1σ) are based on counting statistics at 95% confidence level; error statistics are not valid for concentrations less than 2% (*Basu et al.*, 1981). Subtotals are in parentheses.

collected from the edge of a lava rille and 3.5 km downslope from the Apennine Front sampling site, is made up of about 90% mare material.

Several complications arise in trying to identify the bedrock components that make up a lunar soil. One problem is the fine grain size of the soil itself. The average grain size of lunar soils is only about 60 μm. Thus, the presence of recognizable, polymineralic rock fragments in the smaller size fractions is a function of the mineral grain size in the parent rocks. Rocks composed of minerals >60 μm in size will, when crushed, produce mostly single mineral fragments and it will be difficult to identify the original source rock. However, many basalts in the Apollo 11 collection are very fine grained; crystal size in these basalts averages only about 40–100 μm. Many of these fragments in Apollo 11 soils contain several mineral grains and can be identified as basaltic rocks. On the other hand, many basalts from the Luna 24 site are fairly coarse grained; crystal sizes range from 100–500 μm. As a result, and as expected, many more monomineralic particles are found in Luna 24 soils than in the Apollo 11 soils, although more than 90% of both soils was derived from mare basalts. Similar complications have been observed in studies of terrestrial clastic sediments (e.g., sandstones and siltstones), in which simple modal data also do not necessarily provide direct information about the source rocks.

An additional complication is introduced by the fact that lunar soils show variations in *maturity,* a quantity roughly equivalent to age. Lunar soils change significantly as they develop over time, and a highly mature soil, with an increased degree of comminution and melting, may significantly obscure parent rock compositions (for a discussion of maturity and its effects, see section 7.3).

Even in finely comminuted or mature soils, considerable information about the parent bedrock can be obtained from the chemical composition of individual mineral fragments. These compositions can be measured with an electron microprobe on fragments as small as 10 μm in size. Several studies (*Bence and Papike,* 1972; *J. V. Smith,* 1974; *Smith and Steele,* 1976; *Steele and Smith,* 1975) have shown that the chemical compositions of a few common rock-forming minerals, especially their minor element abundances and ratios, provide clues to the nature of their source rocks. With these data it is possible to infer the parent rocks from which individual mineral grains in lunar soils were derived. For some elements, the compositional ranges of pyroxenes derived from mare basalts are distinctly different from pyroxenes derived from highland rocks. Unfortunately, a large range also exists in which the compositions of pyroxenes from different parent rocks overlap. In addition, different basalts show different chemical trends in pyroxene composition during progressive crystallization (section 5.1.1), so that a range of pyroxene compositions can be obtained from a single lava flow.

The magnesium (or forsterite molecule) content of olivine and the calcium (or anorthite molecule) content of plagioclase can also be used to discriminate between individual grains from different parent rocks. *Vaniman et al.* (1979) made a detailed study of chemical compositions of monomineralic pyroxene grains in soil layers from the Apollo 17 deep drill core. They were able to infer the relative proportions of monomineralic pyroxene grains that were contributed by a variety of bedrock types—high-Ti mare basalts, noritic rocks, and anorthositic gabbros (Table 7.4). Earlier, *Basu and Bower* (1977) used a similar approach to confirm the identification of two different sources for KREEP rocks and mare basalt lavas for the pyroxene grains in Apollo 15 soils. Chemical compositions of monomineralic olivine and plagioclase particles from the Luna 24 soils suggest that a significant fraction of these soil particles was derived from distant sources, including highland rocks (3%) and a mafic cumulate (10%) (*Basu et al.,* 1978).

Completely glassy fragments (glasses without either crystal or rock inclusions) of both impact and volcanic origin are present in all sampled lunar soils. The origins of these glasses, whether impact melting or volcanic eruptions, can often be inferred from their chemical compositions (see section 6.1.7). Because the volcanic glasses are derived from eruptions on the maria, this information provides an additional clue to the proportions of highland and mare materials in lunar soils.

Mature (old) and immature (young) soils from the same area may also have different mineralogical compositions (*Papike et al.,* 1982; *Greene et al.,* 1975; *Engelhardt et al.,* 1976; *McKay et al.,* 1972). In general, mature soils are finer grained. The mineral grains

TABLE 7.4. Modal (vol.%) classification of pyroxene fragments in Apollo 17 deep drill core 70002–70009 by lithic origin (*Vaniman et al.,* 1979).

	High-Ti Mare	Noritic	Anorthositic Gabbro	Total Highland
Unit E	0.66	0.01	0.32	0.33
Unit D	0.92	0.02	0.06	0.08
Unit C	0.61	0.20	0.19	0.39
Unit B	0.57	0.21	0.22	0.43
Unit A	0.63	0.19	0.18	0.37

TABLE 7.5. Particle types and relative abundances (vol.%) in size fractions of soil 64501 (*Houck*, 1982a).

Size (μm)	500–250	250–150	150–90	90–75	75–45	45–20	Σ 500–20
Wt.%	8.9	8.2	10.0	3.5	10.0	15.6	56.2
Monomineralic	29.0	35.3	25.3	30.9	45.0	44.0	36.4
Plagioclase	29.0	34.0	25.0	28.6	43.1	34.2	33.0
Pyroxene	—	1.3	0.3	2.3	1.6	6.5	2.5
Olivine	—	—	—	1.0	0.3	2.0	0.3
Opaques, Oxides, etc.	—	—	—	—	—	1.3	0.4
SiO_2 Phases	—	—	—	—	—	—	—
Crystalline Lithic Clasts	5.8	0.3	—	0.3	—	—	1.0
Anorth., Nor., Troct.	(5.8)	(0.3)	—	(0.3)	—	—	(1.0)
Anorthositic	5.8	0.3	—	0.3	—	—	1.0
Noritic-troctolitic	—	—	—	—	—	—	—
Mare Basalt	—	—	—	—	—	—	—
KREEP Basalt	—	—	—	—	—	—	—
Indeterminate/Other	—	—	—	—	—	—	—
Breccias	31.4	32.7	26.2	24.0	21.6	22.9	26.1
Fragmental/Vitric Matrix	(7.0)	(8.9)	(8.3)	(5.3)	(6.5)	(5.9)	(7.0)
Regolithic/Vitric Matrix	(6.2)	(5.9)	(5.0)	(4.3)	(5.2)	(4.9)	(5.3)
Porous	—	1.3	3.0	1.0	0.3	1.0	1.1
Compact	6.2	4.6	2.0	3.3	4.9	3.9	4.2
Feldspathic/Vitric Matrix	(0.4)	(0.7)	(1.3)	(0.7)	(0.3)	—	(0.5)
Porous	—	—	1.0	0.7	0.3	—	0.8
Compact	0.4	0.7	0.3	—	—	—	0.2
Fragmental Matrix	(0.4)	(2.3)	(2.0)	(0.3)	(1.0)	(1.0)	(1.2)
Unshocked clasts >50%	—	—	—	0.3	0.3	—	0.6
Shocked clasts >50%	0.4	2.3	2.0	—	0.7	1.0	1.2
Crystalline Matrix	(24.4)	(23.8)	(17.9)	(18.7)	(15.1)	(17.0)	(2.7)
Poikilitic	(4.5)	(5.0)	(4.0)	(3.9)	(2.6)	(0.6)	(3.0)
Equant Plagioclase	3.6	4.3	2.3	1.6	2.3	0.3	2.2
Acicular Plagioclase	0.9	0.7	1.7	2.3	0.3	0.3	0.8
Basaltic-Textured	(9.3)	(5.6)	(7.9)	(5.3)	(2.3)	(1.4)	(4.8)
Variolitic	1.3	—	0.3	0.3	—	—	0.3
Subophitic	3.6	4.0	3.3	1.0	0.7	0.7	3.9
Intergranular	1.3	0.3	1.7	0.7	0.6	—	0.7
Intersertal	—	—	0.3	—	—	—	0.1
Porphyritic	—	—	—	—	—	—	—
Other/Indeterminate	3.1	1.3	2.3	3.3	1.6	0.7	1.8
Granulitic	0.4	1.3	0.3	1.6	0.7	0.3	0.6
Other/Indeterminate	11.2	11.9	5.7	7.9	9.5	14.7	10.8
Agglutinates	28.1	27.1	44.0	34.5	25.7	22.5	29.2
Glass	4.3	4.7	4.9	9.2	7.5	9.4	6.8
Clast Laden/Ropy	2.2	2.3	2.3	3.0	2.3	2.3	2.3
Vitrophyric/Quench Crystal	0.4	0.7	0.7	0.3	0.3	1.1	
Cryptocrystalline	0.9	0.3	0.3	2.6	1.3	0.3	0.7
Clast and Crystal Free	(0.8)	(1.4)	(2.3)	(2.9)	(3.6)	(6.5)	(3.4)
Green	0.3	0.1	—	—	—	—	0.1
Yellow	0.4	0.7	0.7	1.0	0.7	0.7	0.7
Colorless/Gray, etc.	0.4	0.7	1.3	1.6	2.3	3.9	2.0
Black/Orange, etc.	—	—	0.3	0.3	0.3	2.9	0.9
Miscellaneous	—	—	—	—	—	0.3	0.1
No. of particles	224	303	300	304	304	307	1742

Subtotals are in parentheses.

that are fine grained in the parent rocks, as well as minerals with good cleavage (e.g., plagioclase) that are easily broken, tend to be concentrated in the finer soil fractions. This concentration is especially pronounced in the extremely fine (<10-μm) fraction (*Devine et al.,* 1982). Experimental studies also support the theory that such differential comminution of mineral grains is an important process in forming lunar soils (*Hörz et al.,* 1984). Examples of plagioclase concentration in the finest-size fractions of actual lunar soil samples are shown in Tables 7.3 and 7.5 (*Basu et al.,* 1981; *Houck,* 1982a; see also *McKay et al.,* 1978b).

7.1.3. Agglutinates

Agglutinates are individual particles that are aggregates of smaller lunar soil particles (mineral grains, glasses, and even older agglutinates) bonded together by vesicular, flow-banded glass. Agglutinate particles (Fig. 7.2a) are small (usually <1 mm) and contain minute droplets of Fe metal (much of which is very fine-grained, single domain Fe°), and troilite (FeS). They have probably formed by the melting and mixing produced by micrometeoritic bombardment of the lunar regolith.

Agglutinates were one of the most interesting features observed in the first returned lunar soil samples. These somewhat unexpected, abundant, heterogeneous, clast-rich particles are made of soil grains (clasts) bonded together by impact-melted glass (*Duke et al.,* 1970a; *McKay et al.,* 1970, 1972; *Heiken,* 1975). In some mature soils agglutinates are the major constituent, and they may make up as much as 60% of the soil by volume. Agglutinates are unique to soils developed on terrestrial planets lacking an atmosphere, such as the Moon and Mercury.

The formation of agglutinates requires (1) a rain of high-velocity micrometeoroids onto the surface of an airless planet and (2) a target consisting of a regolith produced by prior bombardment. Therefore, agglutinates are not found at all on the Earth, even in association with terrestrial impact craters. Although some meteorites may have been derived from regolith-like deposits on some asteroids, no true agglutinates have been observed in them. So far, we have found true agglutinates only in lunar soils.

Figure 7.2 shows a series of scanning electron micrographs of agglutinates. They are typically irregular in shape and often have branching or dendritic morphologies. In thin section (Fig. 7.2d), agglutinates are usually heterogeneous in appearance, with clasts and glass intermixed in varying proportions. Vesicles are present in most agglutinates. Metallic iron droplets are also common and, under high-power reflected-light microscopy, clouds of very fine metallic iron droplets are often visible. Agglutinates frequently display mounds and trains of metallic iron (Fig. 7.2e), as well as attached mineral grains and small lithic fragments. Vesicles are also common on agglutinate surfaces.

Unique properties. Agglutinates differ from other lunar impact glasses and from terrestrial impact glasses in several important respects. First, they always contain Fe metal droplets. Analysis of

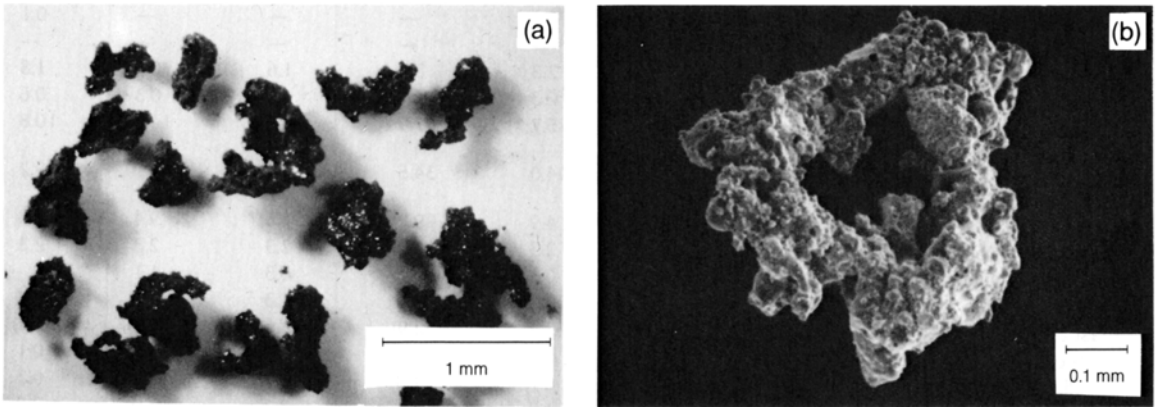

Fig. 7.2. Typical lunar soil agglutinates. **(a)** Optical microscope photograph of a number of agglutinates separated from Apollo 11 soil sample 10084, showing a variety of irregular agglutinate shapes (NASA Photo S69-54827). **(b)** Scanning electron photomicrograph of a doughnut-shaped agglutinate. This agglutinate, removed from soil 10084, has a glassy surface that is extensively coated with small soil fragments. A few larger vesicles are also visible (NASA Photo S87-38812).

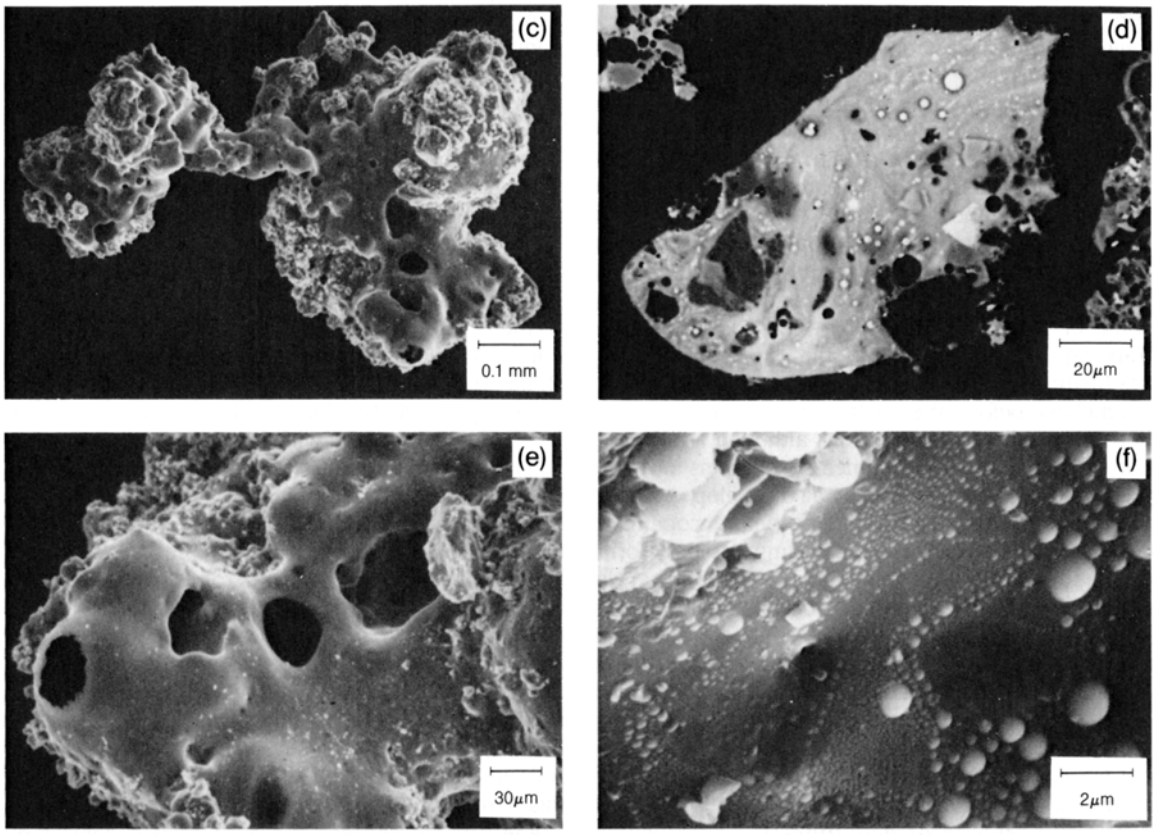

Fig. 7.2. (continued) **(c)** Scanning electron photomicrograph of an irregular agglutinate from soil 10084, showing some vesicular, glassy, fragment-free surfaces adjacent to fragment-laden surfaces. Some agglutinates are very delicate and display narrow bridges, necks, and dendrite-like arms (NASA Photo S87-38811). **(d)** Scanning electron photomicrograph of a polished thin section of an agglutinate using back-scattered electrons. The agglutinate particle contains a variety of vesicles, with circular, elongate, and irregular shapes. Irregular mineral fragments in the glass include plagioclase (darker), pyroxene, and ilmenite (brighter). The bright circular features are metallic Fe, which occurs as isolated droplets, and trains and swirls of small droplets (<5 μm). The metallic Fe has apparently been formed by reduction of FeO in the glass. It is not confined to surfaces, but is present throughout the volume of most agglutinates (NASA Photo S87-38816). **(e)** Closer SEM view of a glassy agglutinate surface, showing vesicular structure. Small mounds and trains of metallic Fe are visible as bright spots that occur over the entire glassy surface (NASA Photo S87-39605). **(f)** Closeup SEM view of a glassy agglutinate surface from sample 10084, showing clusters of Fe mounds, together with groups and trains of smaller Fe mounds (20-Å to 1-μm diameters). Most, if not all, of this Fe has presumably been formed by reduction of the lunar glass by implanted H (and possibly C) during the high-temperature pulse from the micrometeorite impact that created the agglutinate (NASA Photo S87-38846).

this metal shows that it is usually relatively pure Fe, lacking the significant Ni and Co present in meteoritic metal. Second, most of the metal droplets are extremely fine-grained. Ferromagnetic analysis shows that most of the metal is in the single-domain size range (30–100 Å), and this material is therefore not always visible using an optical microscope (*Morris,* 1976; *Pearce et al.,* 1975). Third, agglutinates always contain solar-wind gases, including He and H (*DesMarais et al.,* 1974; *Housley et al.,* 1973b). The abundances of these gases in agglutinates are usually higher than in any other grains of equivalent size in the soil.

The properties of agglutinates are best explained by a model in which agglutinates are formed by impacts of micrometeoroids into a lunar soil that contains previously implanted solar-wind elements, mainly H and He. During the impact event, several

complex processes occur. Some of the soil grains are melted, forming glass and liberating their implanted solar-wind H and He. The liberated H reacts with FeO in the glass, partly reducing it to metallic iron and producing some H_2O, which escapes from the glass (*Housley et al.,* 1973a,b). The vesicles are formed in the glass by the liberated solar-wind gases and possibly by the generated H_2O as well.

After the impact, the iron droplets are formed by the reduction process. The melted glass also engulfs small soil grains before it cools, and it may liberate some of their implanted solar-wind gases, possibly trapping them immediately within the newly-formed agglutinate. The agglutinate generally cools (quenches) before the melt can fully homogenize both physically and chemically, although somewhat homogenized smaller volumes or domains may be present. The reduced iron may also develop complex forms on the agglutinate surface before cooling is complete. Some micrometeoroid impacts may form a single agglutinate, especially if the target is coherent and the impacting body is small, and agglutinates in the form of bowl-shaped craters are not uncommon. Other impacts may form many agglutinates as the impact-produced melt pulls apart and is ejected from the impact site through neighboring soil masses. Most agglutinates probably do not travel far from the site of the impact that formed them, but few data exist on this point.

The importance of agglutinates. Agglutinates make up a high proportion of lunar soils, about 25–30% on average, although their abundances may range from a rare 5% to about 65%. At high abundances, the agglutinates, which have been produced in the regolith itself, obscure the percentages of the comminuted bedrock fragments in lunar soils. Furthermore, agglutinates contain an appreciable amount of metallic Fe° in their glass, which has formed by the reduction of Fe-silicates in the soils. Both the Fe° metal and the glass in the lunar soil obscure and modify infrared and X-ray fluorescence signals from the other soil phases, thereby complicating the mapping of the lunar surface, especially with orbital and Earth-based remote sensing. Finally, because agglutinates are continuously produced by micrometeoroid bombardment at the surface of the regolith, the agglutinate abundance in a soil increases with time and is directly proportional to its cumulative exposure age. Thus, the percentage of agglutinates in a lunar soil is one of the most useful indicators of its maturity.

Agglutinate petrography. Agglutinates are small and, like most other lunar soil grains, can be observed adequately only with a scanning electron microscope (SEM) or in polished thin sections under a petrographic microscope equipped with both transmitted and reflected light. They are best studied using ion-etched thin sections and the backscatter-electron mode of an SEM (Figs. 7.2b–f). Using these tools, agglutinates appear as heterogeneous swirls or bands of glass that contain rock, mineral, and glass fragments of all sizes; irregular lines of fine-grained iron are scattered throughout the glass. There are also fragments stuck to glassy agglutinate surfaces.

The presence of very-fine-grained (300 Å), single-domain Fe° metal is a characteristic feature of agglutinates. Production of this Fe is dependent on (1) the availability of Fe compounds in the target soils, (2) melting by micrometeoritic impacts, and (3) the availability of a reducing agent like solar-wind-implanted H in lunar soils. Because the latter two variables increase with increasing exposure age, other factors remaining constant, the abundance of fine-grained, single-domain Fe° in a soil should be a good indicator of soil maturity. The ratio of single-domain Fe° to original FeO increases as a soil matures because repeated micrometeoroid impacts continuously reduce the FeO-bearing silicates to Fe°. It has been shown that the intensity of ferromagnetic resonance of lunar soils (I_S on an arbitrary scale) is caused by this fine-grained, single-domain Fe°. Thus, the ratio I_S/FeO (with total iron in a soil expressed as FeO) is a good measure of maturity of a lunar soil, and agglutinate glass is the physical carrier of this ferromagnetic resonance (see section 7.3).

Agglutinate chemistry. Agglutinates consist of soil grains bonded by glass, and the glass itself is produced by melting the lunar soil. For these reasons, agglutinates tend to mimic the composition of the soils from which they formed. However, an agglutinate can only incorporate smaller particles than itself. Therefore, agglutinates can only be representative of that fraction of a soil whose grain size is smaller than that of the agglutinates. However, agglutinates can range up to >1 mm in size, and it is reasonable to expect that the average composition of agglutinates will be generally similar to that of the bulk soil. The only anomaly expected should be a higher concentration of Fe in the agglutinates because of the production of metallic Fe from original FeO in the soil. Indeed, analyses of agglutinate-rich magnetic concentrates from soils (*Adams et al.,* 1975; *Rhodes et al.,* 1975; *Blanchard et al.,* 1975b) indicate the presence of such an enrichment of Fe in the agglutinates over the respective bulk soils.

Although the chemical composition of whole agglutinates may be soil-like, the composition of the agglutinate glass is not. The glass that forms the binder in the agglutinate particle is, in contrast, a product of several complex processes. Primarily the glass is a melt from the very small volume of soil

that was directly impacted by a micrometeoroid. This small volume may not have been representative of the total soil. Furthermore, small compositional changes must have occurred during melting, such as the escape (at least in part) of volatile elements, or the extraction of metallic Fe° from silicate melts, leaving the melt slightly depleted in Fe. Additional effects could have been produced by the character of the mineral grains involved. Shocked grains with high internal strain energy and those with high surface-to-volume ratios (i.e., small grains), permit easier heat transfer and are likely to melt preferentially.

This last possibility led *Papike et al.* (1981) to propose that fusion of the finest fraction of soils (F^3 model) is the chief process that produces agglutinitic glass. The best test of this model has been provided by studies of Luna 24 soils, which are extremely immature, relatively pure mare soils (*Basu et al.,* 1978). In these samples, the ratio of agglutinitic glass composition (*Hu and Taylor,* 1978) to the bulk soil composition is quite similar to the ratio of the <10-μm-fraction composition (*Laul et al.,* 1981) to that of the bulk soil. In particular, the enrichment and depletion patterns of specific elements in both agglutinates and in the <10-μm fraction are quite similar (*Walker and Papike,* 1981; Fig. 7.3). This study provides a large-scale demonstration that the chemical composition of agglutinitic glass is indeed biased toward that of the <10-μm fraction of the original soil.

Furthermore, closer examination of the composition of individual agglutinates suggests that the composition of the agglutinate glass is determined by the initial shock-induced melting and is not modified by incorporation (assimilation) of unmelted grains into the glass. Seemingly pure glass is actually riddled with many submicrometer-sized vesicles and clasts. Analyses by *Basu and McKay* (1985) of the "pure" glass, both adjacent to and away from such clasts, both large and small, show no differences in chemical composition between different areas. This observation suggests that assimilation of the clasts by the primary impact melt has not been a major process modifying the final composition of the glass in different areas.

However, special problems are produced by large agglutinates, which may be the result of several generations of impact events. These large multigenerational agglutinates contain small glassy areas that are remarkably homogeneous in chemical composition. These areas are different in different agglutinates, or even within single multigenerational agglutinates, and they show no systematic chemical relationship to the composition of either bulk soils or their finest fractions (Fig. 7.4). These homogeneous glassy areas within agglutinate grains may represent the melt from single impact events, and their homogeneity could reflect total melting of the target (rather than just melting of the finest fraction) upon micrometeoroid bombardment (*Gibbons et al.,* 1976*; Hu and Taylor,* 1978). It seems likely that, when micrometeoroids strike random small targets in lunar soils (i.e., mineral grains approximately 100 μm in size or less), the impacts can produce only extremely small volumes of melt that are not representative of the bulk soil.

Agglutinates, formed as the result of surface exposure, are themselves subsequently exposed to further surface processes, especially to bombardment by extralunar charged particles from the solar wind, solar flares, and cosmic rays. Solar-wind ions implant themselves in a thin outer rind of any soil target (e.g., an agglutinate particle), with varying

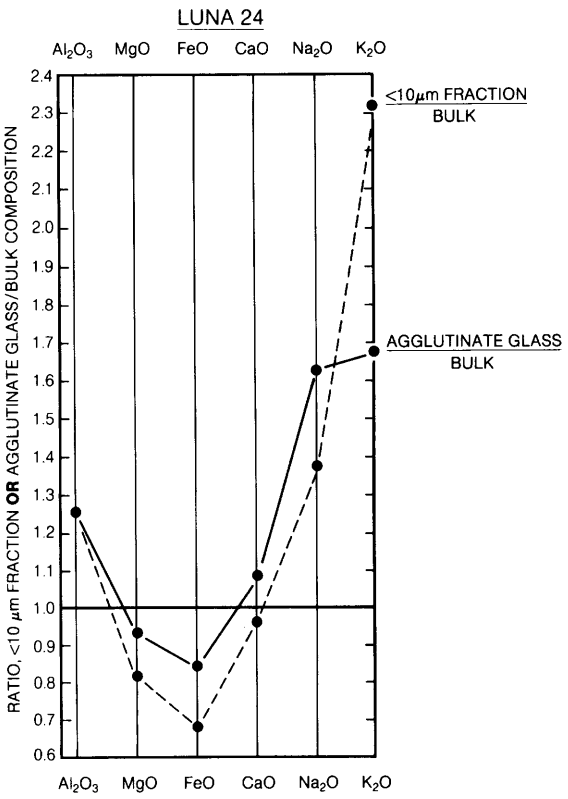

Fig. 7.3. Plot showing similarities in chemical composition between agglutinate glass from the Luna 24 soils and the <10-μm fraction of Luna 24 soils (*Papike et al.,* 1982). The plot shows ratios of key oxides in both the agglutinates and the <10-μm fraction, normalized to the same oxide in the total bulk soil.

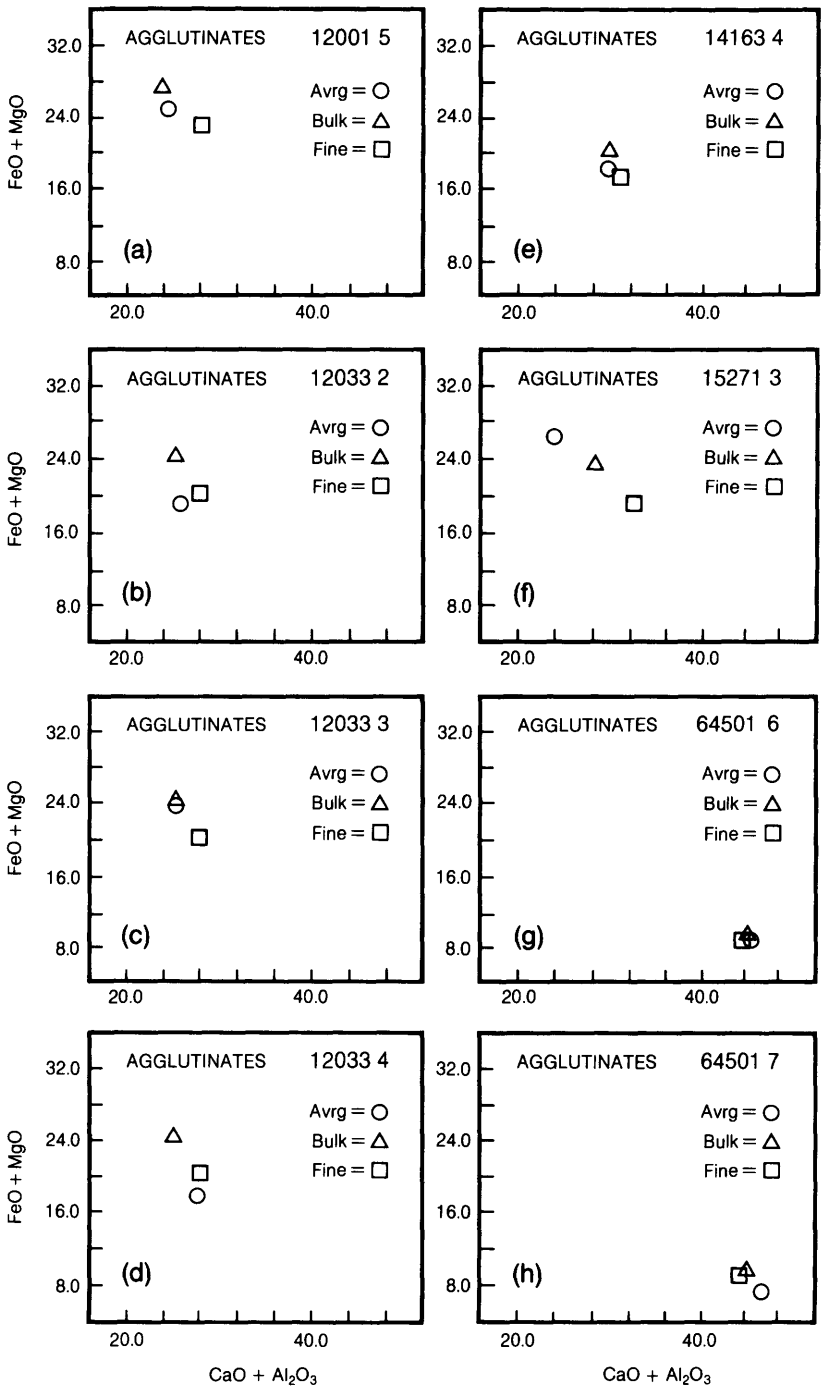

Fig. 7.4. Plots of (FeO + MgO) vs. ($CaO + Al_2O_3$) for isolated glassy areas in large single agglutinates. Note the tight clustering of the agglutinate glass compositions. Data plotted for comparison are the average compositions of agglutinate glass from the soil sample (Avrg), the bulk composition of the soil sample (Bulk), and the composition of the finest fraction (<10 μm) of the soil (Fine). The composition of any single domain of agglutinate glass shows no systematic relation to either the bulk composition of the parent soil or to that of the finest soil fraction (*Basu and McKay,* 1985).

TABLE 7.6. Concentrations of solar-wind elements (in cm^3STP/g) in magnetic agglutinate fractions separated from soil 15601.

	Range of grain size [μm]												
									Repurified				
Isotope	20–30	30–40	40–53	53–75	75–106	106–150	150–250	250–1000	10–20	20–30	30–40	40–53	53–75
$^{3}He[10^{-5}]$	2.02	2.08	1.57	1.10	1.04	0.845	0.778	0.854	2.62	2.34	1.90	1.71	1.25
					0.996			0.663					
$^{4}He[10^{-2}]$	5.21	5.28	3.99	2.88	2.64	2.20	2.01	2.23	6.62	5.94	4.91	4.33	3.23
						2.58			1.60				
$^{20}Ne[10^{-5}]$	142	149	110	88.9	85.8	75.5	65.9	76.7	183	161	136	122	95.9
					83.3			58.0					
$^{21}Ne[10^{-5}]$	0.390	0.417	0.325	0.258	0.262	0.231	0.209	0.240	0.491	0.449	0.381	0.344	0.28
					0.254			0.193					
$^{22}Ne[10^{-5}]$	11.4	11.8	8.96	7.19	6.96	6.07	5.38	6.19	14.8	13.0	11.0	9.94	7.85
					6.74			4.61					
$^{36}Ar[10^{-5}]$	41.4	38.4	29.4	25.9	21.8	19.7	17.6	19.3	52.1	42.0	36.4	31.7	26.3
					22.7			14.6					
$^{38}Ar[10^{-5}]$	7.81	7.22	5.51	4.88	4.16	3.71	3.32	3.65	9.87	7.91	6.93	5.97	4.98
					4.24			2.71					
$^{40}Ar[10^{-5}]$	36.2	33.5	26.7	23.1	19.2	18.7	17.7	16.9	45.1	35.7	30.5	27.1	23.2
					20.2			13.1					
$^{84}Kr[10^{-8}]$	25.7	22.7	19.5	17.0	13.7	13.2	12.5	12.2	35.8	28.7	25.2	22.0	18.7
					14.8			9.9					
$^{132}Xe[10^{-8}]$	4.27	3.36	2.83	2.69	2.01	2.14	1.90	1.79	5.29	4.38	3.69	3.34	2.80
					2.18			1.50					

The weight of the samples analyzed varied between 0.45 and 2.1 mg. Included are also "repurified" agglutinate separates, samples that were received after three sequential magnetic separations to make sure that no nonmagnetic material was left (*Schultz et al.*, 1977).

degrees of efficiency; the penetration depth for an element is no more than a few hundred angstroms. For all practical purposes, therefore, the solar-wind atoms, implanted after the agglutinate formed, can be considered to reside at the surface of the agglutinate. However, older solar-wind particles occur inside agglutinates in the small soil particles contained within the agglutinates. These soil particles had been irradiated by the solar wind for various lengths of time before they were incorporated into the newly formed agglutinates.

Measurements of the isotopes of common solar-wind elements, such as noble gases, in agglutinate concentrates from soil grain-size fractions, clearly show an enrichment in the finer sizes (Table 7.6). The data show a good fit to the equation

$$C = S(d/r)^{-n} + V$$

where C is the concentration of an isotope of a solar-wind element in the grain-size fraction, which has average diameter d; r is an arbitrary reference grain size with a concentration of S of the same trapped isotope; the exponent n corresponds to the negative slope in a plot of log grain size vs. log concentration; and V is the grain-size-independent volume-correlated component (*Schultz et al.,* 1977). These volume-correlated components of solar-wind-implanted noble gas isotopes for a typical lunar soil (sample 15601) are given in Table 7.7. Similar systematic variations are also found for other solar-wind elements such as H and C (*Basu et al.,* 1975). Because agglutinates trap samples of the solar wind at different times, understanding the agglutination process is an essential part of using solar-wind-element systematics in lunar soils for any investigations of the past history of the sun.

TABLE 7.7. Surface and volume correlated concentrations of solar-wind elements (in cm^3STP/g) in agglutinates from soil 15601.

Element	S	V
$^{4}He[10^{-4}]$	106 ± 13	131 ± 20
$^{20}Ne[10^{-4}]$	2.46 ± 0.25	5.45 ± 0.40
$^{36}Ar[10^{-4}]$	0.72 ± 0.06	1.44 ± 0.13
$^{84}Kr[10^{-8}]$	4.12 ± 022	10.4 ± 0.5
$^{132}Xe[10^{-8}]$	0.68 ± 0.04	1.52 ± 0.09

S is the concentration in the fraction of 100 diameter. V is the grain size independent volume correlated component. (Uncertainties given correspond to 1 sigma error of the fit.)

7.1.4. Other Unusual Soil Components

Impact glasses. A significant portion of all lunar soils (~3–5%) consists of small beads or irregular pieces of glass that lack any clastic inclusions. Most of these glass particles were produced by impact melting of preexisting regolith. Chemical analyses of large numbers of these glasses show that some of their compositions form clusters that correspond to the compositions of some rock types identified in larger samples. However, the compositions of many of these glasses represent mixtures of rock types and not primary rocks.

An additional complication in comparing the compositions of regolith glasses and lunar bedrock is that chemical fractionation processes that may accompany impact melting, such as selective volatilization of Si, have given rise to new glass compositions that do not correspond to any lunar bedrock. One such group is the high-alumina, silica-poor (HASP) glasses that have been identified from several areas of the Moon (*Naney et al.,* 1976; *Vaniman,* 1990).

The impact-glass beads in the submillimeter fraction of lunar soils are generally free from inclusions or crystals, but a small population of larger glassy objects, usually >1 mm in size and containing significant numbers of inclusions, has now been identified. Studies indicate that these heterogeneous objects probably formed by the splashing of molten impact melt onto exposed regolith. The impacts responsible for these splashes appear to have been much smaller than those that produced large numbers of the clear glass beads.

Ropy glasses. A set of distinctive, twisted glasses occur as broken pieces in all lunar soils. They contain fine dusty soil grains as inclusions, and some of them even contain skeletal crystals that grew during cooling and solidification of the glass itself (Fig. 7.5). These glasses exhibit a wide variety of chemical compositions, and they are believed to be products of impacts that were intermediate in size between those responsible for producing the impact-melt splashes and those that form large melt sheets, and similar in origin to the glassy impact bombs of the Ries Crater in Germany (*Fruland et al.,* 1977; also see sections 2.3 and 6.4).

Shocked minerals. Lunar soils are generated by the impact-produced comminution and melting of bedrock. Therefore, these soils abound in shock-metamorphosed materials that have been altered by the intense shock waves produced by the impact. A large part of this material is made up of shocked mineral fragments. A complete range of shock effects (reflecting shock waves of different intensities) is observed in both feldspars and pyroxenes. For

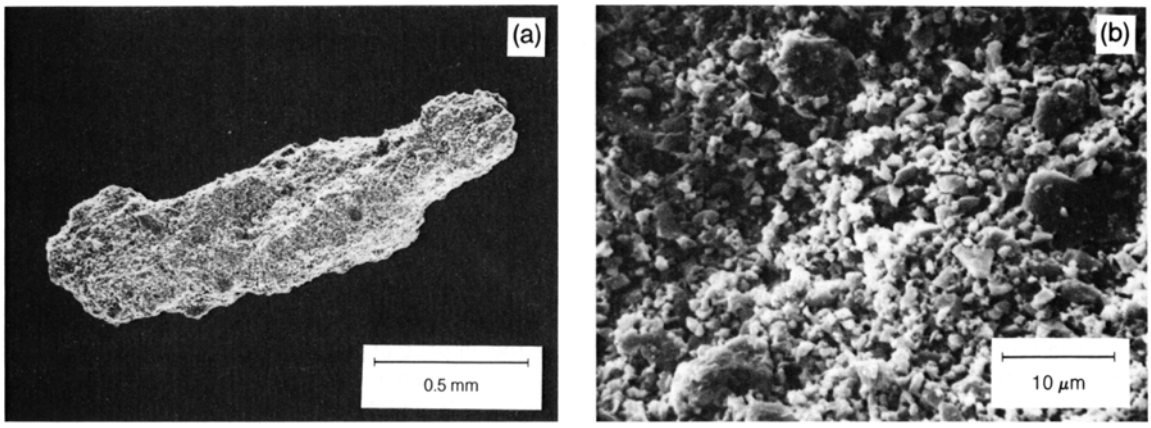

Fig. 7.5. Scanning electron micrograph of typical ropy glass particle from Apollo 12 sample 12033. **(a)** The twisted form (NASA Photo S71-24593), and **(b)** the tightly welded coating of fine fragmental material (NASA Photo S71-24586), are characteristic of many ropy glass fragments. These particles have been interpreted as impact products, which were possibly ejected to great distances as ray material.

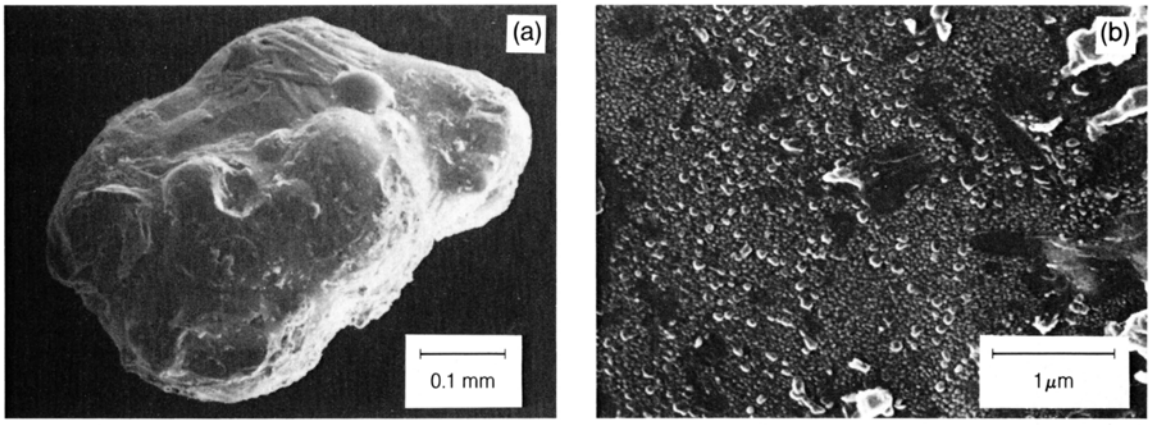

Fig. 7.6. Scanning electron micrograph of a composite volcanic glass droplet from Apollo 17 core 74001/2 (the "orange soil"). **(a)** This grain is composed of multiple droplets that collided in an eruption column while still molten. **(b)** The surfaces of such beads are usually partly coated with complex deposits of material that were possibly formed by sublimation from volcanic gases onto the bead during the volcanic eruption.

example, some plagioclase crystals show no effect of shock, whereas many show various degrees of strained and undulose optical extinction, and others exhibit total solid-state vitrification to a glass (maskelynite). A detailed discussion is provided in section 4.1.2.

Volcanic glasses. Volcanic glass particles in lunar soils are recognized by their uniformity in chemical composition, the presence of a surface coating of condensates of volatile elements, and the absence of any enrichment of siderophile elements derived from impacting meteoroids. The most abundant glasses of this type are green and orange glass spherules (Fig. 7.6), which are inferred to have formed in volcanic fire-fountain eruptions. Many different volcanic glass types have been identified in lunar soils (e.g., *Delano,* 1986). These glasses (mostly droplets and fragments) are probably the only primary lunar materials that have become part of the lunar regolith without any ballistic transport from

impact craters. When erupted, these glass pyroclasts may form layers of pyroclastic debris, such as the orange soil near Shorty Crater at the Apollo 17 site. In particular, this orange soil has grain sizes and other properties that are clearly different from those of the common impact-produced soils on the Moon (*Heiken et al.,* 1974). Section 6.1 covers lunar volcanic glasses in detail.

7.1.5. Grain Shapes and Surfaces

The effects of the interaction between the space environment and the lunar surface are commonly preserved on the exposed surfaces of grains of lunar soil. The resulting alteration features are small in scale and are observable only with a scanning electron microscope. A freshly broken soil grain, newly exposed to the space environment, has characteristic surface fractures, regardless of whether the original grain is crystalline or glassy. With continued exposure at the lunar surface, however, the grain surface characteristics gradually change. The changes are of principally two kinds: (1) the surface may acquire material in the form of added splashes and coatings of glass, or (2) the surface may lose material through erosion. Each of these two changes may also have a continuum of variations. In addition, the processes responsible for these changes operate simultaneously and in opposition, so that a grain may reach a steady state balanced between growth and destruction.

The depositional features on grain surfaces are principally coatings or splashes of impact-melted material that may or may not have come from the same grain (Fig. 7.7).

Erosion of exposed lunar soil grains is caused chiefly by two microscopic processes: (1) the removal of surface material at the atomic level (*sputtering*) by the impact of high-energy ions from the solar wind and cosmic rays (see Chapter 3), and (2) the mechanical melting and ejection of material from microcraters (zap pits) (Fig. 7.8) produced by the high-velocity impact of cosmic dust particles (see Chapter 4).

7.1.6. Grain-size Characteristics

The grain-size characteristics of any unconsolidated fragmental material are mostly controlled by the mechanical processes responsible for its formation. Because of the unique and complex processes responsible for the formation of the lunar soil, it is

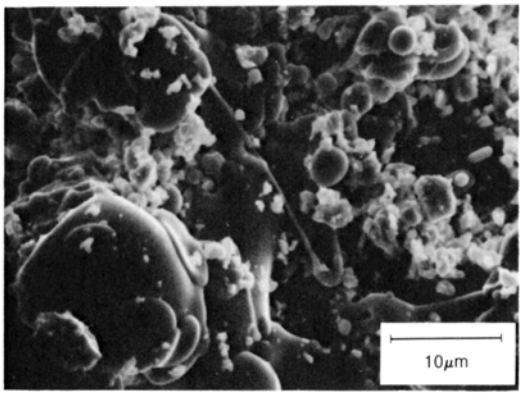

Fig. 7.7. Scanning electron micrograph of a plagioclase grain from lunar soil sample 10084, showing a variety of complex depositional features on the surface of the grain. These depositional features include irregular glass splashes, glass beads, circular "pancake" glass splashes, and adhering fine-grained fragments of crystals and glass. These features indicate that the grain was exposed at the lunar surface, where it was struck by melt ejected from nearby impact craters. Other features possibly present, but not obvious in the photograph, may include vapor-deposited coatings. Such complex surface features tend to build up on individual grains with increasing exposure time at the lunar surface.

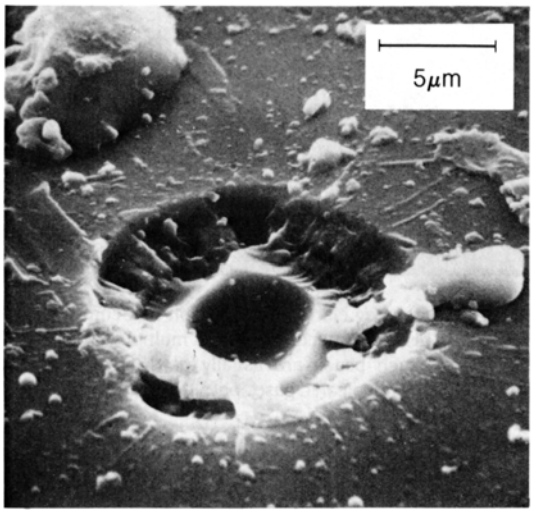

Fig. 7.8. Micrometeoroid impact crater on the surface of a lunar soil particle. This crater consists of a 5-μm-diameter crater (center), surrounded by a 5-μm-wide spall zone. Streamers and droplets of glass (melt) radiate from the crater center. Although material is deposited as shown in Fig. 7.7, competing processes work to remove material from exposed surfaces, including sputter erosion and erosion from micrometeoroid impacts that can remove material by spallation and by melt ejection or vaporization.

TABLE 7.8. The range of mean or median grain sizes for lunar soils.

	Number of Analyses	Medians*	Means†	References
Apollo 11	13	4.40 ϕ (48 μm) to 3.25 ϕ (105 μm)		*Carrier* (1973)
Apollo 12	55	4.58 ϕ (42 μm) to 3.40 ϕ (94 μm)		*Carrier* (1973)
Apollo 14	8	3.74 ϕ (75 μm) to 0.32 ϕ (802 μm)		*McKay et al.* (1972)
Apollo 15	19	4.3 ϕ (51 μm) to 3.22 ϕ (108 μm)		*Carrier* (1973)
Apollo 16	14		3.29 ϕ (101 μm) to 1.89 ϕ (268 μm)	*Heiken et al.* (1973)
Apollo 17	42		4.59 ϕ (41.5 μm) to 2.59 ϕ (166 μm)	*McKay et al.* (1974)
Luna 16	4	3.8 ϕ (70 μm) to 3.05 ϕ (120 μm) to		*Vinogradov* (1971)
Luna 20		~3.8 ϕ (70 μm) to 3.62 ϕ (80 μm)		*Vinogradov* (1973)

* Median, half of the particles are coarser than the median and half are finer; corresponds to the 50% mark on a cumulative curve.
† Mean (M_z), the graphic mean is based on three points on a cumulative curve (see *Folk,* 1968).
Phi units (ϕ), grade scale for granular sediment $\phi = -\log_2 \xi$ (ξ equals the diameter in millimeters).

not surprising that the grain-size distributions of lunar soil samples do not match those of terrestrial sediments that have been deposited by wind or water. Nor do lunar soil samples match the expected size distribution for impact-comminuted rock debris.

The process of lunar soil formation is obviously more complicated than simple impact comminution. Although meteoroid and micrometeoroid bombardment reduces lunar rocks and their debris to fine particles, the micrometeoroid bombardment of the soil itself produces, with each impact, small amounts of melt that adhere to nearby soil particles, bonding them together to produce the larger constructional particles called *agglutinates.* At the same time, bombardment by larger meteoroids churns (gardens) the lunar regolith and mixes together different soils produced under many different conditions. Thus, lunar soil grain size is controlled by three principal processes: comminution (which reduces the grain size), agglutination (which increases the grain size), and mixing.

Many comprehensive grain-size analyses of lunar soils have been made at the NASA Johnson Space Center (e.g., *McKay et al.,* 1974). Data from this laboratory have been reported mostly in terms of a few standard parameters (mean grain size, median grain size, sorting, etc.) that were calculated using procedures developed by *Folk and Ward* (1957) for terrestrial sediments. Most lunar soils fit a log-normal grain-size distribution, so that their grain-size-frequency data are plotted on a logarithmic scale, using a phi scale [$\phi = -\log_2$ (grain size, mm)], in which they approximate a Gaussian distribution. It has also been claimed that they more closely follow a Rosin's size-frequency distribution (*King and Butler,* 1977). However, in either case the approximations using parameters of *Folk and Ward* (1957; described in section 9.1) are still valid.

In general, for a given site, both the grain size of the finest-grained soil collected, as well as the average mean grain size of all soil samples collected, are different from those at any other site. This result appears to be related to the regolith thicknesses at each landing site. Thicker regoliths imply longer exposure ages and longer periods of meteoroid bombardment. The exposure age thus determines how the grain-size distribution will reflect the combined processes of mixing, comminution, and agglutination. This same relation between mean grain size and regolith thickness is also observed in lunar soil samples from a single mission, but which were collected at different locations within one landing site.

Mean grain size and sorting. With no wind or water on the Moon it is difficult to apply grain-size parameters that have been developed on Earth for a full range of clastic sediments (deposited by wind and water). However, some statistical descriptions can be made. The mean grain size of lunar soils ranges from 40 to 800 μm, with most means falling between 45 and 100 μm (Tables 7.8 and A9.1). Using conventional terrestrial descriptions, most lunar

regolith samples would correspond to pebble- or cobble-bearing silty sands (Fig. 7.9). Sorting values (the standard deviation of *Folk,* 1968) range from 1.99 to 3.73 ϕ); in other words, the lunar soils are poorly to very poorly sorted. There is also an inverse correlation between mean grain size and sorting (standard deviation); the coarsest samples are the most poorly sorted (Fig. 7.9). Soils from all the Apollo sites are nearly symmetrically to coarsely skewed (skewness = 0 to 0.3).

Exceptions to these generalizations are the green-glass and the dark-mantle deposits sampled at the Apollo 15 and 17 sites, respectively. These pyroclastic deposits are finer-grained (mean grain sizes of 40.0 and 37.9 μm) and better sorted (σ = 1.57 and 1.69 ϕ,) than any of the sampled lunar soils. These deposits have been interpreted as deposits of volcanic ash and are not true impact-produced soils (see section 6.1.7 on lunar pyroclastic deposits). When these glass spheres become mixed into neighboring layers of ordinary lunar soil, their presence significantly lowers the mean grain size of the soil.

Attempts to estimate the grain-size distribution of lunar soils from photographs and electronic images have not been successful. On the basis of a comparison between Surveyor 3 television images, obtained in 1967, and soils sampled nearby during the Apollo 12 mission in 1969, *Carrier* (1973) determined that accurate estimation of grain-size distribution from the television images was not possible. *Jaffe et al.* (1968), using the Surveyor images, had predicted that the lunar soil at the Apollo 12 site was composed of particles between 2 and 60 μm in size. In fact, the mean grain size of soils collected from the Apollo 12 site (<1-mm fraction) ranged from 70 to 220 μm. This difficulty of estimating regolith grain size using televised images should be kept in mind when planning future unmanned missions on the lunar surface.

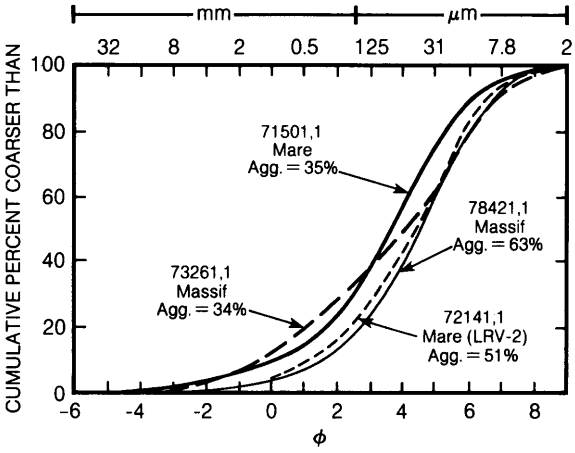

Fig. 7.9. Cumulative size-frequency diagram for typical lunar surface soil samples. Data are shown as cumulative percent by weight greater than a given particle size. Particle sizes are given in both mm and μm and 41 classes (see text for discussion). "Agg" refers to the agglutinate content of individual soil samples.

7.1.7. Chemical Composition of Lunar Soils

The chemical compositions of lunar soils reflect their mixed origins. All regolith samples brought back from the Moon contain some components exotic to the collection site. Although Apollo 11 landed in the middle of a mare basalt plain, the soils do not have compositions equivalent to 100% mare basalt. There is chemical evidence for the presence of additional rock and mineral fragments from the anorthositic highlands, rare KREEP-bearing material, and a small meteoroid component.

Certain minerals, including potassium feldspar, apatite, whitlockite, and zircon, are rare in the lunar soil, but they carry the bulk of such important trace elements such as K, the rare earth elements (REE), P, and Zr. The abundance of major elements can be used to indicate roughly the proportions of highland anorthositic (Ca,Al-rich) and mare basaltic (Fe,Ti-rich) rocks that are present in the soil (see section 8.3). The trace elements K, REE, and P can be used to estimate the percentage of KREEPy source rocks in a soil (see section 8.4).

The proportions of different petrologic components in a soil vary with grain size, and therefore the bulk chemical compositions will also vary with grain size. Minerals that were originally present as small crystals in parent rocks may dominate the composition of the finest-grained sizes of a lunar soil, even though they made up only a small percentage of the parent rock.

Multivariate analysis of a large array of chemical elements can provide insights into the variety of rock types represented in any lunar soil. *Laul and Papike* (1980) chose several common lunar rock types as end-members, and then carried out mixing-model calculations based upon 35-element analyses of lunar soils. The results can be used to interpret the chemical composition of any lunar soil in terms of the principal rock types present in the immediate area, and can provide estimates of the amount and nature of exotic material introduced into the soil from beyond the landing site.

This chemical-statistical approach is especially useful because most lunar soils have abundant fused material, making petrographic identification of

source rock types difficult. For example, the Apollo 11 soils contain 60% agglutinates and 20% dark-matrix breccias, leaving only a small part of the sample composed of easily identified rock fragments and mineral grains. *Laul and Papike* (1980) determined, from their chemical analyses and mixing calculations, that the source rocks for these soils are (1) high-K mare basalt (10%); (2) low-K mare basalt (62%); (3) anorthosite, norite, and troctolite (ANT rocks) (14%); and (4) low-K KREEP (13%).

Determination of the abundances of K, Rb, Sr, and Ba in nine grain-size fractions of Apollo 17 mare soil 71501 showed that these incompatible elements are systematically enriched in the finer-grained fractions. *Korotev* (1976) and *Haskin and Korotev* (1977) show that this enrichment is produced by the differential comminution of feldspathic and mesostasis portions of the original bedrock. These materials, which carry the bulk of the incompatible elements in the bedrock, are both finer grained and more easily broken than the other bedrock components, which accounts for their preferential incorporation into the finer size fractions. A more quantitative treatment of soil chemistry is provided in Chapter 8.

7.2. SPECTRAL PROPERTIES OF THE LUNAR REGOLITH

Although diagnostic absorption bands are present in the visible and infrared spectra of lunar rocks (sections 6.2 and 6.5) and in their mineral constituents, these bands are subdued in the reflectance spectra from the regolith because of the regolith's high content of dark, absorbing agglutinates. The reflectance spectral properties of mature soils from each of the Apollo sites are shown in Fig. 7.10. In particular, the complex multicomponent agglutinates, which are the products of prolonged exposure to the space environment, are also responsible for the characteristic slope in the spectra, which increases toward longer wavelengths.

Superimposed on this sloping continuum are the weak but diagnostic absorption bands characteristic of the mineral fragments present in the soil. These weak features are seen more clearly in the residual spectra of Fig. 7.10, which are obtained by normalizing to remove the effects of the continuum. The absorption band near 1.0 μm largely reflects the presence of different varieties of the mineral pyroxene (section 5.1.1). Soils with abundant orthopyroxene exhibit a band centered near 0.91 μm, and soils with abundant clinopyroxene exhibit a band centered at longer wavelengths, near 1.0 μm.

The reflectance spectra of immature regoliths, whose agglutinate content is lower, have more prominent absorption features. As the agglutinate abundance decreases, the spectra of these regoliths become comparable to those of fresh samples of lavas, plutonic rocks, and breccias (sections 6.2 and 6.5). Areas of immature regoliths on the Moon can readily be identified by Earth-based telescopic observations. The special spectral character of these regoliths can be easily seen in the spectra obtained from small areas of the Moon (5–10 km in diameter) shown in Fig. 7.11.

In the blue and ultraviolet wavelengths, the slope of the reflectance spectrum is notably less steep for the darker, more TiO_2-rich mature mare soils (*Charette et al.,* 1974). This property has been useful for mapping the spatial extent of different mare soil types on the Moon (*Pieters,* 1978).

7.3. REGOLITH EVOLUTION AND MATURITY

The lunar regolith is produced by meteoroid impacts that shatter exposed lunar bedrock, which may consist of a wide variety of rock types—lavas, coarse crystalline rocks, and fragmental breccias (see Chapter 6). When this process begins, the resulting regolith material is both fresh and young. If the newly formed regolith is exposed at the lunar surface, it continues to be progressively modified by micrometeoroid impacts and by high-energy solar and cosmic charged particles. This modification process, described below, is called *maturation,* and regolith exposed to these processes for long periods of time becomes *mature.* If the fresh, young regolith soon becomes deeply buried (e.g., by ejecta from a nearby impact crater), it is not exposed to these surface processes, and it therefore remains fresh or *immature.*

However, such buried regoliths may not remain buried indefinitely. Subsequent impacts may turn the regolith over (gardening) and bring young, buried regolith to the surface. At this point, it again becomes subjected to micrometeoroids and charged particles, and the maturation process continues.

This potential for alternate burial and exposure of lunar regolith gives rise to the concept of *surface exposure age.* This age is defined as the cumulative length of time that a given lunar soil has been exposed at (or near) the surface, as measured by the effects of some alteration process—micrometeoroid impact pits, solar-wind implantation, or the effects of high-energy cosmic rays. The effects of solar-wind, solar-flare, and galactic-cosmic-ray exposure are summarized in Table 7.9.

To estimate surface exposure ages, it is generally assumed that the lunar surface environment has remained constant over the time span in question. Even so, calculations of exposure ages are compli-

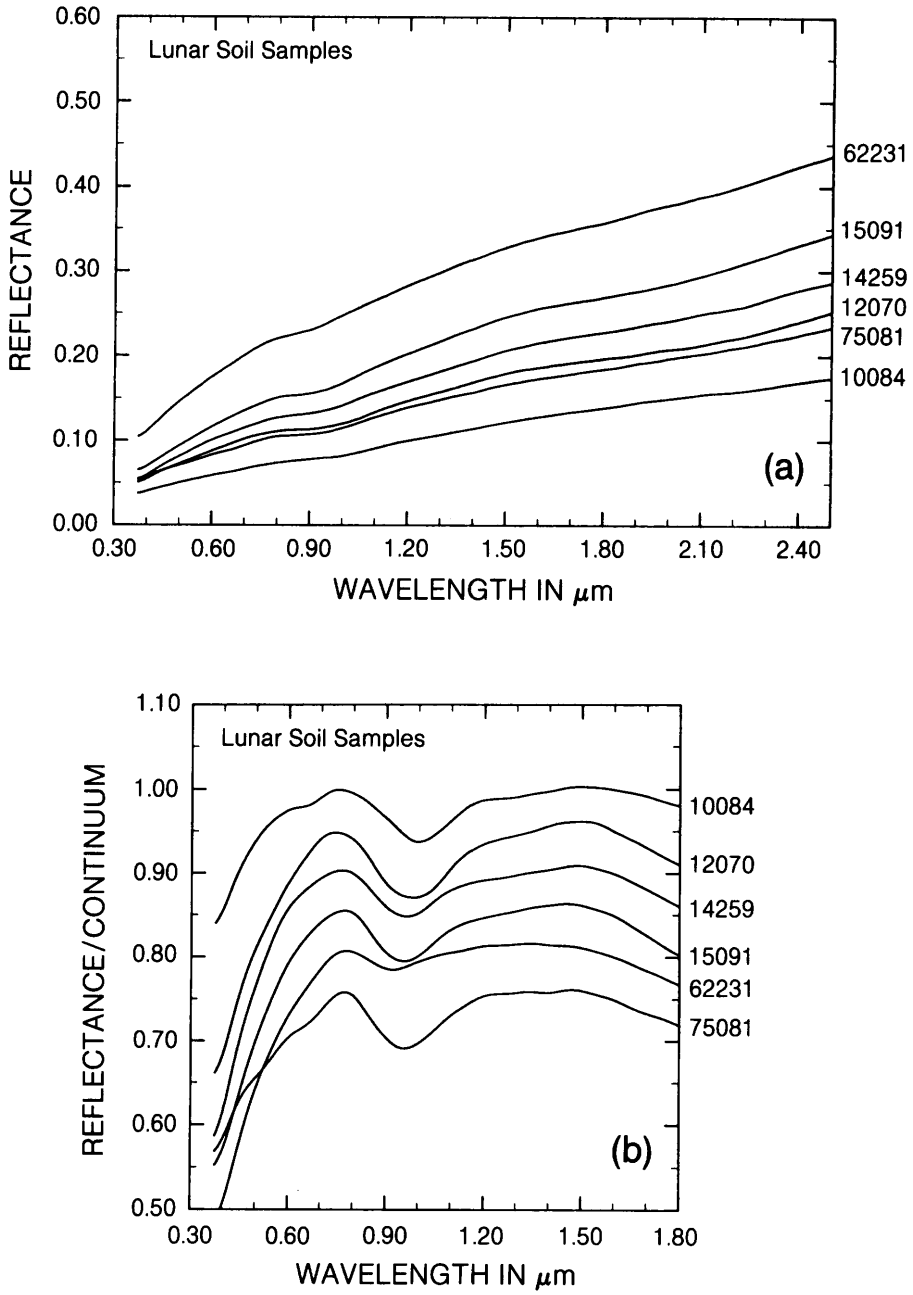

Fig. 7.10. Spectral properties of lunar soils in the ultraviolet and near-infrared, as measured in the laboratory. **(a)** Reflectance spectra, shown as the ratio of total radiant flux reflected by the soil to the total incident on the surface, of lunar soil samples 10084 (mature mare regolith), 12070 (submature mare regolith), 14259 (mature soil developed on breccias), 15091 (mature soil at a highland-mare boundary), 62231 (mature highland soil), and 75081 (submature mare soil). **(b)** Residual absorption features of the spectra in **(a)** after removal of the steeply sloped continuum reflectance.

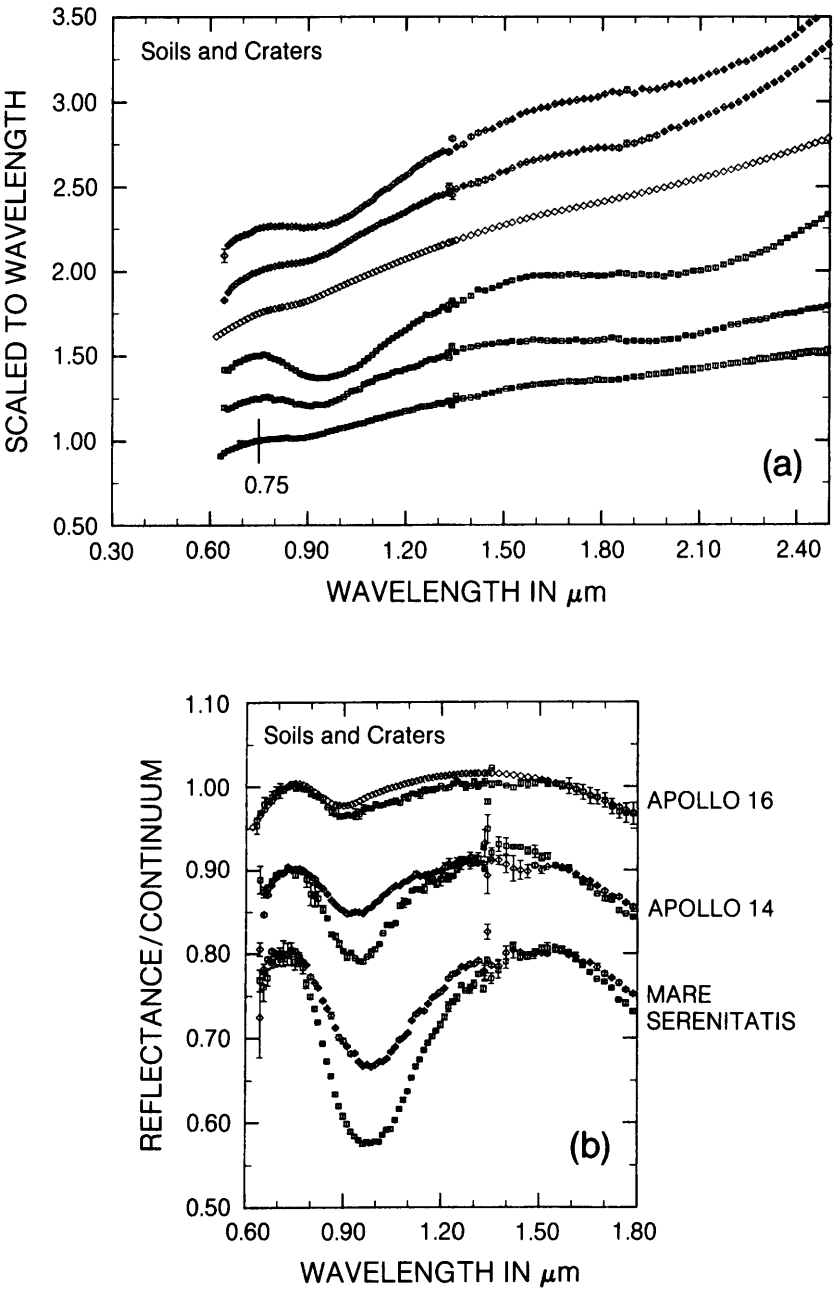

Fig. 7.11. (a) Reflectance spectra of mature and immature lunar soils obtained remotely (using instruments on Earth-based telescopes). The areas measured on the lunar surface are 5–10 km across. All spectra are normalized to unity at 0.75 μm and are offset vertically for comparison. **(b)** Residual absorption features of the spectra in **(a)** after removal of the steeply sloped continuum reflectance. Residual absorption curves for mature soils and immature soils (fresh crater ejecta) from the same geologic region are superimposed; absorption features tend to be subdued in the more mature soils. The location of mineral absorption features, e.g., the deep absorption at 0.8–1.0 μm, varies from region to region (e.g., between the Apollo 14 and 16 highland sites), consistent with observed changes in geology and geochemistry. However, when mature and immature soils from the same site are compared, the chief variation is in the intensity of the reflectance rather than in the location of absorption features.

TABLE 7.9. Nuclear particle effects in extraterrestrial materials (from *Walker,* 1980).

Radiation Source	Energy and Characteristic Penetration Distance	Major Observable Effects
Solar wind	1 keV/amu several hundred angstroms	Direct implantation (e.g., surface-correlated rare gases) Reimplantation of lunar-atmospheric species (e.g., ^{40}Ar excess in lunar soils) Radiation damage (e.g., amorphous layers on lunar dust grains)
Solar flares	<1 MeV/amu to ≳100 MeV/amu millimeters to centimeters many more low-energy than high-energy particles	Radionuclide production (e.g., ^{26}Al, ^{53}Mn) Track production (principally tracks produced by slowing down VH nuclei) Electronic defects (e.g., thermoluminescence)
Galactic cosmic rays	≥100 MeV/amu typically –3 geV/amu centimeters to meters	Radionuclide production Stable isotope production (e.g., ^{21}Ne, ^{15}N) Nuclear effects due to buildup of nuclear cascades with depth (e.g., N-capture in Gd) Tracks (spallation recoils in addition to slowing down heavy nuclei)

cated by the fact that different alteration processes operate at different depths within the regolith. Micrometeoroid craters (zap pits) and solar-wind-ion implantation occur at the very surface, and regolith particles that show these effects have been exposed to free space. The radioactive transformations produced in the lunar regolith by high-energy solar-flare and cosmic-ray particles develop at depths of a few centimeters to a few meters and indicate exposure near (but not necessarily at) the surface. These complications produce a situation in which the resulting exposure age is depth dependent.

In addition to exposure ages, lunar soils can be distinguished on the basis of different degrees of maturity (usually *immature, submature,* and *mature*) by measuring how greatly the soil is altered on average by some particular external process.

This view of the maturation of the lunar regolith is necessarily oversimplified. In fact, regolith formation, surface exposure ages, and observed degree of maturity are inextricably mixed. Nevertheless, a simple perspective, in which maturity and exposure ages are treated separately, is useful for describing lunar regolith processes, because most regolith was deposited early in the history of the Moon, before ~3.5 b.y. ago. At this time, the impact flux was higher, large impacts were more frequent, and exposure times were short because of the high probability of subsequent burial. As meteoroid impacts subsequently became less frequent, the more gradual maturation processes active today became more important in producing and modifying the presently observed regolith.

7.3.1. Maturation by Meteoroid Bombardment

Bombardment by meteoroids, both large and small, produces the most significant changes in lunar soils:

1. Large particles are broken down into smaller ones.
2. Large impacts shock-indurate the regolith, producing coherent regolith breccias.
3. Micrometeoroid impacts produce small amounts of melt at the point of impact; the melt then cements nearby small grains to make agglutinates.

4. Impacts of all sizes may produce vaporized projectile and target material that is dispersed from the impact site and deposited on the exposed surfaces of regolith particles.
5. With moderate to large impacts that form craters more than a few meters in diameter, the ejected regolith material forms a layer that covers up neighboring soils. Such impacts may also excavate previously buried regolith soils, reexposing them to surface processes.
6. Continued bombardment produces a continuous churning of the regolith, thus mixing soils together at random.
7. Large impacts, which penetrate the regolith layer, also eject deep-seated bedrock fragments, often to significant distances, where they form the exotic component of the regolith at that site. These impacts may also generate a sheet of impact melt that covers regolith in and around the crater.
8. Finally, material ejected from a large crater may also produce secondary craters when it lands. These craters produce additional ejecta, and many other effects of the primary impacts, although at decreasing energy levels.

Therefore, meteoroid bombardment controls the maturation of the lunar soil in several different ways. It produces physical and chemical changes in the soil itself—comminution, vapor fractionation, the formation of aggregates (agglutinates and regolith breccias), and the addition of a meteoritic component. In addition, impacts produce other and more widespread changes—breaking up bedrock and adding it to the regolith, mixing together layers of soil that were originally discrete, introducing exotic rock components from distant sites, and turning over or reworking the exposed soil to depths that depend on the meteoroid size-frequency distribution and impact flux rate (see Chapter 4). Meteoroid impact also determines what volumes of the regolith are brought to or near the lunar surface, where they can be affected—and matured—by other processes.

Production of new particles. Meteoroid impacts control the maturation of the regolith by regulating its excavation and exposure to near-surface processes, but they also produce their own maturation effects. Micrometeoroids comminute soil particles, a process that changes the distribution of particle sizes by producing smaller particles and removing larger ones. Therefore, the mean grain size of the <250-μm soil fraction is an index of maturity; finer-grained soils are more mature.

Meteoroid impacts also produce agglutinates, bits of welded soil fragments, glasses, and mineral and rock fragments (see sections 7.1.3 and 7.1.4). Agglutinate content is one index of soil maturity; higher agglutinate contents imply more mature soils. This index conflicts to some extent with the previous one because agglutinate formation results from the welding of smaller particles into larger ones, and therefore acts to increase the overall grain size.

Vapor fractionation. The intense and transient shock-wave heating produced by a meteoroid impact has several distinctive effects. Volatile elements are vaporized from the regolith and bedrock targets. Because the gravity of the Moon is low, some of these vaporized elements can escape the Moon's gravitational field. As a result, the lunar soils can become progressively depleted in these elements with increasing maturity.

In addition, volatile elements that do not escape exhibit a measurable mass fractionation of their isotopes, probably produced during this vaporization process. Analyses of 0 and Si isotopic ratios in lunar rocks and soils indicate that lunar soils are enriched in the isotopes ^{18}O and ^{30}Si relative to the crystalline rocks (*Epstein and Taylor,* 1972). These workers also found that these large enrichments of the heavy isotopes of 0 and Si in lunar soils are directly related to the amount of solar-wind-derived H present. Successive partial fluorinations of soil grains, a technique that enables the extraction of Si and O from successively deeper layers in the grains, show that the enrichment of ^{18}O and ^{30}Si is essentially *surface-correlated* (i.e., restricted to the grain surface) (*Epstein and Taylor,* 1972; Table 7.10). These measurements also show that this apparent vaporization of the light isotopes, ^{16}O and ^{28}Si (or, conversely, a fractional condensation of the heavy isotopes, ^{18}O and ^{30}Si) is accompanied by a reduction of the bulk O/Si ratio; it is therefore likely that more O than Si escapes during the fractional vaporization process.

The concentrations of other volatile elements (e.g., Zn, Ga, Ge, Cd, Sb, Te, and Hg) in different grain-size fractions of lunar soil samples also show a negative correlation with grain size, indicating that these elements are enriched in the finer fractions. Because the small grains have higher surface-to-volume ratios than do larger ones, these results indicated that these elements have been deposited on grain surfaces (*Krähenbühl et al.,* 1977; Tables 7.1 1 and 7.12). Calculations by *Boynton et al.* (1975) suggest that, even with the maximum possible introduction of some of these elements into the lunar regolith from meteoroids, there is still an excess of volatile elements on the surfaces of lunar soil grains. Lunar volcanism has been suggested also as the source of this excess (*Boynton et al.,* 1976a). (Establishment of a volcanic source for these condensable volatiles would be of special significance in understanding the formation of the volcanic glass spherules that are

TABLE 7.10. Isotopic compositions of oxygen and silicon extracted by successive partial fluorination of Apollo 14 and Apollo 15 lunar samples (*Epstein and Taylor*, 1972).

Sample	Cum. μmole O_2 / mg original sample	δO^{18}	μmole O_2	δSi^{30}	μmole SiF_4	Ratio O_2/SiF^4
14298,14 fines (0.772 g)						
a. 30 min/80°C	0.036	+57.7	28	+24.8	28	1.00
b. 60 min/121°C	0.049	+34.9	9.5	+7.65	7.5	1.27
c. 30 min/143°C	0.070	+30.9	16.5			
				+4.20	39	1.39
d. 30 min/197°C	0.118	+23.8	37			
e. 30 min/209°C	0.177	+15.66	46	+1.16	31	1.48
f. 30 min/247°C	0.303	+11.93	97	+1.31	65	1.49
Total			234		170.5	1.37
14422 12 fines (1.265 g)						
a. 20 min/87°C	0.020	+56.6	25	+23.2	25	1.00
b. 60 min/121°C	0.033	+30.0	16.5			
				+6.51	30	1.48
c. 45 min/146°C	0.055	+26.7	28			
d. 25 min/190°C	0.113	+20.6	73	+3.07	55	1.33
e. 25 min/217°C	0.177	+15.40	82	+2.87	55	1.49
f. 30 min/247°C	0.336	+11.29	201	+0.47	154	1.31
g. 30 min/279°C	0.559	+8.24	281		167	1.68
h. 30 min/299°C	0.774	+8.13	277		175	1.58
i. 30 min/345°C	1.097	+7.38	404		258	1.57
Total			1387.5		919	1.51
14148,7 trench fines, top (0.6639 g)						
a. 30 min/77°C	0.035	+51.4	23	+22.3	23	1.00
b. 30 min/120°C	0.049	+27.6	9.5			
				+5.97	15	1.37
c. 30 min/145°C	0.066	+28.9	11			
d. 30 min/200°C	0.132	+19.8	44	+2.62	29	1.52
e. 30 min/247°C	0.341	+11.31	139		93	1.49
f. 50 min/266°C	0.645	+8.40	202		138	1.46
g. 30 min/296°C	0.935	+7.01	192		127	1.51
h. 30 min/303°C	1.186	+6.63	167		111	1.50
Total			787.5		536	1.47
14156,4 trench fines, middle (0.6273 g)						
a. 30 min/77°C	0.021	+56.3	13	+26.4	12	1.17
b. 30 min/121°C c. 30 min/147°C	0.040	+33.3	12	+8.97	12	1.00
d. 30 min/198°C	0.096	+26.3	35	+4.50	24	1.46
Total			60		48	1.25

TABLE 7.10. (continued)

Sample	Cum. μmole O_2 / mg original sample	δO^{18}	μmole O_2	δSi^{30}	μmole SiF_4	Ratio O_2/SiF^4
14149,23 trench fines, bottom (0.7696 g)						
a. 30 min/77°C	0.017	+42.4	13	+20.6	12	1.08
b. 30 min/121°C	0.038	+25.9	16	+8.91	10	1.60
c. 30 min/147°C	0.064	+24.4	20	+6.36	9	2.22
d. 30 min/200°C	0.146	+15.47	63		45	1.4
e. 30 min/247°C	0.326	+10.31	139		96	1.45
f. 50 min/266°C	0.585	+7.79	199		138	1.44
g. 30 min/297°C	0.823	+6.95	183		130	1.41
h. 30 min/303°C	1.046	+6.73	172		114	1.51
Total			805		554	1.45
14321,59 rock breccia (0.963 g)						
a. 30 min/80°C	0.021	+7.81	20	+1.48	11	1.82
b. 30 min/123°C	0.032	+9.12	11			
				-0.13	17	1.21
c. 30 min/156°C	0.042	+8.90	9.5			
d. 30 min/202°C	0.066	+7.78	23	-1.32	17	1.35
Total			63.5		45	1.41
15021,25 fines (0.8811 g)						
a. 30 min/80°C	0.040	+49.7	35	+24.5	29	1.07
b. 60 min/118°C						
	0.042	+24.6	20			
c. 45 min/144°C						
				+7.74	24	1.17
d. 25 min/190°C	0.085	+26.0	20			
e. 25 min/217°C	0.125	+18.64	35	+4.15	23	1.35
f. 30 min/247°C	0.187	+15.16	55	+2.17	40	1.38
g. 30 min/294°C	0.439	+8.33	222	-0.02	166	1.34
h. 30 min/303°C	0.691	+6.32	222	-0.74	168	1.32
i. 30 min/311°C	0.928	+5.28	209	-0.92	129	1.62
j. 30 min/342°C	1.239	+5.07	274	-0.37	175	1.57
k. 30 min/371°C	1.546	+6.25	270	-0.20	141	1.91
Total			1362		895	1.52
15251,24 fines (0.8847 g)						
a. 30 min/67°C	0.020	+51.8	18	+25.4	12	1.50
b. 60 min/119°C	0.037	+37.0	15	+12.9	8	1.88
c. 45 min/144°C	0.052	+35.0	13	+8.87	6	2.17
d. 25 min/190°C	0.094	+26.7	37	+6.24	31	1.19
e. 25 min/216°C	0.144	+18.2	44	+2.66	36	1.22
f. 25 min/259°C	0.270	+12.40	112	+1.04	80	1.40
g. 30 min/291°C	0.527	+8.01	227	-0.06	154	1.50
h. 30 min/303°C	0.729	+6.86	179	-0.24	139	1.32
i. 35 min/319°C	0.931	+6.13	179	-0.41	143	1.28
j. 30 min/343°C	1.241	+5.06	274	-0.33	152	1.83
k. 30 min/369°C	1.552	+5.66	275	-0.10	141	1.98
Total			1373		902	1.52

TABLE 7.11. Weight distribution of grain-size fractions in samples 72501 and 72461 and results for the volatile elements determined by radiochemical procedures (*Krähenbühl et al.*, 1977).

Grain-size Size interval (μm)	Mean (μm)	Weight mg	Cd ppb	Ge ppb	Hg ppb	In ppb	Sb ppb	Te ppb	Zn ppm
72501									
1000–350	540	47.5	28±2	250±25	1.0±0.1	4.1±0.5	1.3±0.3		7.3±0.7
350–149	250	54.8	31±3	665±65	1.9±0.2	2.1±0.3	2.9±0.7		9.8±0.9
149–74	110	51.7	41±3	350±35	1.6±0.2	2.1±0.3	2.8±0.65		12 ±1.1
74–45	60	55.45	37±3	250±25	2.4±0.3	2.0±0.3	2.1±0.5		14 ±1.3
45–30	36	49.2	34±3	280±30	2.5±0.3	2.0±0.3	2.1±0.5		20 ±1.8
30–15	22	33.5	40±3	290±30	4.8±0.5	1.9±0.3	4.1±1		20 ±1.8
15–7	11	34.1	72±6	375±40	6.3±0.7	3.4±0.4	2.9±0.7		33 ±3
7–2*	3	36.5	59±5	435±45	8.3±0.9	4.7±0.5	4.5±1		36 ±3.2
<2*	1.25	6.7	106±8	520±50	22 ±2	6.0±0.7	7.7±2		54 ±5
Mean†	—		42±3	368±40	3.6±0.3	2.8±0.4	2.8±0.7		18.2±1.6
Bulk		82.3	39±3	400±45	3.1±0.3	2.1±0.2	2.5±0.5		17 ±1.5
72461									
1000–350	540	31.4	25±2	235±27	4.5±0.5	4.0±0.5	1.2±0.3	14 ±3	6.0±0.5
350–149	250	45.4	33±3	510±58	1.3±0.1	1.3±0.2	2.0±0.5	14 ±3	8.5±0.7
149–74	110	36.8	35±3	485±55	1.3±0.1	2.0±0.2	1.6±0.4	17 ±3	11.5±1
74–45	60	49.7	53±4	320±37	2.0±0.2	1.9±0.2	1.5±0.4	20 ±4	13 ±1
45–30	36	40.1	43±3	260±30	2.5±0.3	1.8±0.2	1.7±0.5	24 ±5	18 ±2
30–15	22	37.7	34±3	315±36	6.6±0.7	4.3±0.5	2.9±0.7	22 ±4	17 ±2
15–7	11	47.9	49±4	365±42	4.8±0.5	3.1±0.3	1.9±0.4	33 ±7	26 ±2
7–2*	3	17.3	65±5	370±42	7.4±0.7	4.0±0.4	4.0±1.0	42.5±8	35 ±3
<2*	1.25	6.2	130±10	510±58	12.5±1	10.7±1.2	1.5±0.4	101 ±20	54 ±5
Mean†		—	43±3	364±42	3.6±0.4	2.8±0.3	2.0±0.5	24 ±5	16.5±2
Bulk		47.8	44±3	295±34	3.6±0.4	2.0±0.2	4.0±0.8	22 ±4	17.5±2

* Obtained by sedimentation.
† Taking in account weight of fractions.

TABLE 7.12. Estimated percentages of volatile elements contributed to Apollo 16 lunar soils by lunar bedrock, the known flux of extralunar particles (C1 chondrite composition), and "excess" volatiles possibly due to volcanism (mean and standard deviation; *Boynton et al.*, 1976a).

	From Lunar Rocks				Extralunar*				Excess			
	Zn	Ga	Cd	In	Zn	Ga	Cd	In	Zn	Ga	Cd	In
60002	3.3	66.5	2.2	3.2	73.6	11.1	32.7	32.1	23.1	22.4	65.1	64.7
	±0.2	± 5.5	±0.4	±0.5	± 6.9	± 0.2	± 4.5	± 3.4	± 6.9	± 5.2	± 4.8	± 3.8
Stations 1,2,13	3.2	63.9	2.0	2.6	35.1	4.7	15.6	12.2	61.7	31.4	82.4	85.2
	±0.6	± 2.6	±0.3	±0.9	± 6.5	± 1.0	± 5.3	± 2.2	± 6.7	± 2.7	± 5.6	± 3.1
Station 11	5.1	75.8	3.2	9.7	34.1	2.5	16.2	28.8	60.8	21.7	80.6	61.5
	±1.0	± 0.6	±0.8	±1.2	±16.4	± 0.9	± 8.7	±11.3	±17.5	± 0.6	± 9.5	±12.3

*The extralunar contribution is an upper limit.

found in lunar soils, because we still do not know which gases drove explosive volcanic eruptions on the Moon.)

Impact-produced heating also releases the solar-wind H that has been trapped in the outermost surfaces of lunar soil grains. This release produces an important additional effect. Hydrogen is a strong reducing agent, and it reacts with FeO in the impact melt to form micrometer-sized grains of native Fe metal (see sections 5.4 and 7.1.3). This is the mechanism proposed to produce the amounts of single-domain Fe particles that generate the ferromagnetic resonance observed in lunar soils (*Tsay et al.,* 1971; *Housley et al.,* 1973b). With increasing exposure to micrometeoroids, the amount of single-domain Fe in the soil increases, and so does the ferromagnetic intensity. The ratio of ferromagnetic resonance intensity (I_s) to the total Fe content (expressed as FeO, written as I_s/FeO), is an additional index of soil maturity (*Morris,* 1976).

7.3.2. Maturation by Ionizing Radiation

Ionizing radiation on the Moon comes in the form of atomic particles from the solar wind, solar flares, and extrasolar high-energy cosmic rays. Each source contains a wide variety of atomic particles, mostly protons accompanied by an approximately "cosmic" distribution of heavier atoms. Particles from different sources differ essentially in the magnitude of their energy distribution, which determines their depth of penetration into lunar materials. In addition to penetrating into lunar surface particles, the charged extralunar particles can ionize atoms of gas in the tenuous lunar atmosphere. The gas ions can then be accelerated by magnetic fields associated with the solar wind and implanted onto regolith grains (*Manka and Michel,* 1971). Table 7.9 (after *Walker,* 1980) summarizes the effects of ionizing radiation on lunar materials. A more detailed discussion of ionizing radiation can be found in section 3.11.

Solar wind. Solar-wind particles, which have an average energy of 1 keV/amu, penetrate to about 150 nm (0.15 μm) in lunar materials. The particles interact with the atoms in the target grains to create an amorphous outer layer in dielectric crystals, especially in grains of lunar plagioclase (Fig. 7.12; *Dran et al.,* 1970). These trapped solar-wind elements gradually accumulate in exposed grains. It is estimated that a saturation value for such trapped elements, balanced between implantation and loss by sputtering, is reached in approximately 100 yr (*Borg et al.,* 1980). The accumulation of solar-wind H is especially important because it enables the subsequent chemical reduction of FeO in lunar materials involved in micrometeoroid impacts. The accumulation of solar-wind elements, especially H, He, and other noble gases, is a measurable parameter of surface maturity, and more mature soils have higher contents of these elements.

A second effect of the solar wind is destructive; the ions act to sputter off the outer micrometer or so of exposed lunar soil particles (cf. section 7.1.5). This effect is most significant and easily observed on micrometer-sized particles, which are usually rounded in lunar soils.

Solar flares. Solar-flare particles, with energies from 10^4 to 10^8 eV/amu, penetrate on the order of a few millimeters to several centimeters into lunar rocks and soil particles. Their flux is much lower than that of solar-wind particles, and their accumulation is negligible by comparison. Being more energetic, however, heavy solar-wind particles (atomic number, Z >20) form trails of ionization damage in dielectric materials (crystals and glass). These damage trails can be etched into visible tracks (*particle tracks*) with suitable reagents (Fig. 7.12; *Fleischer et al.,* 1975). The density of the tracks provides an indicator of the exposure age of the sample, i.e., the length of time that it resided within a few centimeters of the surface. The track length can be used to estimate the composition (atomic number, Z) of the particles that produced them.

Cosmic rays. Cosmic-ray protons and neutrons are sufficiently energetic (>1 GeV/amu) that they penetrate into lunar materials to depths of about 1 m. These particles produce nuclear reactions, and the products of these reactions can be used to measure the incoming flux, the exposure age of the sample, and the depth of the sample in the regolith. In the laboratory, stable products, such as spallogenic noble gas isotopes and neutron-induced isotopes of Gd and Sm, can be measured by mass spectrometry. Radioactive products, such as the isotopes ^{26}Al and ^{53}Mn, can be measured by sensitive detectors. The cosmic-ray production curves for spallogenic isotopes as a function of penetration depth have been calculated by *Reedy and Arnold* (1972) and *Hohenberg et al.* (1978); the production curves for neutron-induced isotopes, with depth, have been calculated by *Lingenfelter et al.* (1972). If these cosmogenic isotopic profiles can be measured in the lunar regolith, then the experimentally-determined profiles can be used to calculate surface exposure ages from the measured production profiles. This approach is valid, however, only when the thickness of the regolith layer is at least a significant fraction of a meter.

Both solar flares and cosmic rays produce particle tracks in lunar soil grains. At depths of less than about 1 cm the lower-energy solar-flare particles dominate track production because the low-energy

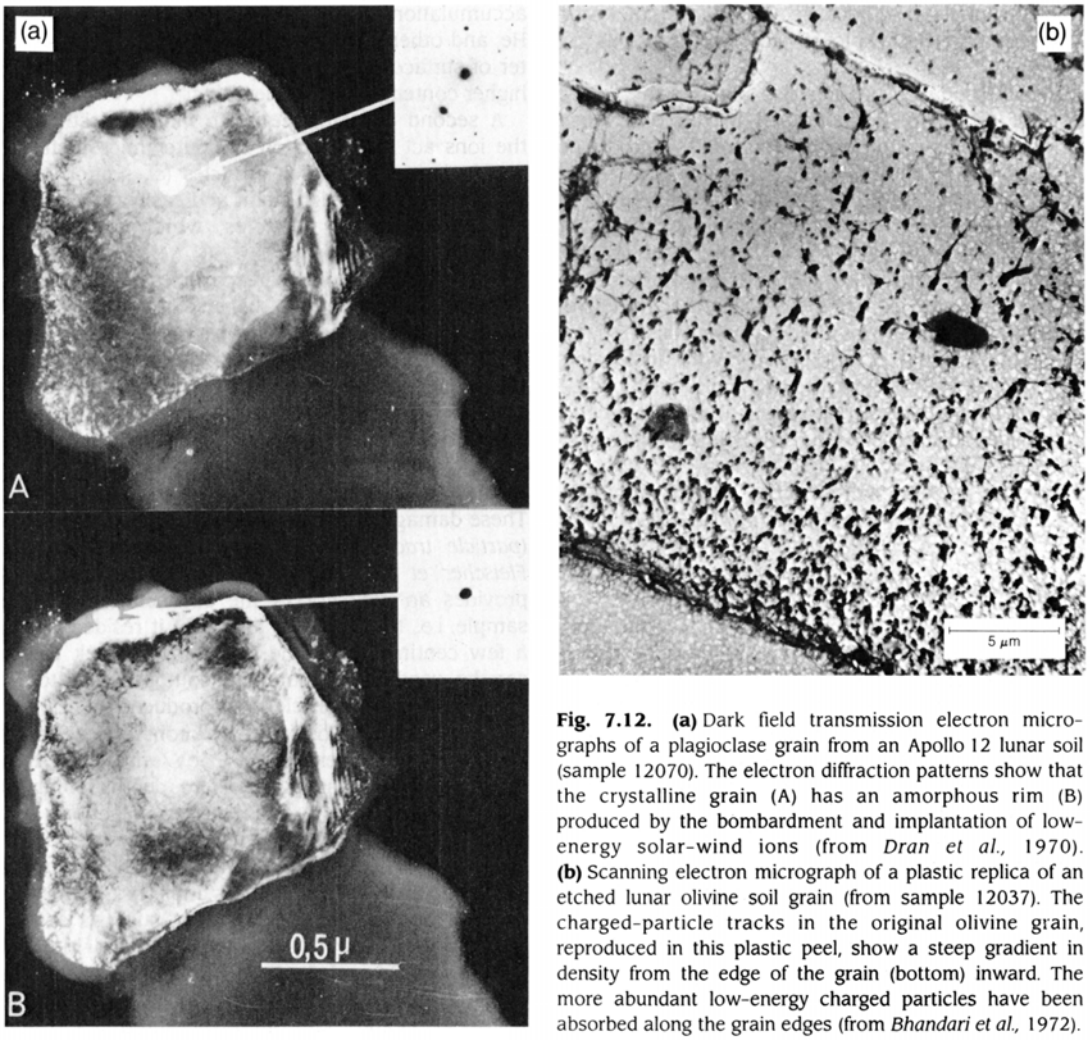

Fig. 7.12. **(a)** Dark field transmission electron micrographs of a plagioclase grain from an Apollo 12 lunar soil (sample 12070). The electron diffraction patterns show that the crystalline grain (A) has an amorphous rim (B) produced by the bombardment and implantation of low-energy solar-wind ions (from *Dran et al.,* 1970). **(b)** Scanning electron micrograph of a plastic replica of an etched lunar olivine soil grain (from sample 12037). The charged-particle tracks in the original olivine grain, reproduced in this plastic peel, show a steep gradient in density from the edge of the grain (bottom) inward. The more abundant low-energy charged particles have been absorbed along the grain edges (from *Bhandari et al.,* 1972).

cosmic-ray particles that would be stopped at these depths have been already modulated out of the solar system by solar magnetic fields. The production of particle tracks in lunar materials as a function of depth has been measured by a number of groups; results are shown in Fig. 7.13. The track production rates follow a negative power law that depends on depth, so that the production rate for tracks drops off rapidly with increasing depth. The quality of these measurements is reviewed by *Zinner* (1980), who concluded that the production curve of *Blanford et al.* (1975) (64455 in Fig. 7.13) is probably within a factor of 2 of the recent long-term flux.

Particle-track densities in individual grains can be used to measure the exposure age of the sample in which they are found. If a soil sample has a significant fraction of fresh grains, then these grains will have the minimum track density possible for any of the soil grains from the sample. If the depth at which the sample was collected can be determined or estimated, this measured minimum-track density can be used to calculate a maximum exposure age for the sample (*Crozaz et al.,* 1970). Lunar soil grains exposed within millimeters of the surface, i.e., to solar-flare particles, accumulate particle tracks rapidly, and in only 10^3 to 10^4 yr have track densities

in excess of $10^9/cm^2$. In sharp contrast, soil grains exposed deeper than about 1 cm (i.e., only to cosmic rays), will rarely have track densities in excess of $10^8/cm^2$. Consequently, mature soils or mature soil components, which have been exposed for longer periods of time and whose upper parts are relatively well-mixed, will have large numbers of grains with track densities $>10^9/cm^2$, while immature and submature soils or soil components will have large numbers of grains with track densities below $10^8/cm^2$. The percentage of soil grains with track densities greater than $10^9/cm^2$ is called the *track maturity index,* and it increases as the maturity of the soil increases.

7.3.3. Maturity Indices and Their Use

The physical processes caused by exposure of lunar regolith at or near the lunar surface (section 7.3.2) have been used to define a number of maturity indices: I_s/FeO, mean grain size, the

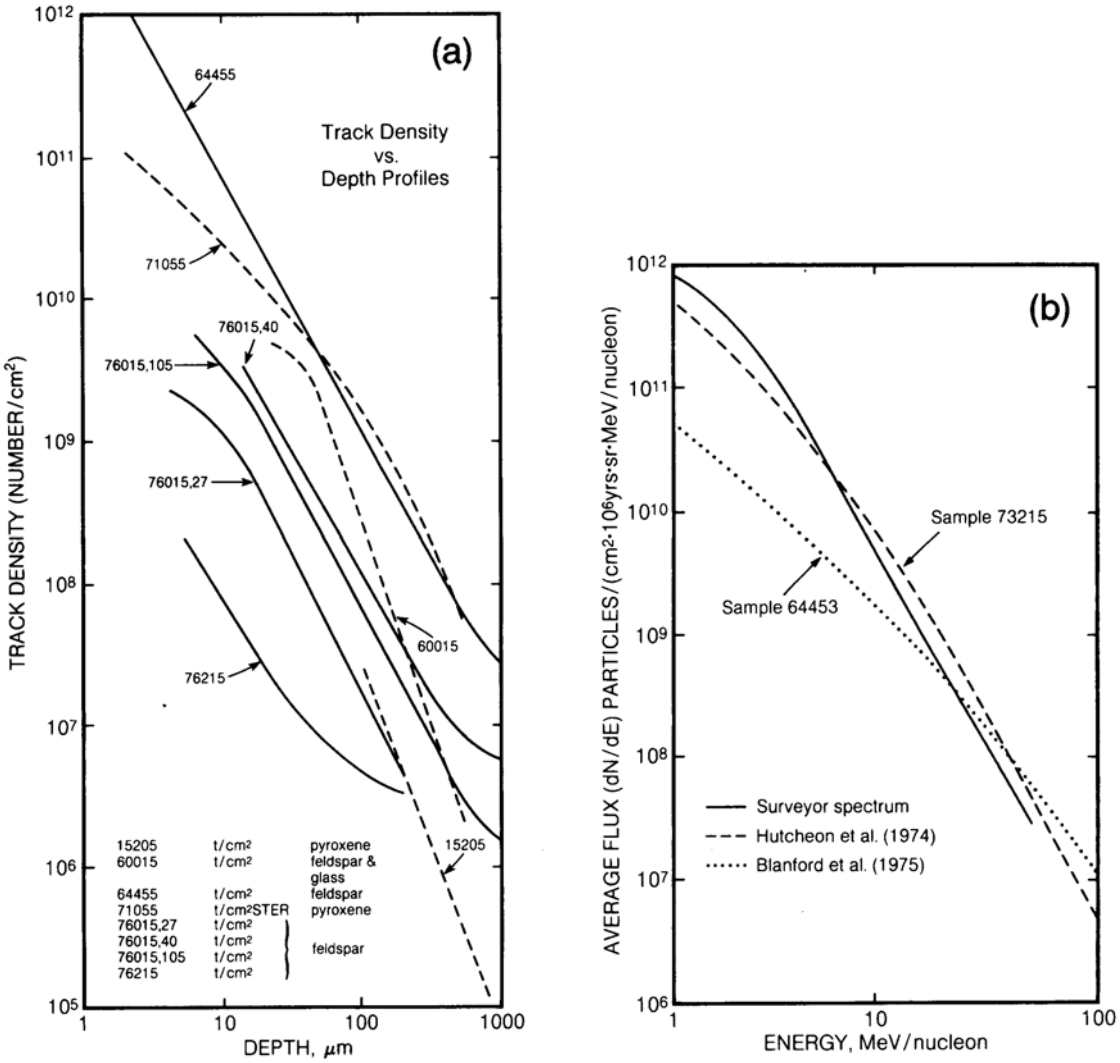

Fig. 7.13. (a) Profiles of solar-flare track densities as a function of depth, measured in single mineral and glass grains from several soil samples (*Zinner,* 1980). Track densities are given either as t/cm^2 or as t/cm^2-steradian, as indicated in the figure, depending on the original orientation of the soil grain. Different line types are only for clarity. **(b)** Energy-flux spectra for Fe-group solar flare particles, measured over 2.6 yr between 1967 and 1969 (Surveyor lunar lander spectrum) and from lunar rocks 64455 and 73215 (from *Zinner,* 1980).

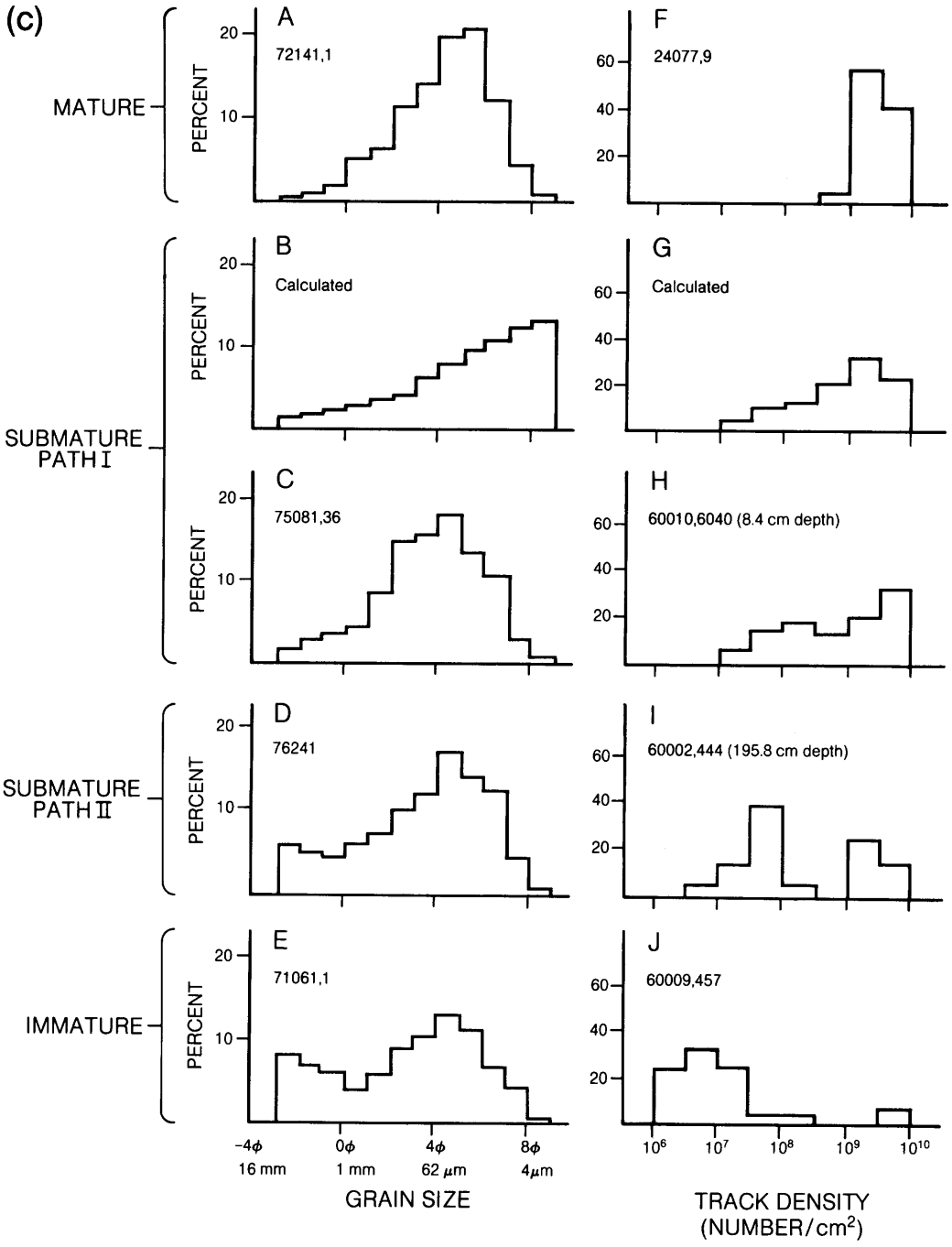

Fig. 7.13. (continued) **(c)** Histograms showing frequency distributions of grain sizes and track densities for lunar soils that show a range of maturities. Ordinates in percent. *Mature* soils (A and F) show a concentration of grain sizes and track densities into single peaks (*Blanford et al.,* 1979), while *immature soils* (E and J) show a wider, bimodal distribution. Two types of *submature soils* can be distinguished: those matured in place (path I; C and H), which show a single broad distribution, and those matured by mixing (path II; D and I) (*McKay et al.,* 1974), which show a bimodal distribution. Calculated distributions for submature path I soils (B and G) are from *Shoemaker* (1971) and *Duraud et al.* (1975).

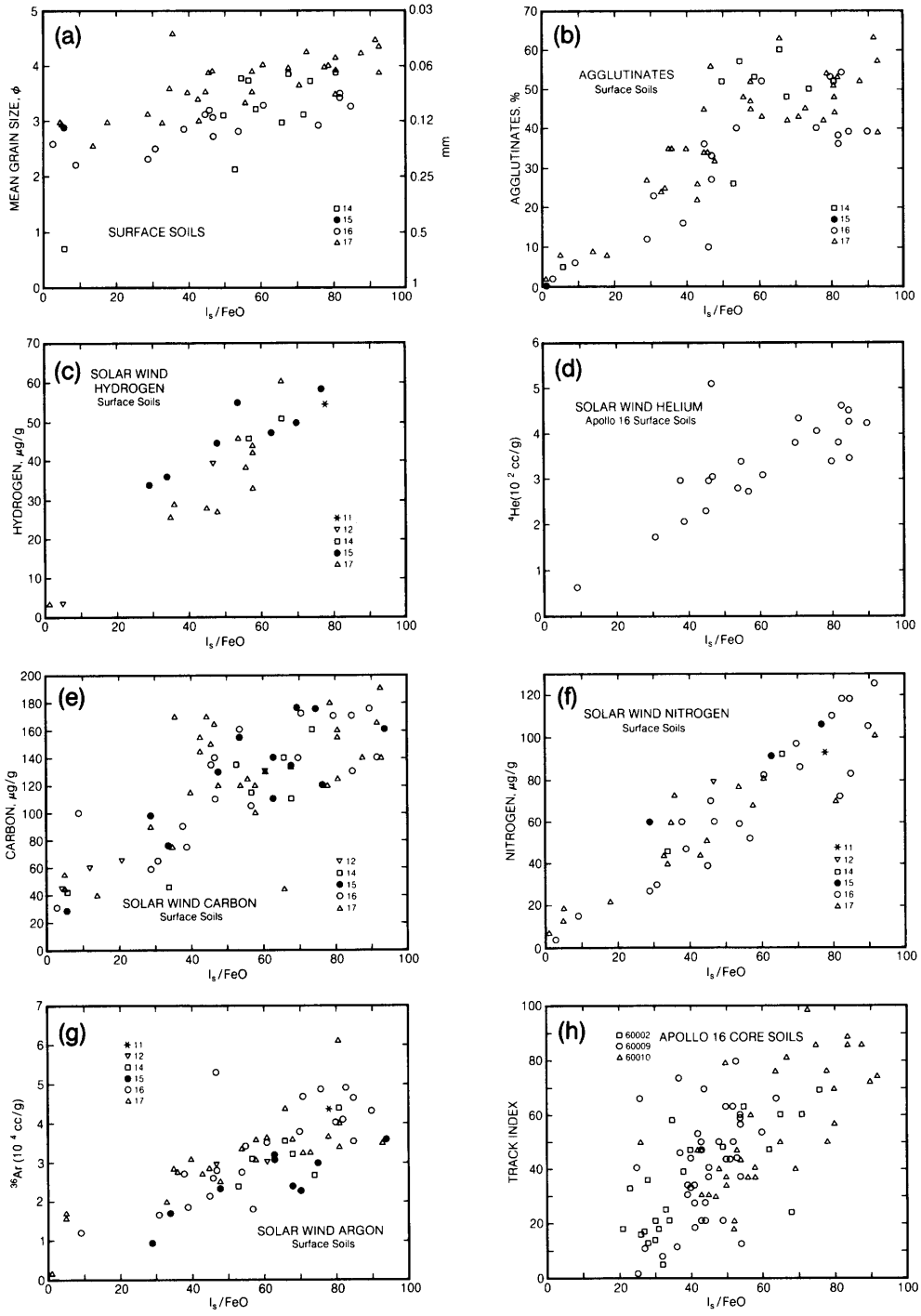

Fig. 7.14. Diagrams showing correlations between I_s/FeO and other maturity indices in lunar surface soils and core soil samples. **(a)** Mean grain size, in ϕ and mm; **(b)** percentages of petrographic agglutinates. Several solar-wind elements, including **(c)** H, **(d)** He, **(e)** C, **(f)** N, **(g)** Ar; and **(h)** the percentage of grains with track densities $>10^9/cm^2$. Data are from *Morris* (1976), except for **(c)** from E. K. Gibson (personal communication, 1985) and **(h)** from *Morris and Gose* (1976) and *Blanford et al.* (1979). Numbers for different symbols indicate different Apollo missions.

TABLE 7.13. Concentrations of metallic iron (in equivalent wt.%) contributed by three metal particle diameter ranges for 79 lunar soils (from *Morris,* 1980).

Soil	FeO (wt.%)	I_s/FeO (arb.) <250 μm	Equivalent wt.% Fe^0			Soil	FeO (wt.%)	I_s/FeO (arb.) <250 μm	Equivalent wt.% Fe^0		
			Fe^0_A	Fe^0_B	Fe^0_C				Fe^0_A	Fe^0_B	Fe^0_C
10084,853	15.8	78.0	0.34	0.61	0.81	67960,30	4.6	20.0	0.030	0.069	0.13
12001,7	16.8	56.0	0.28	0.47	0.67	69921,11	5.6	90.0	0.19	0.43	0.65
12003,11	15.4	57.0	0.22	0.37	0.55	70251,1	16.6	43.0	0.22	0.39	0.61
12024,46	14.6	30.0	0.14	0.27	0.49	70271,4	16.2	56.0	0.28	0.47	0.71
12030,122	14.3	14.0	0.072	0.11	0.31	70311,3	17.5	39.0	0.21	0.36	0.68
12033,45	14.2	4.6	0.022	0.13	0.27	71131,8	18.2	33.0	0.20	0.34	0.68
12037,23	17.3	21.0	0.13	0.22	0.34	71151,2	18.0	34.0	0.20	0.34	0.59
12042.24	16.8	61.0	0.32	0.54	0.69	71501,18	18.3	35.0	0.21	0.39	0.60
12044,12	15.7	57.0	0.27	0.45	0.69	72131,4	17..2	60.0	0.29	0.51	0.72
12070,104	16.5	47.0	0.24	0.40	0.64	72701,24	8.8	61.0	0.20	0.33	0.59
15041,34	14.3	94.0	0.41	0.61	0.78	72161,61	14.9	87.0	0.41	0.66	0.83
15071,19	16.4	52.0	0.27	0.40	0.54	72221,2	9.6	58.0	0.18	0.28	0.58
15091,34	11.6	74.0	0.28	0.42	0.57	72241,2	9.1	64.0	0.18	0.29	0.47
15101,179	11.6	70.0	0.27	0.40	0.61	72261,5	9.6	59.0	0.20	0.34	0.50
15211,56	11.8	54.0	0.25	0.37	0.56	72431,1	9.8	63.0	0.21	0.33	0.53
15221,36	11.5	63.0	0.25	0.38	0.55	73131,2	6.8	16.0	0.044	0.090	0.23
15231,51	11.6	71.0	0.27	0.40	0.51	73151,4	9.3	68.0	0.21	0.32	0.58
15251,56	12.0	75.0	0.27	0.40	0.60	73211,1	9.4	39.0	0.13	0.21	0.38
15271,115	12.2	63.0	0.29	0.43	0.54	74111,1	10.2	31.0	0.11	0.19	0.47
15301,120	14.0	53.0	0.24	0.36	0.62	74220	22.0	1.0	0.013	0.043	0.07
15401,14	16.6	5.6	0.044	0.083	0.18	76031,4	11.7	64.0	0.23	0.36	0.55
15431,17	11.9	39.0	0.14	0.23	0.35	76121,10	15.2	71.0	0.33	0.54	0.75
15471,18	16.4	34.0	0.21	0.33	0.47	76131,4	12.3	70.0	0.24	0.35	0.57
15501,41	16.6	51.0	0.28	0.45	0.58	76221,7	10.9	66.0	0.22	0.37	0.53
15531,48	20.2	27.0	0.16	0.27	0.31	77511,4	12.3	80.0	0.31	0.50	0.73
15601,103	19.2	29.0	0.21	0.34	0.44	78121,3	14.2	68.0	0.30	0.51	0.69
60601,9	5.5	85.0	0.14	0.27	0.57	78221,7	11.7	93.0	0.32	0.53	0.76
61141,57	5.3	56.0	0.096	0.18	0.66	78231,4	13.1	81.0	0.35	0.59	0.76
61121,12	4.9	9.2	0.018	0.059	0.29	78441,45	12.4	77.0	0.30	0.51	0.77
61241,14	5.4	47.0	0.087	0.20	0.45	78481,61	13.1	82.0	0.32	0.56	0.87
61501,103	5.6	53.0	0.10	0.20	0.60	79121,10	16.5	57.0	0.32	0.56	0.80
62231,3	5.1	91.0	0.16	0.29	0.58	79241,30	15.6	51.0	0.26	0.45	0.63
64501,11	5.2	61.0	0.10	0.18	0.50	79511,55	15.3	61.0	0.28	0.49	0.73
64801,35	5.2	71.0	0.15	0.28	0.56	24077,7	19.9	39.0	0.20	0.32	0.51
64811,84	5.6	54.0	0.11	0.23	0.58	24109,14	20.6	31.0	0.18	0.29	0.46
65701,8	5.7	106.0	0.21	0.39	0.73	24149,16	20.3	21.0	0.11	0.20	0.33
65901,104	5.8	99.0	0.18	0.33	0.71	24174,17	20.9	27.0	0.11	0.19	0.37
66031,8	5.5	102.0	0.17	0.32	0.65	24182,12	20.2	19.0	0.077	0.14	0.30
67461,103	4.3	25.0	0.037	0.065	0.13	24210,10	21.1	19.0	0.15	0.19	0.33
67511,11	4.2	8.8	0.012	0.024	0.076			Average	0.20	0.33	0.54
								Std. Dev.	0.10	0.15	0.18

The values of FeO and I_s/FeO were obtained from *Morris* (1978b). I_s/FeO was measured for the <250-μm size fraction. Diameter range of metallic iron particles: Fe^0_A = 40–330 Å; Fe^0_B = 40 – >330 Å; Fe^0_C = ~20 – >1000 Å.

percentage of grains with high track densities (>10^9/cm^2), agglutinate content, content of solar-wind elements, depletion of volatiles, and the presence and degree of isotopic mass fractionation.

Many of the maturity indices are of limited value for estimating soil maturity because, after a period of initial increase, they tend to saturate and become constant with time. For example, mean grain size will reach some equilibrium value as comminution is balanced by agglutinate formation. Similarly, the concentration of implanted solar-wind elements tends toward a saturation level at which implantation of new atoms is balanced by the removal of the particle surface—and the solar-wind atoms it contains—by sputtering.

However, the value of I_s/FeO appears to increase steadily with increasing maturity and shows no tendency to saturate with time (*Morris,* 1976).

Consequently, I_s/FeO has become widely used to establish a soil's maturity level, and the quantity has been measured for every lunar soil. These data are catalogued in the *Handbook of Lunar Soils* (*Morris et al.,* 1983).

Figure 7.14 shows typical correlation plots of I_s/FeO with other maturity indices; Table 7.13 gives numerical I_s/FeO values for a set of lunar soils. There is considerable scatter in these plots, indicating that determination of the maturity level of a soil should be based on more than one maturity index. For example, *McKay et al.* (1974) have effectively used grain size, sorting, and agglutinate content to define immature, submature, and mature soil groups at the Apollo 17 site (Fig. 7.15).

7.3.4. Regolith Processes and Maturity

Regolith turnover by meteoroid impacts does not simply take a volume of lunar soil with a given maturity and then expose or bury it; impacts also mix discrete volumes of soil together. This soil mixing is a complex process, but most measures of soil maturity make no distinction between soils matured *in situ* (i.e., which underwent very small-scale mixing) and those subjected to large-scale mixing. However, if soil mixing is sufficiently gross, and the mixed components have sufficiently different levels of maturity, then grain-size and track-density frequency distributions can demonstrate that a soil has been mixed. Submature soils can thus be distinguished on the basis of whether they matured by small-scale or large-scale mixing.

McKay et al. (1974) designated the two processes for producing submature soils as path I (matured *in situ* with only small-scale mixing) and path II (matured with large-scale mixing).

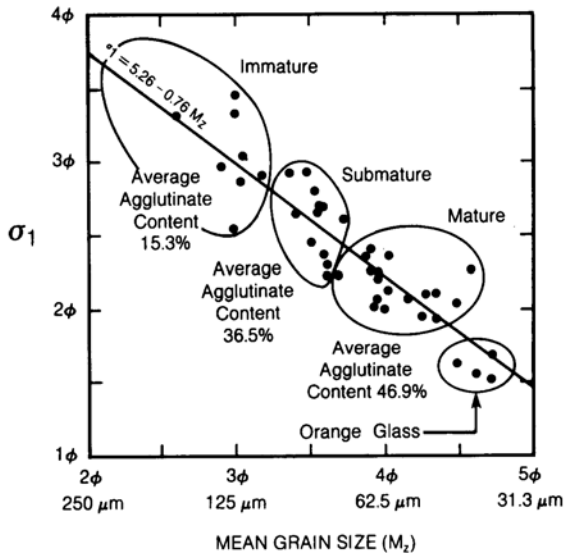

Fig. 7.15. Diagram showing the relationship between grain size, sorting, and agglutinate content for 42 Apollo 17 soils (*McKay et al.,* 1974). Mean grain size (M_z, abscissa) is shown in both millimeter and ϕ scales; smaller grain sizes are to the right. Sorting (ordinate) is expressed as the inclusive graphic standard deviation σ_1, in ϕ. Better-sorted soils are toward the bottom. The diagram shows that increasingly mature soils become progessively finer-grained, better-sorted, and composed of a greater proportion of agglutinates.

7.4. VARIATION OF SOILS WITH DEPTH: THE LUNAR CORE SAMPLES

7.4.1. General Characteristics of Lunar Regolith Core Samples

Core samples of the lunar regolith have provided the most dependable information about the evolution of the regolith and about its textural and structural complexities. Identification of individual soil layers within the core samples has been based mostly on discrete changes in grain size and particle proportions from layer to layer. Depths of regolith sampled by coring range from 10 cm (Apollo 11) to 298.6 cm (Apollo 17). At the time of this writing, about 85% of the cores have been studied. (See sections 2.2 and A2.1 for a description of cores and drive tubes.)

Core studies (and some observations of shallow trenches dug by Surveyor spacecraft and later by astronauts) indicate that the lunar regolith is made up of discrete layers of material ejected from both large and small impact craters. Within a single layer, the observed grain size is related to the depth of catering in the impact event, the ratio of bedrock to regolith in the excavated material, and the duration of subsequent exposure to micrometeoroid bombardment at the lunar surface. With a high percentage of bedrock in the ejecta layer, the material is coarsest grained; conversely, the finest-grained regoliths have a smaller bedrock component. The relationship between grain size and regolith thickness—that thicker regoliths have generally finer grain sizes—has been well-documented by *McKay et al.* (1980).

Throughout a section of multilayered regolith, however, the grain size varies randomly from layer to layer. Exposure to micrometeoroid bombardment at the lunar surface further comminutes fragments in the regolith, but also builds up an increasing volume of agglutinates with time. Eventually, a

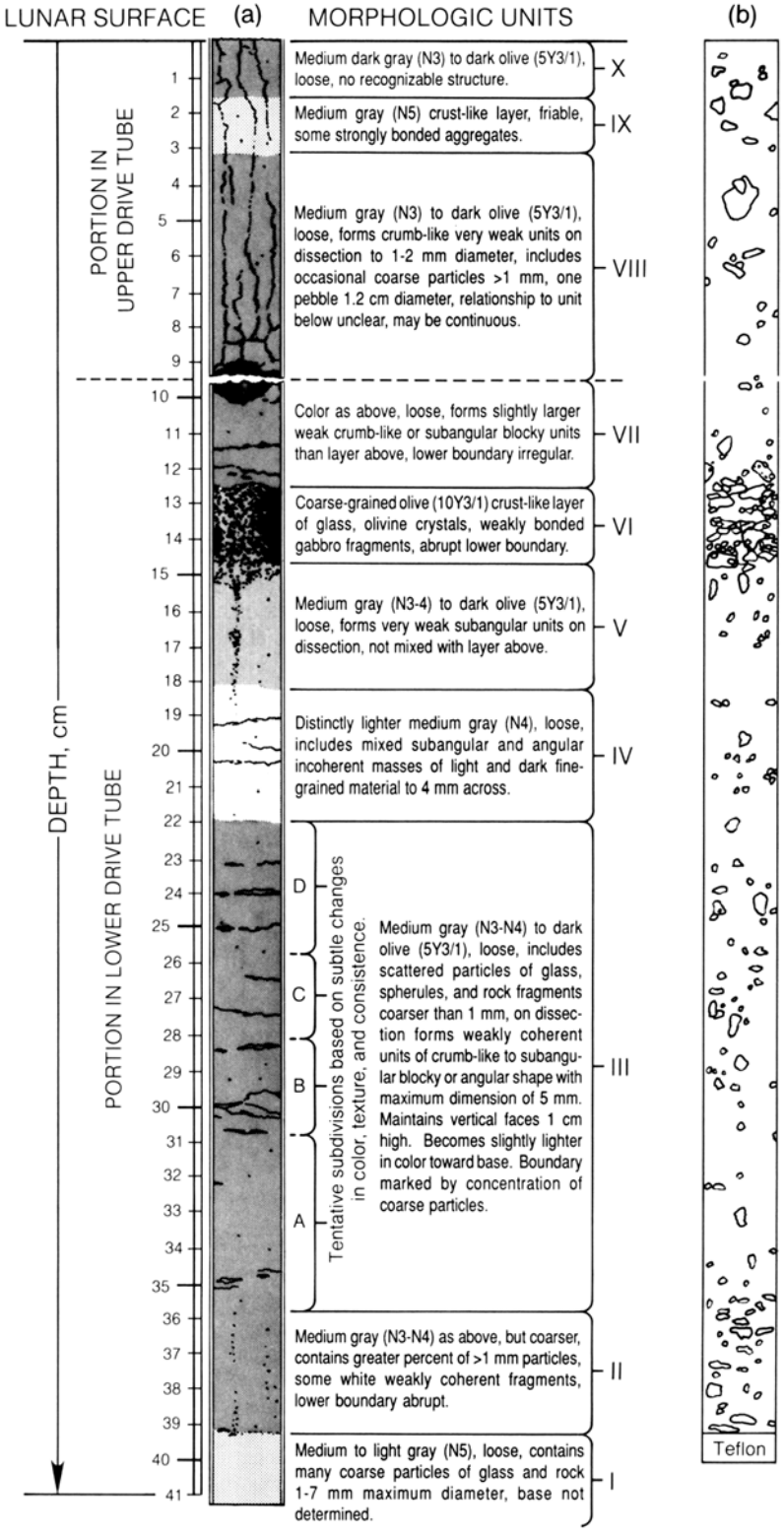

Fig. 7.16. Drawing of the Apollo 12 double drive-tube core (samples 12025-12028). **(a)** Within the core, 10 discrete layers have been identified, mostly on the basis of sharp changes in grain size and grading between adjacent layers (stratigraphic diagram by R. Fryxell; *Fryxell and Heiken,* 1974). Color designations are according to the Munsell standard. **(b)** Location of coarser lithic fragments.

steady-state grain size develops as the agglutinate content increases and balances comminution (*Morris,* 1976; Fig. 7.14a,b).

In studying the core samples, similar grain-size measurement techniques have been used, but different workers have preferred to use slightly different statistical parameters to describe and compare the grain sizes of individual layers. Some investigators have preferred to designate the average grain size by the *median* (half the particles by weight are coarser than the median sizes, and half are finer). Others have used the *mean,* a quantity calculated or determined graphically by measuring the percentage of particles corresponding to three points on a cumulative size-frequency curve, summing the weights at 16%, 50%, and 84% and dividing by three (*Folk,* 1968). These parameters are discussed in more detail in section 9.1.1.

The first cores from lunar regolith were collected at the Apollo 11 site, using hollow drive tubes that were hammered into the soil. These drive tubes were short (about 30 cm) and the incomplete sections they secured gave little indication of the textural complexity that is characteristic of the regolith sampled more deeply at other Apollo and Luna landing sites. A double drive-tube core sample (sample 12025/12028), collected at the Apollo 12 site on the rim of a 10-m-diameter crater, provided the first evidence that lunar regolith is layered. This 42-cm regolith sample is composed of ten discrete layers; the median grain sizes of the soils from the individual layers range from 61 μm to 595 μm (Fig. 7.16).

A more complete view of the textural characteristics of the regolith, layer by layer, has been obtained from analyses of regoliths sampled by drilling at the Apollo 15, 16, and 17 sites. The 236-cm-deep section sampled by a core drill at the Apollo 15 site (no. 15001–15006) consists of 42 distinct textural units, with median grain sizes from 44 μm to 89 μm; all the layers are poorly sorted (*Heiken et al.,* 1973, 1976). Most of the samples from these layers form a tight grouping around a median grain size of 50 μm.

At the same Apollo 15 landing site, a shorter drive tube, inserted only 20 m from the edge of Hadley Rille, penetrated the upper 60 cm of a 1-m-thick immature regolith (lunar core sample 15010/11; *McKay et al.,* 1980). Because of this sample's close proximity to bedrock, together with the process of continuous mass wasting of regolith material into the rille, the regolith at this location is coarser grained than regolith samples collected elsewhere; it has an average mean grain size (average of several samples) of *85* μm (Fig. 7.17) (*McKay et al.,* 1980 used mean rather than median grain size).

At the Apollo 16 site on the Cayley Plains, a 221-cm-thick section of highland regolith was sampled by drilling (*Allton and Waltz,* 1980). In this core, three major subdivisions were recognized by *Meyer and McCallister* (1977) and 46 textural units by *Duke and Nagle* (1974). Only samples from the individual layers in the upper 20 cm of the core have been sieved; median grain sizes for the <1-mm fraction range from 56 to 72 μm, and all are poorly sorted. A systematic study of changes in grain size with depth (to 65 cm) was made by *McKay et al.* (1977) for another Apollo 16 sample, core 60009/60010. In this core, there is a general increase in mean grain size with depth, with the exception of a layer at the bottom of the core, from 85 μm at the surface to 200 μm at a depth of 55 cm (Fig. 7.18). The upper 12 cm of the core shows the highest degree of *in situ* maturation and reworking, and it is the finest-grained unit sampled in this regolith section.

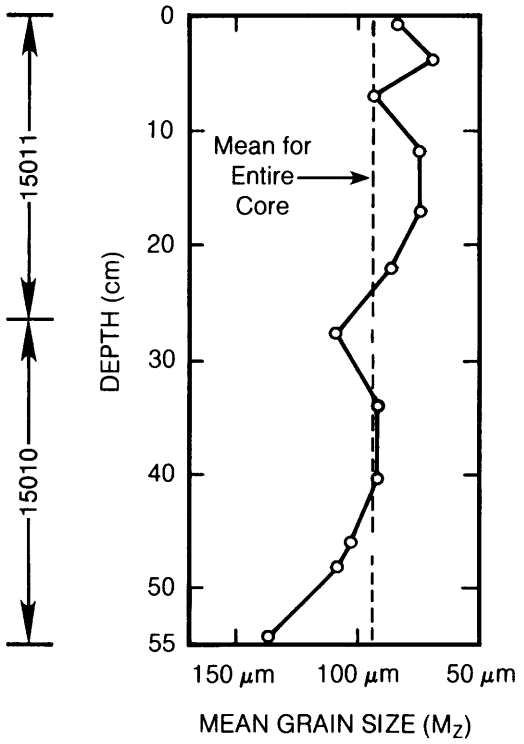

Fig. 7.17. Plot of data from the Apollo 15 drive-tube core 15010/11, showing sample locations and mean grain sizes for individual samples. This core was collected close to the rim of Hadley Rille, where regolith is thin and immature, as indicated by the relatively large mean grain size (about 100 μm) for all portions of the core.

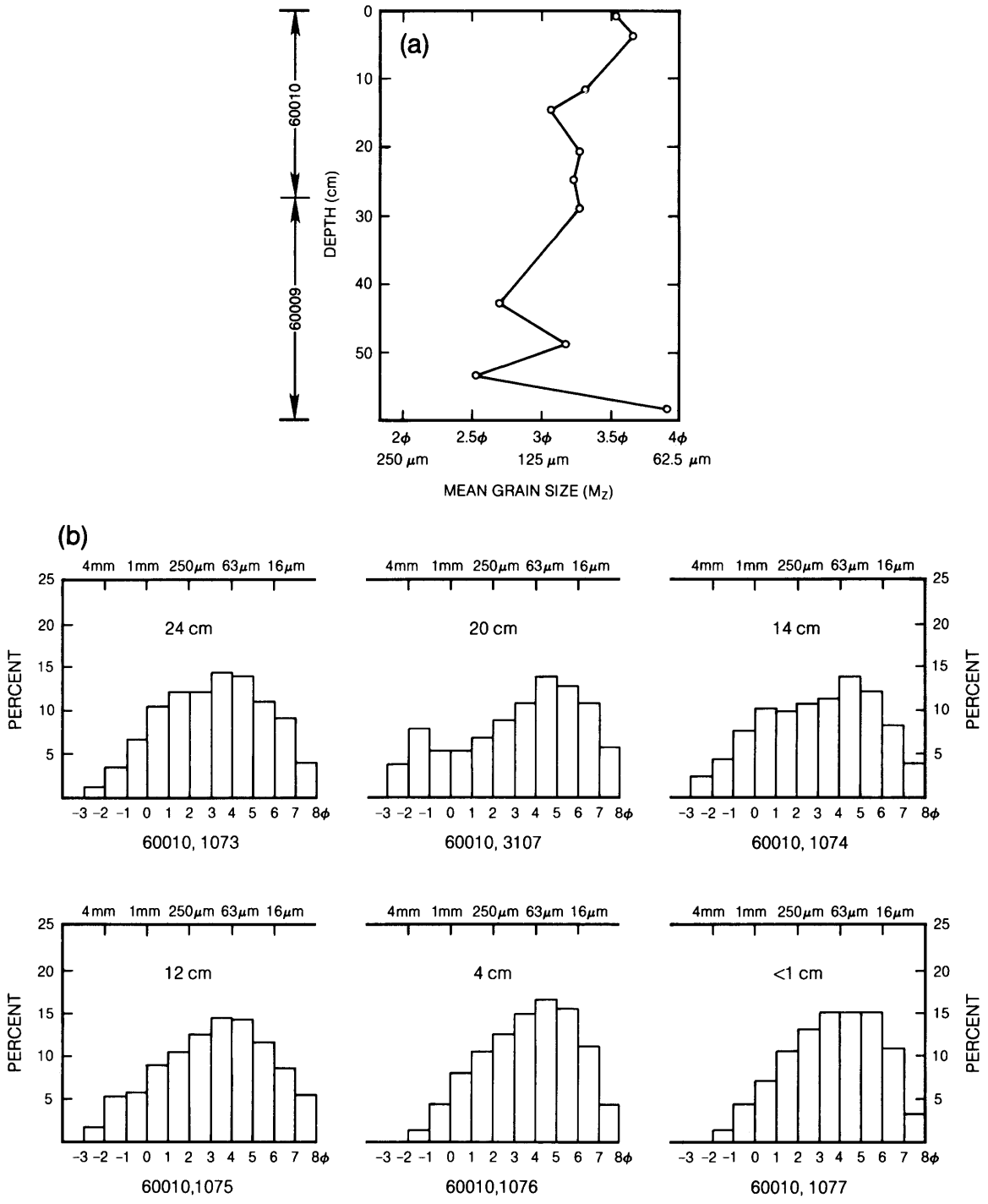

Fig. 7.18. Variation with depth of grain size characteristics of lunar soil samples from the Apollo 16 core 60009/10. **(a)** Variation in mean grain size as a function of depth in the core. **(b)** Histograms of grain-size distribution for six soil samples (depths given in centimeters) from core 60010 **(a)**. The samples show a gradual increase in mean grain size with increasing depth, except at the bottom of the core, where a new layer may have been penetrated. The upper core layers tend to be finer-grained and slightly better sorted than the lower ones.

The showpiece of regolith core samples was collected by deep drilling at the Apollo 17 site. Sampling a total regolith thickness of 284 cm, drill core 70009–70002 was collected between two 650-m-diameter craters. *Vaniman et al.* (1979) identified five stratigraphic units, and *Taylor et al.* (1979) identified eight stratigraphic units in this core, based upon textural (grain size) and petrographic differences. Detailed grain-size analyses of the individual depositional units have not been completed; however, maturity indices such as I_s/FeO (*Morris et al.,* 1979) and core descriptions indicate that a wide range of grain size and sorting is present from layer to layer (*Duke and Nagle,* 1974).

A unique core sample (sample no. 74001/2) was collected on the rim of an impact crater (Shorty Crater) at the Apollo 17 site; it sampled not a true lunar soil, but a deposit of volcanic ash (the "orange and black soils") in the overturned rim flap of the impact crater. This deposit has a mean grain size of 40 μm. Variations of grain size (Fig. 7.19; *McKay et al.,* 1977) and sorting appear to have been controlled by eruption processes and do not reflect comminution by meteoroid impact processes after the material was deposited.

In a study of the Luna 24 regolith sample from Mare Crisium, *McKay et al.* (1978b) determined that the individual layers are composed of mixtures of

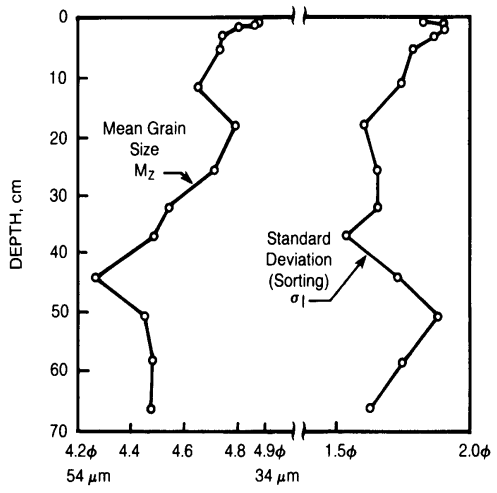

Fig. 7.19. Variations of mean grain size (M_z) and sorting (σ_1) within Apollo 17 core 74001/2, the orange "soil" from the rim of Shorty Crater. The deposit is not a lunar soil, but a pyroclastic (volcanic ash) deposit, and the grain size and sorting reflect eruption processes rather than maturation processes within a lunar soil (*McKay et al.,* 1974).

coarse-grained, immature components, together with finer-grained, more mature components. The grain-size distributions are thus bimodal, with peaks at 1 mm and 100 μm (Fig. 7.20). Within the regolith sampled, there appears to be a general decrease in mean grain size with depth, from 139 μm at the surface to *72* μm at an approximate depth (distance along the core tube) of 200 cm. This result is the reverse of the trend observed in the Apollo 16 core samples.

In summary, the analysis of regolith core samples has shown that regolith properties vary in a complex and not entirely predictable way with depth. A trend to coarser-grained samples with depth is present in some of the cores (e.g., Apollo 16), but there are exceptions (e.g., Luna 24).

7.4.2. Variations with Depth in Regolith Core Samples

Drilling of the Earth has often supplied the valuable third dimension needed to interpret its history and structural complexity. Even though the mechanism (meteoroid impact) that produces most of the layered deposits on the Moon is not a major process on Earth, core samples of the lunar regolith have the same potential to provide a chronology of the depositional and erosional events that have been responsible for the Moon's formation.

Cores have been retrieved from seven landing sites on the Moon; the deepest core reached a depth of 298.6 cm. Not all of these cores have yet been studied (Table 7.14), but most have been examined for variations in physical, chemical, and geologic properties with depth. These variations have been used to identify discrete layers (strata) and to infer maturation rates.

Unfortunately, despite the detailed study of the Apollo cores, it has not been possible to identify any single layer as ejecta from a known impact crater at the landing site. A tenuous correlation has been made at the Apollo 17 site between Camelot Crater and a coarse-grained, immature layer in the drill core.

Study of the lunar cores has confirmed that our general understanding of cratering mechanics and regolith formation seems to be correct. However, we still do not completely understand the interconnections of different stratigraphic features, such as grain size, sorting, the presence or absence of graded bedding, and the identification of former surface horizons.

A wide range of stratigraphic data have been measured in the cores: visual color and texture, bulk chemistry, petrography, various maturity indices (section 7.3), the amounts of cosmogenic nuclides and particle tracks (which can be related to exposure

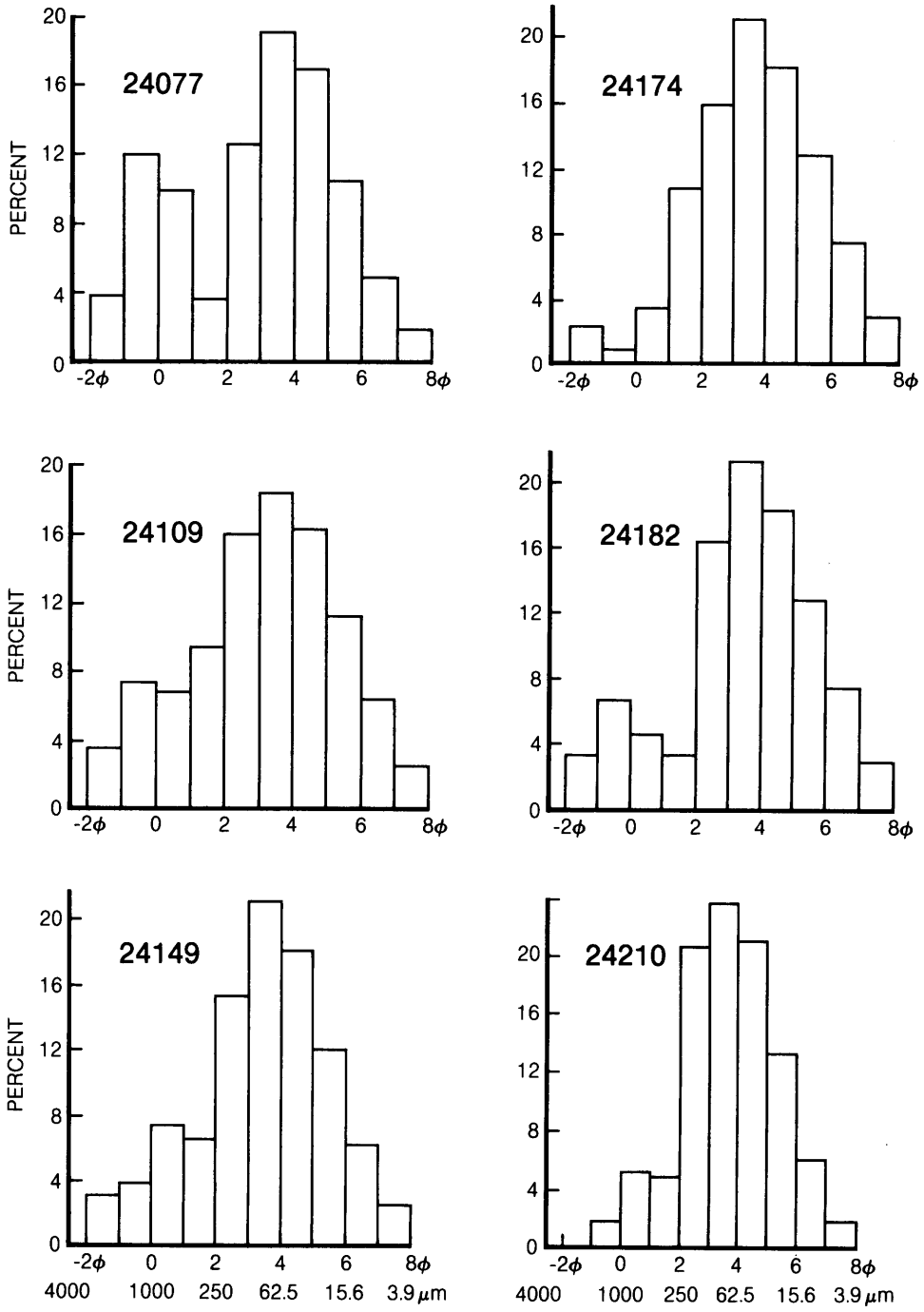

Fig. 7.20. Histograms of grain-size distributions for Luna 24 core samples (*McKay et al.,* 1978b). The grain-size distributions are generally bimodal, with peaks at 1 mm and 100 μm. Approximate sample depths: 24077 (10 cm), 24109 (110 cm), 24149 (150 cm), 24174 (175 cm), 24182 (180 cm), and 24210 (220 cm). There is a general increase in mean grain size with depth.

TABLE 7.14. Core samples collected by the Apollo missions and current status of investigation.

Core Number	Station	Landmark	Diameter and Type	Approximate Dissection Date	Depth (cm)	Dissection Length (cm)	Bulk Density (g/cm^3)	Peel	Epoxy Impreg-nation	Thin Section	Spectral Reflec-tance	Comments
10004	LM		2 cm Drive	3/78	<32	13.5	1.59	N	N	N	N	
10005	LM		2 cm Drive	3/78	>25	10.5	1.71	N	N	N	N	
12025		Halo Crater	2 cm Drive	12/69	*	9.5	1.98	N	N	N	N	Upper tube - paired with 12028
12026	LM		2 cm Drive	11/69	37	19.3	1.74	N	N	N	N	
12027		Sharp Crater	2 cm Drive	1/80	~37	17.0	—	Y	Y	Y	Y	
12028		Halo Crater	2 cm Drive	12/69	9.5*	31.6	1.96	N	N	N	N	Lower tube - paired with 12025
14210	A	Weird Crater	2 cm Drive	1/79	~64	32	1.75	Y	Y	Y	Y	Lower tube - paired with 14211
14211	A	Weird Crater	2 cm Drive	11/78		7.7	1.73	Y	Y	Y	Y	Upper tube - paired with 14210
14220	G	Triplet	2 cm Drive	5/79	<36	16.0	1.60	Y	Y	Y	Y	
14230	G	Triplet/Cone	2 cm Drive	7/71	45	12.5	—	Y	Y	N	N	Core driven twice
15001	8		2 cm Drill	4/72	236	36.9	1.93	Y	Y	Y	N	6 of 6
15002	8		2 cm Drill	1/72		39.2	1.64	Y	Y	Y	N	5 of 6
15003	8		2 cm Drill	8/72		39.3	1.74	Y	Y	Y	N	4 of 6
15004	8		2 cm Drill	3/72		40.1	1.74	Y	Y	N	N	3 of 6
15005	8		2 cm Drill	1/72		41.0	1.78	Y	Y	N	N	2 of 6
15006	8		2 cm Drill	4/72		40.7	1.58	Y	Y	N	N	1 of 6
15007	2	St George Crater	4 cm Drive	10/80	70.1	34.1	1.69	Y	Y	Y	N	Lower tube - paired with 15008
15008	2	St George Crater	4 cm Drive	4/80		23.1	1.36	Y	Y	Y	Y	Upper tube - paired with 15007
15009	6	Appenine Front	4 cm Drive	12/87	34.6	29.3	1.30	Y	Y	Y	N	
15010	9A	Hadley Rille	4 cm Drive	9/78	67.6	29.9	1.91	Y	Y	Y	N	Lower tube - paired with 15011
15011	9A	Hadley Rille	4 cm Drive	2/79		26.4	1.69	Y	Y	Y	N	Upper tube - paired with 15010
60001	LM		2 cm Drill	5/72	223	5.5	1.67	N	N	N	N	7 of 7
60002	LM		2 cm Drill	7/74		35.8	1.81	Y	Y	Y	N	6 of 7
60003	LM		2 cm Drill	8/76		39.5	1.67	Y	Y	Y	N	5 of 7
60004	LM		2 cm Drill	11/72		38.3	1.62	Y	Y	Y	N	4 of 7
60005	LM		2 cm Drill	11/74		14.6	1.62	N	N	N	N	3 of 7
60006	LM		2 cm Drill	10/72		32.0	1.58	Y	Y	Y	N	2 of 7
60007	LM		2 cm Drill	2/74		22.4	1.44	Y	Y	Y	N	1 of 7
60009	LM		4 cm Drive	6/76	71	31.5	1.72	Y	Y	Y	N	Lower tube - paired with 60010
60010	LM		4 cm Drive	12/76		27.3	1.47	Y	Y	Y	N	Upper tube - paired with 60009
60013	LM		4 cm Drive	Unopened	70.5	—	1.63	N	N	N	N	Lower tube - paired with 60014
60014	LM		4 cm Drive	Unopened		—	1.48	N	N	N	N	Upper tube - paired with 60013
64001	4	Stone Mountain	4 cm Drive	7/81	65.5	34.1	1.66	Y	Y	Y	N	Lower tube - paired with 64002
64002	4	Stone Mountain	4 cm Drive	7/81		26.4	1.40	Y	Y	Y	N	Upper tube - paired with 64001

TABLE 7.14. (continued).

Core Number	Station	Landmark	Diameter and Type	Approximate Dissection Date	Depth (cm)	Dissection Length (cm)	Bulk Density (g/cm^3)	Peel	Epoxy Impreg-nation	Thin Section	Spectral Reflec-tance	Comments
68001	8	South Ray Crater	4 cm Drive	Unopened	68.6	—	1.80	N	N	N	N	Lower tube - paired with 68002
68002	8	South Ray Crater	4 cm Drive	Unopened		—	1.59	N	N	N	N	Upper tube - paired with 68001
69001	9	South Ray Crater	4 cm Drive	Unopened	27.5	—	—	N	N	N	N	
70001	LM	Camelot Crater	2 cm Drill	1/73	~300	5.5	1.66	N	N	N	N	9 of 9
70002	LM	Camelot Crater	2 cm Drill	2/77		34.5	1.84	Y	Y	Y	N	8 of 9
70003	LM	Camelot Crater	2 cm Drill	3/78		39.5	1.84	Y	Y	Y	N	7 of 9
70004	LM	Camelot Crater	2 cm Drill	4/76		39.2	1.86	Y	Y	Y	N	6 of 9
70005	LM	Camelot Crater	2 cm Drill	8/77		40.3	1.83	Y	Y	Y	N	5 of 9
70006	LM	Camelot Crater	2 cm Drill	5/77		38.0	1.85	Y	Y	Y	N	4 of 9
70007	LM	Camelot Crater	2 cm Drill	10/75		30.5	1.80	Y	Y	Y	N	3 of 9
70008	LM	Camelot Crater	2 cm Drill	3/73		37.8	2.07	Y	Y	Y	N	2 of 9
70009	LM	Camelot Crater	2 cm Drill	5/75		25.1	1.75	Y	Y	Y	N	1 of 9
70012	LM		4 cm Drive	Unopened	28	—	1.77	N	N	N	N	
73001	3	Lara Crater	4 cm Drive	Unopened	70.6	—	1.73	N	N	N	N	Lower tube - paired with 73002
73002	3	Lara Crater	4 cm Drive	Unopened		—	1.60	N	N	N	N	Upper tube - paired with 73001
74001	4	Shorty Crater	4 cm Drive	1/77	71	34.3	2.29	Y	Y	Y	N	Lower tube - paired with 74002
74002	4	Shorty Crater	4 cm Drive	1/77		32.0	2.04	Y	Y	Y	Y	Upper tube - paired with 74001
76001	6	North Massif	4 cm Drive	10/78	37.1	31.4	1.57	Y	Y	Y	Y	
79001	9	Van Serg Crater	4 cm Drive	4/87	71	29.3	1.74	Y	Y	Y	N	Lower tube - paired with 79002
79002	9	Van Serg Crater	4 cm Drive	10/86		17.4	1.67	Y	Y	Y	N	Upper tube - paired with 79001

A *peel* is prepared by pouring a thin coating of epoxy onto a flat, dissected surface of the core. See *Fryxell and Heiken* (1974) for a description of the technique.

* 12025 and 12028 were a double drive tube.

ages), and their variations with depth. The most intensively studied cores are the Apollo 15 deep drill core (15001–15006), the Apollo 16 double drive tube 60009/60010, and the Apollo 17 deep drill core (70001–70009). The results obtained for these cores are summarized below.

Petrographic variations. One of the simplest and most valuable techniques for understanding the nature and history of a section of regolith is to determine the variations, with depth, of the relative amounts of the different *petrographic components* of the lunar soil, i.e., the particles that can be identified using an optical (petrographic) microscope or a scanning electron microscope. These components are principally of two kinds: (1) those derived from bedrock, such as rock and mineral fragments; and (2) those produced as the result of exposure at the lunar surface—agglutinates, regolith breccias, and impact-produced glasses (sections 7.1 and 7.3). Petrographic variations with depth have helped to identify different layers in the lunar regolith at every station where a core has been collected. In particular, abrupt changes in the petrographic components have made it possible to locate the boundaries between discrete layers. Where such boundaries also coincide with breaks in the chemical and maturity profiles, a significant break in the history of regolith development may be inferred.

Agglutinates are a petrographic component formed during surface exposure, and the variation of agglutinate abundances in all lunar cores closely follows the profiles of other maturity indexes. This effect is seen in all lunar cores; an example is the covariance seen in the depth profiles of I_s/FeO and agglutinate content in the Apollo 16 core 60009/60010 (Fig. 7.22a; *McKay et al.,* 1977).

The variation of other petrographic constituents—rock and mineral fragments—with depth in the lunar regolith depends essentially on the extent to which these bedrock-derived materials are introduced from both local and distant bedrock, and especially on the relative contributions of highland and mare sources (Fig. 7.21). As shown above (see also *Papike et al.,* 1982) it has not proved possible to correlate different stratigraphic layers, sampled by coring and identified on the basis of the variety of rock fragments, over any distance on the Moon. Therefore, the petrographic variations of the lunar regolith with depth can only be understood in terms of the mixing together of different lithologic components.

Two of the Apollo 16 cores have been studied in considerable detail. *McKay et al.* (1977) showed that the content of mineral and rock fragments in core 60009/60010 can be successfully modeled by mixtures of nearly pure anorthositic plagioclase feldspar and crystalline breccias (metamorphosed breccia plus poikilitic breccia) (Fig. 7.22c), with modification by subsequent maturation. In a study of the core 64001/64002, *Houck* (1982b) and *Basu and McKay* (1984) showed that a more complex situation existed. These cores contain a significant amount of mare basalt fragments. Although their abundance is low (mare basalts being exotic to the Apollo 16 site), there is a positive correlation between mare basalt fragments and monomineralic pyroxene fragments that may have been derived from the mare basalts (Fig. 7.23). The variation of other constituents, such as monomineralic plagioclase grains, crystalline-matrix breccias, and glass show negative correlations with the exotic mare basalts, which is consistent with mixing of local components (anorthosites and breccias) and exotic components (mare basalts). In a separate chemical investigation of this core, *Korotev et al.* (1984) discovered the presence of a mafic (basaltic) component at depths of 5.5 cm and 42 cm. *Basu and McKay* (1984) suggest that this mafic component is probably present as regolith breccias rather than as fragments of mare basalt bedrock.

Another very-well-studied core is the Apollo 17 deep drill core 70001–70009, which sampled a 298-cm-thick section of regolith and is the deepest core from the Moon. Detailed petrographic and mineral chemistry investigations are reported by *Vaniman and Papike* (1977a,b), *Vaniman et al.* (1979), and *Taylor et al.* (1979). These studies show that the core is composed of several stratigraphic units, each of which had a complex history of mixing and emplacement. The conclusion that at least three different rock types contributed pyroxene crystals to these soils in various proportions (*Vaniman et al.,* 1979) indicates both the power of petrographic techniques and the complexity of regolith formation.

Chemical variations. Because the lunar regolith is a mechanical mixture of several kinds of broken and melted rocks, variations in the chemical composition of the regolith with depth also provide a record of the influx and mixing of these materials through time. The chemical variations go in tandem with petrologic variations, but they have the advantage of including data from the fine-grained soil fractions that cannot be examined with petrographic methods. Variations in trace-element abundances also record the input of different parent rocks and the mixing process.

Analyses of 36 soil samples from various depths of the Apollo 16 core 60009/60010 by *Ali and Ehmann* (1977) show that Al and Ca dominate over Mg and Fe, reflecting the dominance of plagioclase feldspar over such mafic minerals as olivine and pyroxene. Although Mg and Fe are lower in abundance, there is a weak positive correlation between

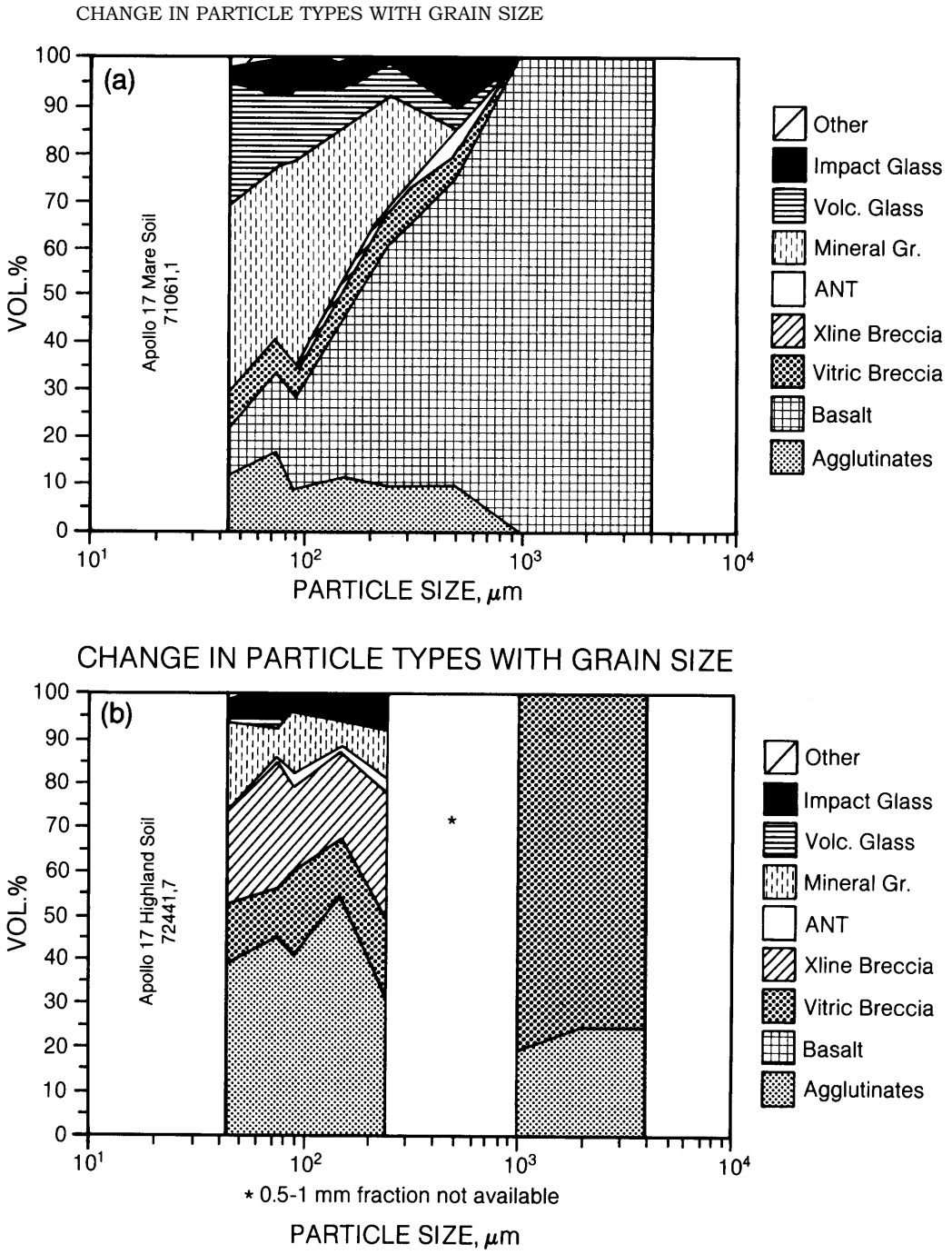

Fig. 7.21. Diagrams showing variations between grain size and relative percentages of different particle types in two Apollo 17 surface soils, **(a)** sample 71061 (mare surface) and **(b)** sample 72441 (highland surface). The two soils show wide variations in the amount of different particles (agglutinates, breccias, basalt and anorthosite fragments, and mineral and glass fragments) present in different grain-size fractions. The main differences reflect the different bedrock sources (mare basalts and highland rocks, respectively) from which the two soils have been derived (Xline = crystalline; ANT = anorthosite-norite-troctolite rock; gr = grain; volc = volcanic).

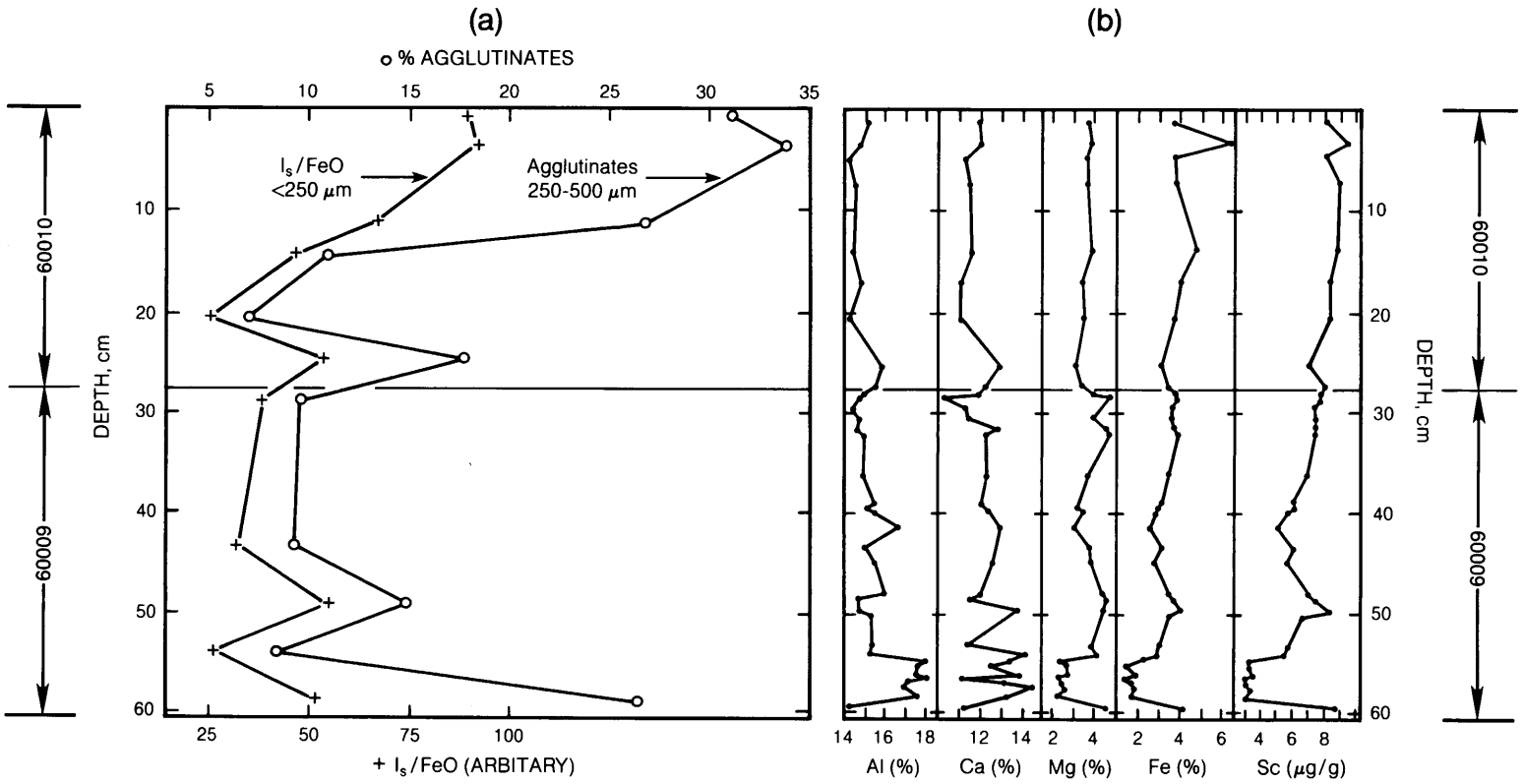

Fig. 7.22. (a) Variation with depth (in centimeters) of two maturity indices: I_s/FeO in the <250-μm size fraction, and agglutinate abundances in the 250–500-μm size fraction of the Apollo *16* drive core *60009/10* (*McKay et al.,* 1977). The two indices correlate closely, despite the irregular variations in both throughout the core. Note the mature zone in the upper 15 cm of the core. **(b)** Variations in chemical composition, plotted for Al, Ca, Mg, Fe, and Sc as a function of depth in the Apollo 16 drive core 60009/10 (from *Ali and Ehmann,* 1977). The vertical scales give depth in centimeters. Significant chemical variations occur over depths of only a few centimeters, especially in the lower part of the core.

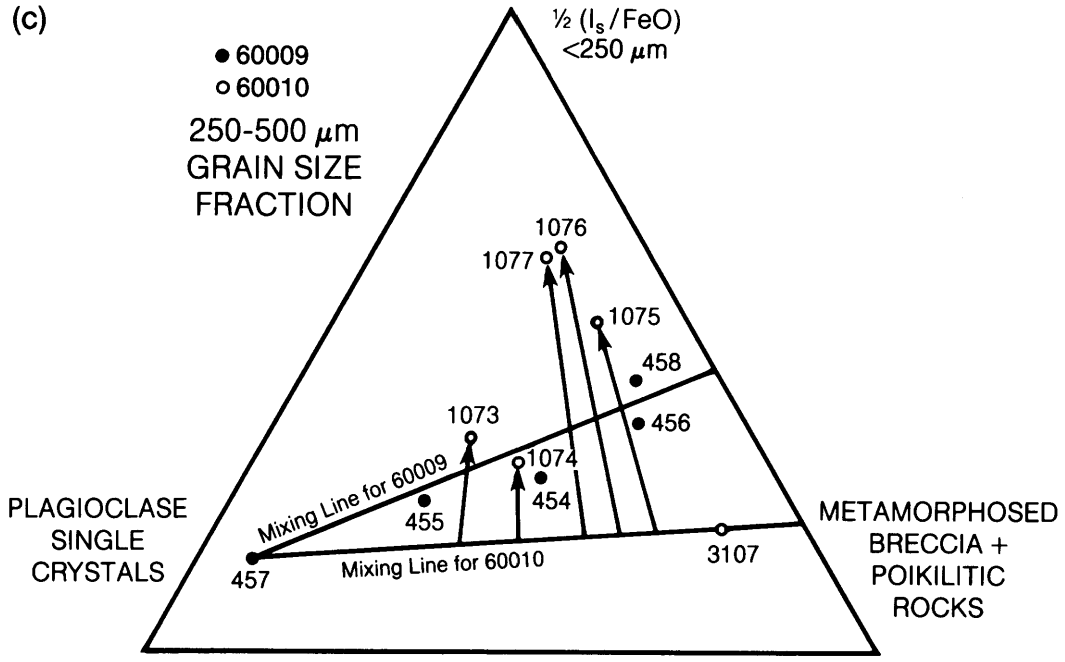

Fig. 7.22. (continued) **(c)** Triangular plot showing the dual effects of lithological mixing and maturation for samples from the Apollo 16 drive core 60009/10. Lithological mixing lines for the two cores lie approximately between the lower corners of the diagram, which represent the two most common rock components, plagioclase single crystals (left) and metamorphosed and poikilitic rocks (right). Most 60010 samples (1073, 1074, 1075, 1076, 1077, and 3107) show considerable displacement from the 60010 mixing line in the direction of increasing maturity (i.e., toward the I_s/FeO apex), indicating that maturation occurred after the samples were mixed together. In contrast, the 60009 samples (454, 455, 456, 457, and 458) have no systematic displacement from the mixing line toward the ls/FeO apex, and therefore show no evidence of postmixing maturation.

them, and there is a strong positive correlation between Fe and Sc, which indicates that they are both present in mare basalt components (Fig. 7.22b).

Korotev et al. (1984) analyzed samples of the lower half of a different Apollo 16 core (sample 64001/64002) at 5-mm intervals. They found that Fe, Cr, and Sc (indicators of mare basalt) are strongly correlated, indicating that a mare basalt component is present. Abundances of Na, Eu, and Ba show a fair correlation (Fig. 7.24). Although all three of the latter group of elements occur together in plagioclase, they are also found in the late crystallizing phases—K-feldspar and glass—of mare basalts. Because they are found in two unmelted components, their covariance is weaker than those of the former group.

Laul and Papike (1980) analyzed 3 grain-size fractions of soil samples from 30 levels of the Apollo 17 deep drill core 70001–70009, and their data show the same systematic variations mentioned above. In addition, they carried out mixing calculations using 25 chemical elements (allowing a 10% uncertainty for each), attempting to duplicate the lunar soil compositions with four components that represent common rock types identified at the Apollo 17 site. Their results show that the chemical compositions of each of the 30 soils analyzed can be adequately expressed in terms of contributions from these four end members (Fig. 7.25). These chemical results are also consistent with the five stratigraphic units that have been recognized on the basis of petrologic work (*Vaniman et al.,* 1979), and this consistency between the two techniques strengthens the identification of these layers as discrete depositional units.

Finally, these studies show that certain elements record the effects of soil maturation processes on the Moon. Comparison of the I_s/FeO profile in the Apollo 17 deep drill core with the abundance of Zn, a volatile element, clearly shows a strong negative correlation (Fig. 7.26; *Laul and Papike,* 1980), implying that Zn has been progressively lost, probably by impact vaporization, as the soil matured.

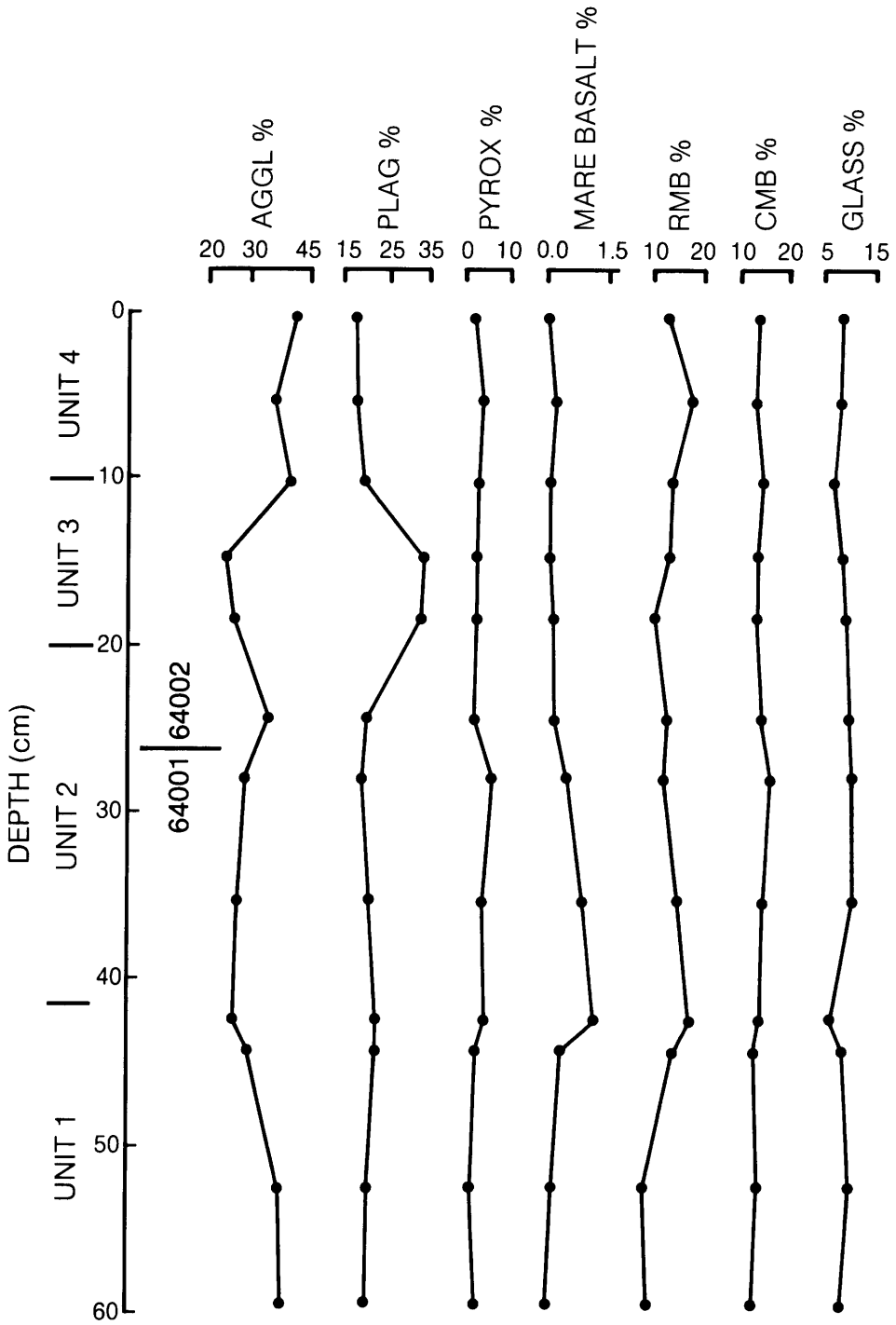

Fig. 7.23. Variations in the abundance of particle types with depth in the Apollo 16 core 64001/2 (*Basu and McKay,* 1984; *Houck,* 1982b). Scale at left shows the depth, sample locations, and boundaries between four distinct layers. Aggl = agglutinate, Plag = plagioclase, Pyrox = pyroxene, RMB = regolith matrix breccia, and CMB = crystalline matrix breccia.

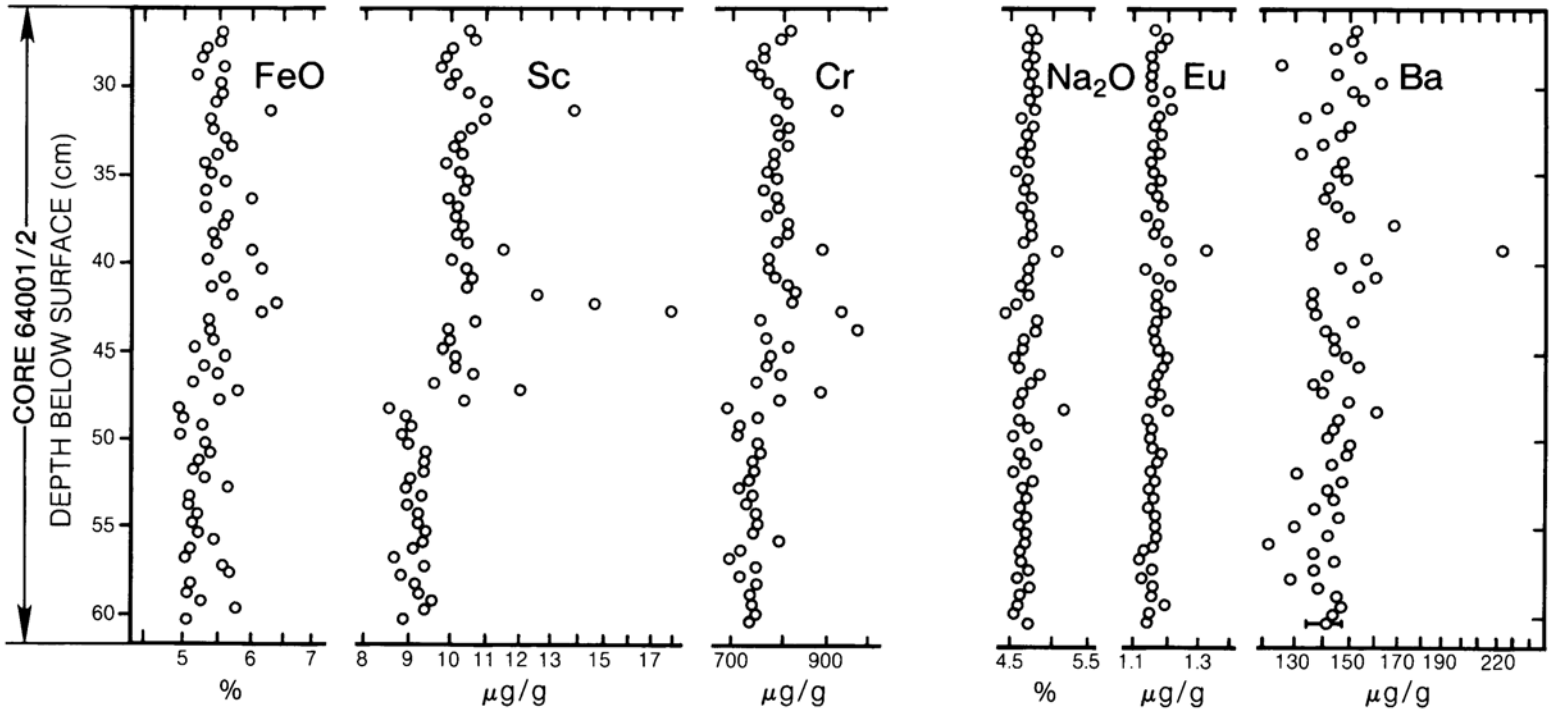

Fig. 7.24. Variations, with depth, of specific elements associated with ferromagnesian minerals (Fe, Sc, and Cr), and with plagioclase feldspar (Na, Eu, and Ba) in soil samples from the Apollo 16 core 64001/2 (*Korotev et al.,* 1984). Variations in these elements correlate approximately with the relative abundances of mare and highland materials, respectively, in the soil.

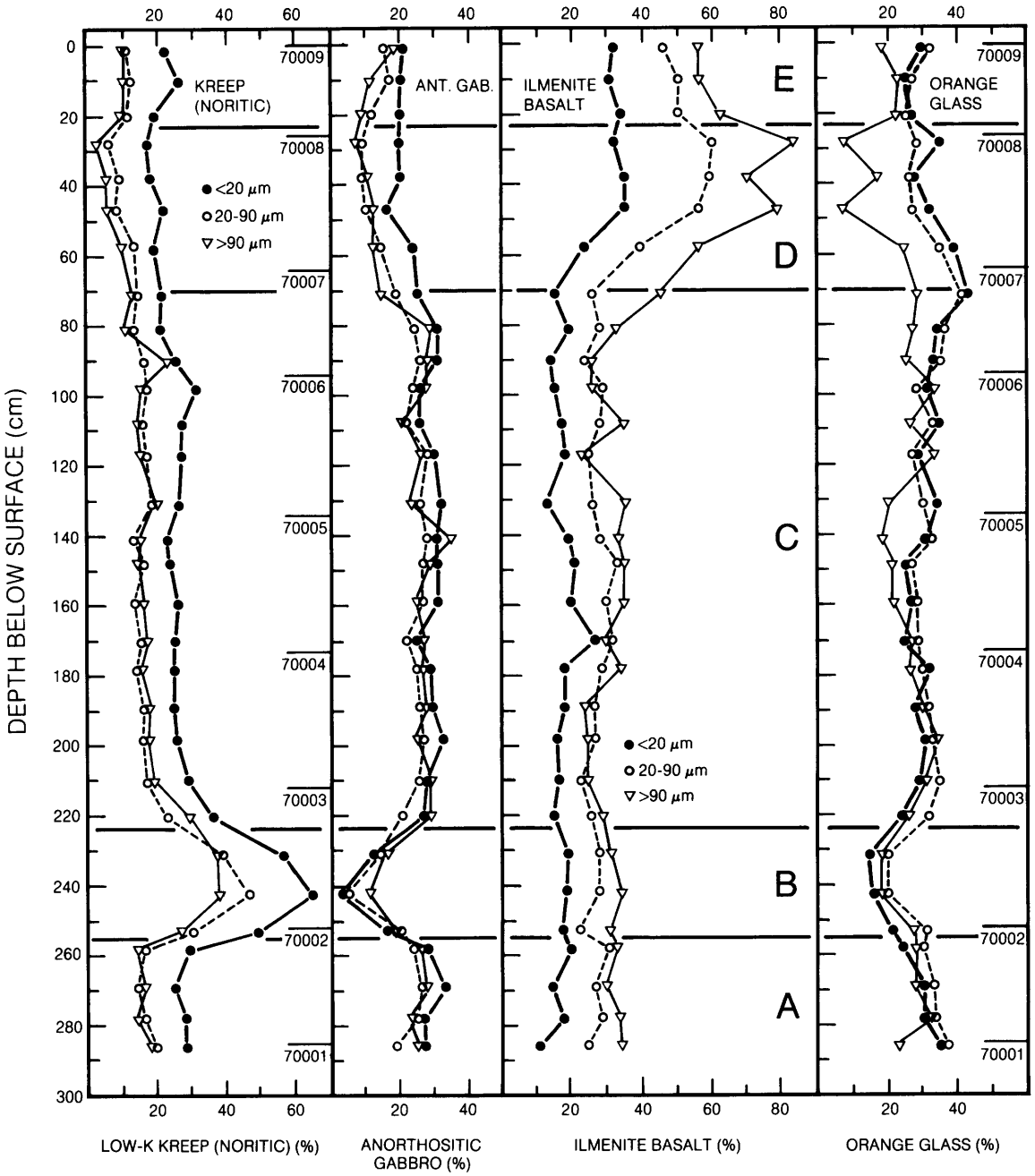

Fig. 7.25. Calculated percentages of different lithologic components as a function of depth for soil samples from the Apollo 17 core 70001–70009 (*Papike et al.,* 1982). For each sample data represent analyses for 25 chemical elements in each of 3 size fractions: <20 μm, 20–90 μm, and >90 μm. Mixing models then use the chemical data to determine the best match for the amounts of four rock types present: low-K noritic KREEP, anorthositic gabbro, ilmenite basalt, and orange glass. Vertical axis gives depth in core; horizontal axes give percentages for each component. Note that the boundaries (horizontal lines) of the five stratigraphic units (A–E) identified on the basis of petrographic studies coincide with significant variations in the abundances of different components.

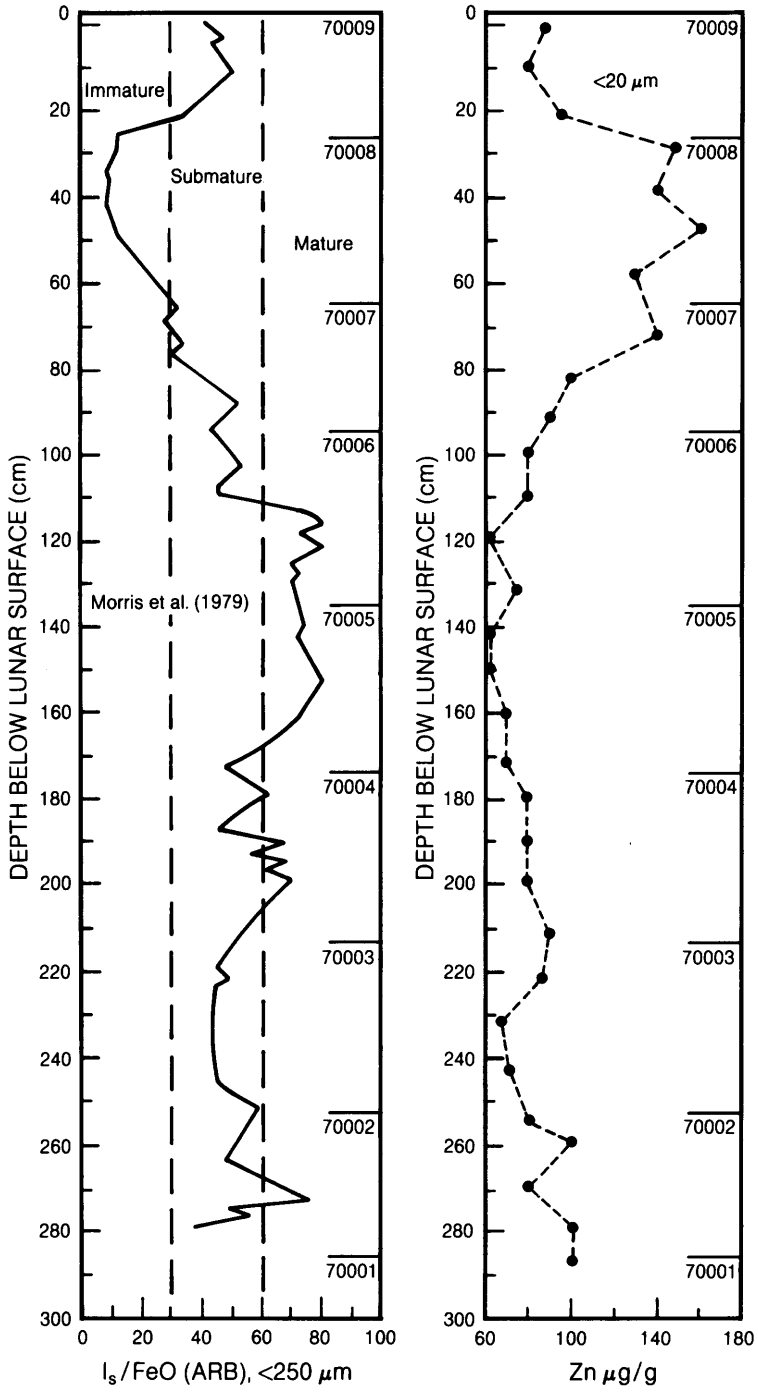

Fig. 7.26. Depth profiles of the abundance of Zn, a volatile element, and I_s/FeO, a maturity index, in the <20-μm size fraction of soil samples from the Apollo 17 drill core 70001–70009. These two quantities show a strong negative correlation, especially in the upper part of the core. This relationship suggests that Zn may be depleted in mature lunar soils, possibly having been expelled by vaporization during agglutinate production (*Laul and Papike,* 1980).

7.4.3. Regolith Stratigraphy

Nature of the regolith sections. The study of layered lunar regolith has many of the same goals as terrestrial stratigraphy—to determine the composition, formation, historical sequence, and correlation of a series of layered deposits. However, the lunar regolith presents special complications. Simply viewed, the regolith is built up as a series of layers of material ejected from individual meteorite craters over a period of time, and interbedded lava flows and pyroclastic deposits. At the same time, however, other large impacts may destroy, overturn, or bury a layered sequence. Furthermore, the near-surface part of the regolith, which is subjected to more frequent small impacts, tends to become uniformly mixed (gardened) and to lose many of the characteristics of the original discrete layers.

At any given time, the regolith ideally consists of two zones: (1) a near-surface *reworked* or *gardened* zone, typically a few centimeters to tens of centimeters thick, in which all layers have been homogenized or mixed together; and (2) an underlying *slab* or sequence of slabs in which the original layering is still undisturbed. The lowest section of regolith may grade downward into highly fractured bedrock into which regolith has been mixed or has seeped into the fractures.

In the reworked zone or layer, observed maturity indices have nearly constant values from top to bottom. (The term "layer" can be used, even though the zone described may have originally included more than one layer of ejecta. Mixing has been so complete that no trace of the original layering remains.) The soils from such a reworked layer are mature, and their maturity indices (with the exception of I_s/FeO) tend to be saturated.

Reworked zones are developed at or near the surface, where impacts are small and frequent. The resulting mixing and turnover of this zone occurs often enough to expose most of the soil particles to the near-surface environment for periods of time that are longer than needed to saturate such exposure indicators as solar-flare track densities and trapped solar-wind gases. The time needed to saturate solar-wind and solar-flare effects is less than a few thousand years.

The uppermost part of any lunar core should consist of such a reworked layer, unless the core has been drilled into fresh ejecta from a young crater. With prolonged surface exposure, more large impacts affect the exposed regolith, and the thickness of the reworked layer gradually increases. In the returned Apollo cores, the thickness of this uppermost reworked layer varies between about 10 cm and 50 cm.

Beneath the reworked layer may be layers of material that have remained unmixed since they were deposited. These *slab*s may consist of several layers that still preserve their original depositional relationship to each other. The slabs are shielded by the overlying zone of reworked regolith from near-surface effects such as solar-wind implantation and solar-flare tracks, but more energetic particles (solar-flare protons and cosmic rays) may penetrate the slabs and produce distinctive effects to depths of several meters. Because these effects vary with depth, distinctive *in-situ exposure profiles* develop within the slabs. In core samples, the presence of such profiles indicates that the overall slab, no matter how complexly layered, has remained in place and undisturbed for a significant period of time.

Large impacts excavate and deposit thick ejecta layers. Because the impacts may excavate a significant thickness of layered regolith, much of the material in the resulting ejecta may have been previously exposed, and this material brings the records of that exposure with it into the new ejecta layer. Near the crater, the ejecta layer is thick, and the original regolith layers may be preserved (often overturned) in the new ejecta deposit. Further from the crater, the ejecta layer is thin, and the preimpact regolith components, with their different exposure histories, may be mixed together.

Figure 7.27 shows depth profiles of several maturity indices and indicators of surface (or near-surface) exposure for the Apollo 15 deep drill core, the Apollo 16 double drive tube 60009/60010, and the Apollo 17 deep drill core. The parameters that are plotted, I_s/FeO, the track maturity index, agglutinate content, solar-wind gases, cosmogenic isotopes, and minimum track densities, are discussed in section 7.3. These are the basic data upon which many of the interpretations of lunar regolith stratigraphy have been based.

It would be difficult to resolve such complexities in detail, even with a large number of carefully collected samples. With the relatively few Apollo core samples available, it is not surprising that there is no general consensus on how to interpret the stratigraphic data contained in the lunar regolith cores. The sections below provide general stratigraphic interpretations for three core samples and attempt to account for all of the observations. The interpretations here are not always the same as those presented by the scientists who made specific measurements. The references cited in the sections below and in Fig. 7.27 should be consulted to obtain other points of view.

Apollo 15 deep drill core (sample numbers 15001–15006; 242 cm long). The upper 40-

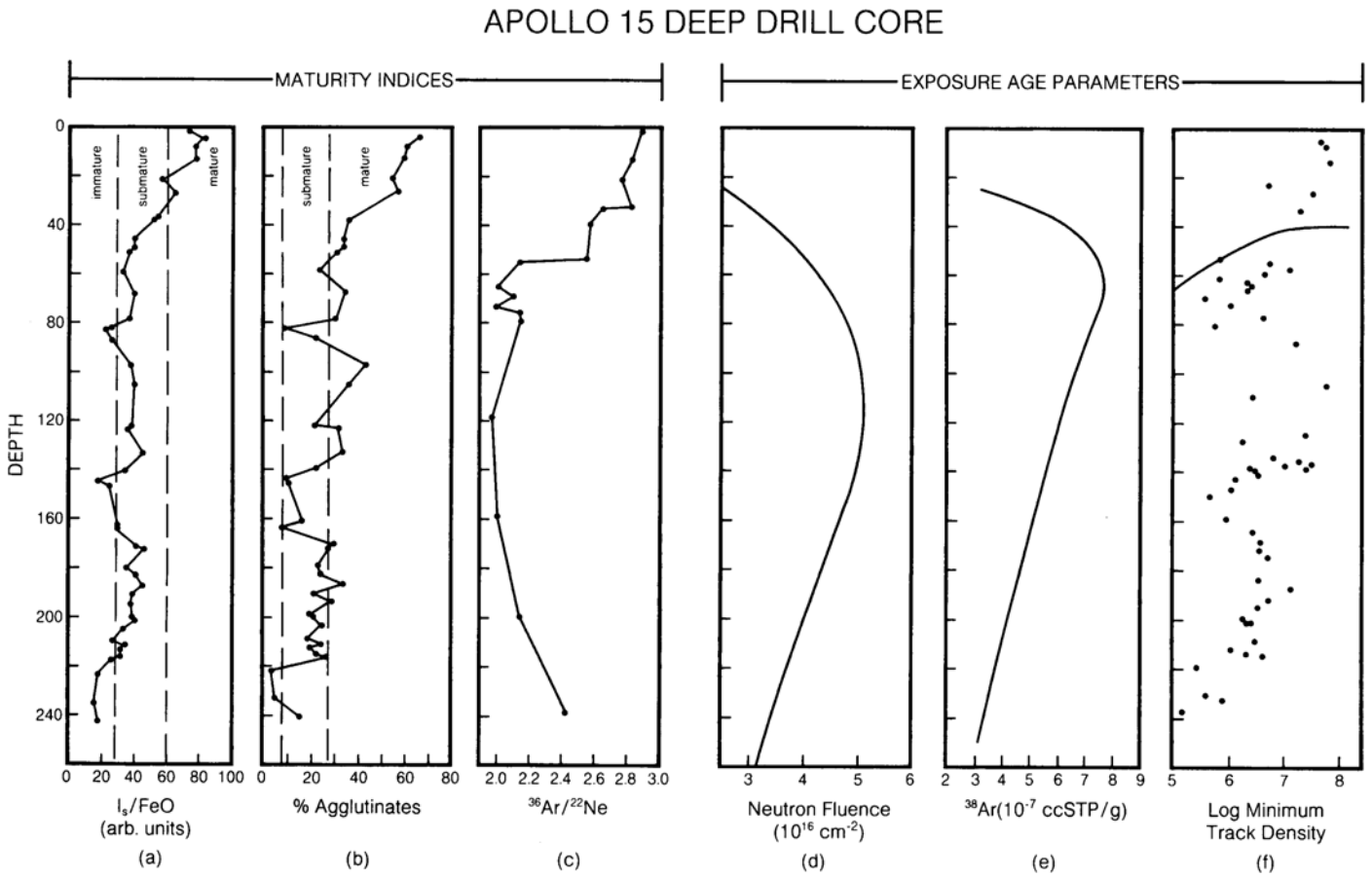

Fig. 7.27. Depth profiles of maturity indices and exposure age parameters for the Apollo 15 deep drill core 15001–15006, Apollo 16 core 60009/10, and the Apollo 17 deep drill core 70001–70009. In general the maturity indices shown (I_s/FeO, agglutinate percentages, and trapped solar-wind noble gases) show a gradual increase upward in the regolith and are highest within a few tens of centimeters of the surface. In contrast, some exposure age parameters (neutron fluence, ^{38}Ar content, and track densities) reflect charged-particle interactions or nuclear reactions that reach a maximum at depths of 50–200 cm in the regolith, where the incoming primary charged particles have been slowed by absorption. *Apollo* 15—15001–15006: **(a)** I_s/FeO, and **(b)** petrographic agglutinate percentages, after *Heiken et al.* (1976); **(c)** solar-wind rare-gas data after *Bogard and Hirsch* (1975); **(d)** neutron fluences after *Curtis and Wasserburg* (1977); **(e)** spallogenic argon (^{38}Ar), after *Pepin et al.* (1974); and **(f)** minimum track densities (number/cm^2) after *Goswami and Lal* (1977).

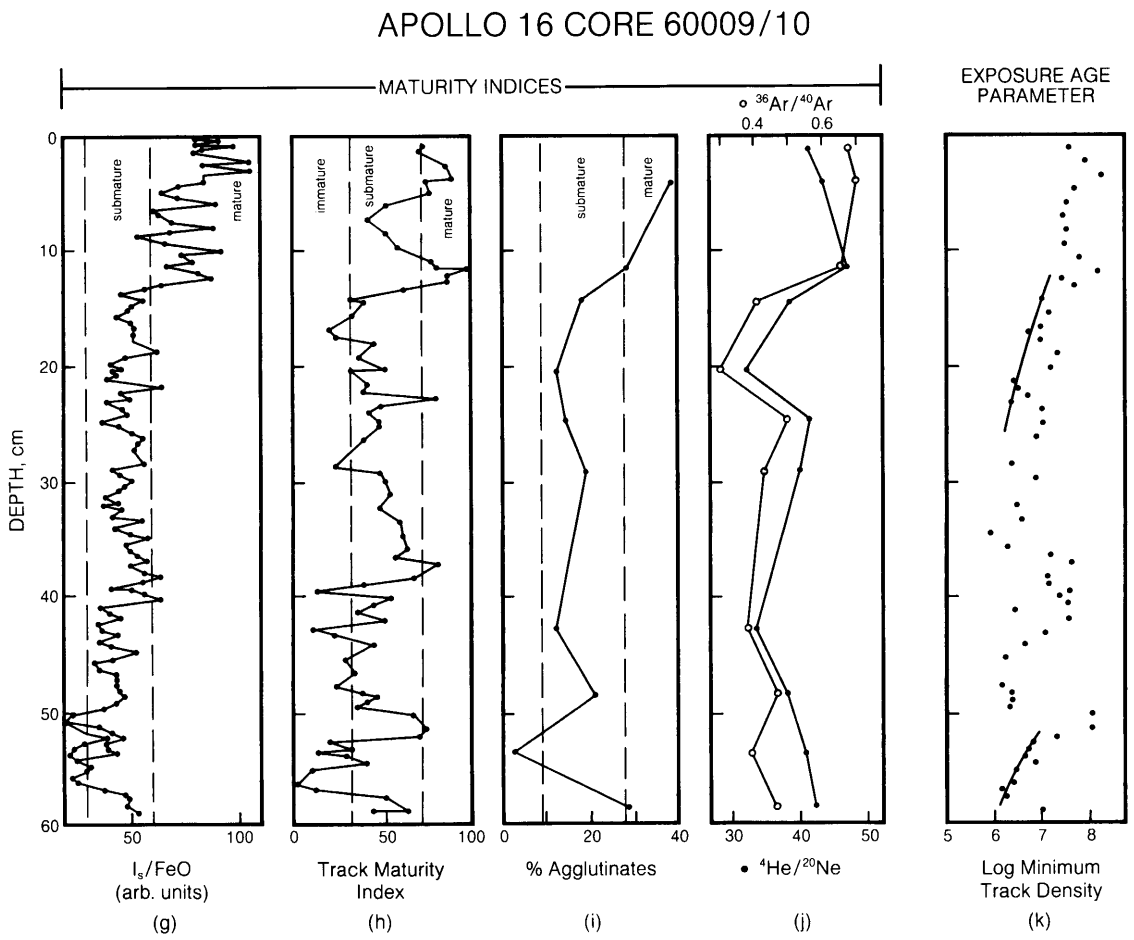

Fig. 7.27. (continued) *Apollo* 16—60009/10: **(g)** Is/FeO after *Morris and Gose* (1976); **(h)** track maturity index after *Blanford et al.* (1979) (track maturity index = % grains with track densities $>10^9/cm^2$; **(i)** petrographic agglutinate percentages, after *McKay et al.* (1977); **(j)** solar-wind rare gases after *Bogard and Hirsch* (1977); and **(k)** minimum track density after *Blanford et al.* (1979).

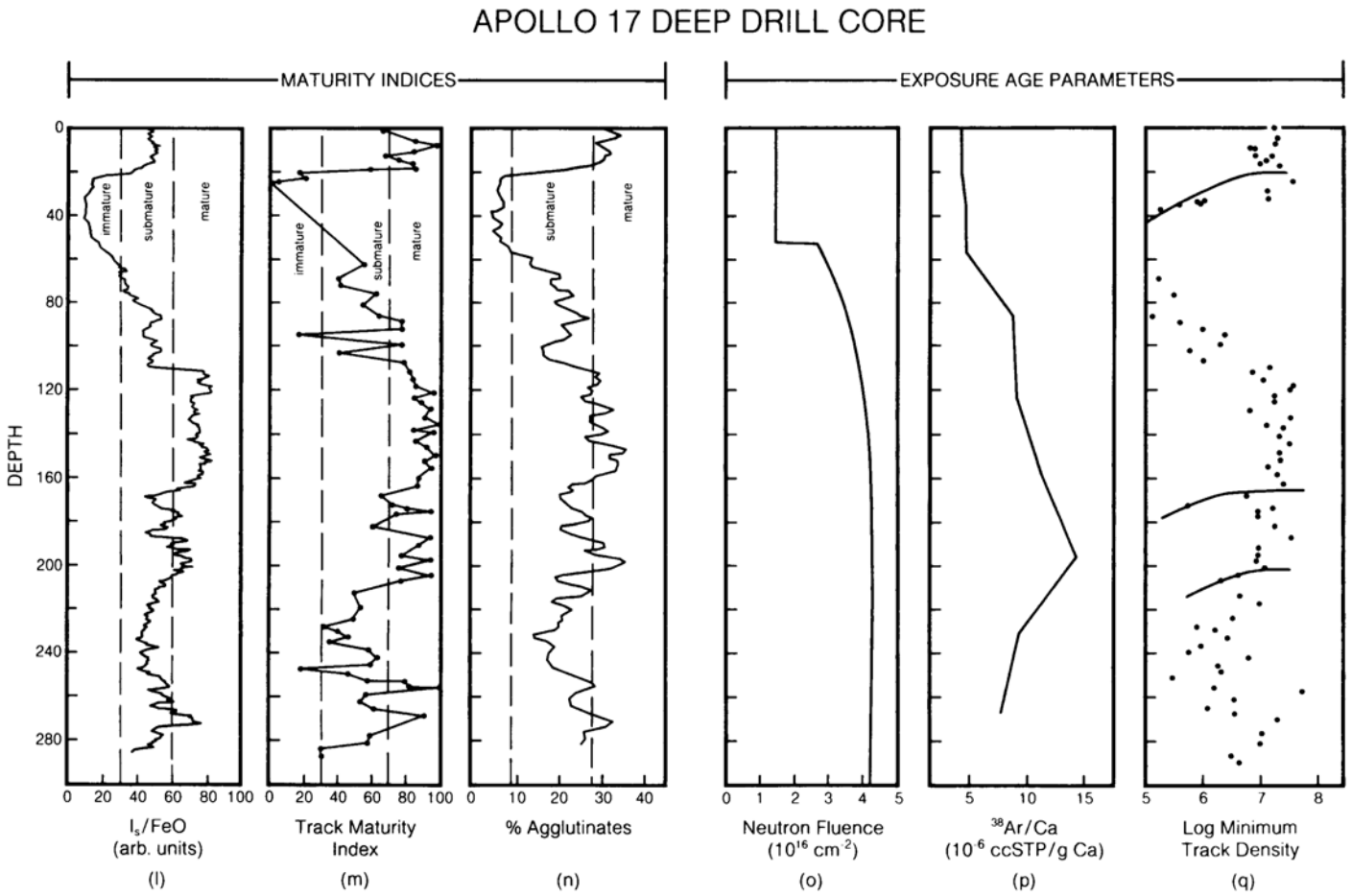

Fig. 7.27. (continued) *Apollo* 17—70001–70009: **(l)** I_s/FeO after *Morris et al.* (1979); **(m)** track maturity index after *Goswami and Lal* (1979); **(n)** petrographic agglutinate percentages, after *Taylor et al.* (1979); **(o)** neutron fluence after *Curtis and Wasserburg* (1977); **(p)** spallogenic argon (^{38}Ar) after *Pepin et al.* (1975); and **(q)** minimum track density after *Goswami and Lal* (1979). The track densities, in numbers/cm^2, show at least three levels where soils were buried by fresh ejecta (curved lines); these correlate also with changes in maturity indices.

45 cm of the Apollo 15 deep drill core has been identified as a reworked zone. Below this zone, the remainder of the core (200 cm) has lain undisturbed *in situ* for ~4.2 × 10^8 yr. The upper reworked zone is distinguished by the fact that all the maturity indices in this part of the core reach equilibrium values, which persist from the surface to a depth of ~40 cm (Fig. 7.27a–c). Petrographic and chemical variability, still preserved within this zone, reflect the lithologic heterogeneity of the site.

The remainder of the core below a depth of 40 cm must have been undisturbed *in situ* because the deeper profiles of cosmogenic nuclides are well-formed and well-preserved (Fig. 7.27d–e). These profiles have scale lengths on the order of a meter, and sizable variations on scales smaller than this would produce highly variable profiles, which, in fact, are seen in all other measured lunar cores.

The emplacement of this slab on the lunar surface was an ancient event. The measured exposure ages of the slab are 4.2 × 10^8 yr (*Pepin et al.,* 1974), 4.5 × 10^8 yr (*Curtis and Wasserburg,* 1977), and 4.0 × 10^8 yr (*Blanford,* 1980). This slab can be divided into several distinct layers, which show great heterogeneity in track densities, surface correlated gases, petrographic characteristics, and chemistry. These variations reflect the heterogeneities within the soil at the time of emplacement. In fact, the inherited track densities at the time of deposition were so high that there are no meaningful track profiles, reflecting later irradiation, which can be distinguished (Fig. 7.27f).

Apollo 16 core (sample numbers 60009/60010; 65.4 cm long). Examination of the I_s/FeO profile for this core (Figs. 7.27g–k) reveals that a reworked zone is present from the surface to a depth of ~12 cm. The track maturity index shows some variation from the ideal uniform profile at a depth of ~2 cm, implying some nonuniform disturbance, but no well-developed track profile can be established below this point because the inherited track densities are too high.

If this zone at ~2 cm depth did result from some specific lunar event, the thickness and location of the zone suggest an event about 10^6 yr ago. At the Apollo 16 site, South Ray Crater (0.5 km in diameter, located 6 km south of the core sample) has been dated at 2.0 × 10^6 yr (*Drozd et al.,* 1974). The track maturity index in the core sample may have been sufficiently sensitive to respond to this event, and to the sudden deposition of the resulting ejecta, but the data provide only suggestive support for this interpretation.

The track profile that developed in the regolith below a depth of 12 cm corresponds to an exposure age of <1.2 × 10^8 yr (*Bogard and Hirsch,* 1977) or 5–14 × 10^7 yr (*Blanford et al.,* 1979). This age is about the same as that of North Ray Crater (0.8 km in diameter, located 5 km north of the core sample) (5 × 10^7 yr; *Drozd et al.,* 1974). This connection is problematical, however. The track data require that the impact ejecta must be at least as thick as the reworked zone (12 cm) and possibly as thick as 39 cm. These are minimum estimates that neglect any overburden that may have originally been present and then subsequently removed. In contrast, the impact ejecta from North Ray Crater are estimated to be only ~1 cm deep at the lunar module site where core 60009/60010 was collected (*Stöffler et al.,* 1974).

There are no clearly defined strata in this core from ~24 cm to ~50 cm. From 12 to 50 cm, all maturity indexes indicate that the material is a submature soil that shows little variation with depth. Because there are no clear reworking zones in this interval, it is probable that this zone was emplaced as a unit in a single impact event. At 50 cm depth, a reworking zone, ~2 cm thick, has been identified; the zone can be seen clearly in both the I_s/FeO and track profiles (Fig 7.27g,h).

Below this thin reworked zone, there is a slab of material that shows a well-developed track density exposure profile from 52–58 cm deep. This profile corresponds to an exposure age of 4.5–9 × 10^6 yr (*Blanford et al.,* 1979), implying that the slab was deposited by a nearby impact at that time. However, any small crater corresponding to this event has probably been severely modified or eroded away by smaller subsequent impacts.

The bottom centimeter of the Apollo 16 60009/60010 core appears to be composed of more mature soil than the material above it, and this lowermost zone may represent a new stratum, but not enough of it was penetrated to conclusively state anything about the exposure history of this soil.

Apollo 17 deep drill core (sample numbers 70001–70009; 298.6 cm long). The upper 20 cm of the Apollo 17 deep drill core is a reworked zone. Immediately below the reworked zone is a slab, 40 cm thick, composed of the freshest lunar soil recovered in the Apollo program. The boundary between the two layers is clearly marked by every observable property of lunar soil (Figs. 7.27l–q). The lower, 40-cm-thick layer, which is extremely coarse-grained, has remained undisturbed since its deposition, and the exposure profiles for cosmogenic nuclides are well developed. The exposure ages estimated for the time of deposition of this layer are >3 × 10^7 yr (*Crozaz and Plachy,* 1976); <8 × 10^7 yr (*Curtis and Wasserburg,* 1977); 1.1 × 10^8 yr (*Drozd et al.,* 1977); and 7 × 10^7 yr (*Blanford,* 1980).

Below this layer, the core has not been studied (with particle-track techniques) in sufficient detail to

give a full history for the entire core. The I_s/FeO profile (Fig. 7.271) suggests that there may be several distinct strata in this section, deposited at different times. However, *Curtis and Wasserburg* (1977) prefer an interpretation involving rapid emplacement of the entire section sampled by the core. The maturity index profiles (Figs. 7.27l–n) suggest that reworked zones exist below the coarse layer at depths of approximately 112–166 cm and 188–203 cm. Profiles of cosmogenic nuclides have not been made with sufficiently close sampling to establish whether this interpretation is correct. However, unpublished spallogenic rare gas profiles and related calculations of neutron fluence based on this interpretation are consistent with the available data (*Pepin et al.,* 1975; *Curtis and Wasserburg,* 1977).

If this view is correct, the lower part of the core contains two more undisturbed slabs at about 40–112 cm and 166–188 cm, separated by reworked zones, and the *in situ* exposure-age estimates are 3–10 × 10^7 yr for the second undisturbed slab (40–112 cm deep), and 6–60 × 10^7 yr for the third undisturbed slab (166–188 cm deep). The cumulative *in situ* residence time of the lowest portion of the core (188–298 cm deep) would be 1.8–8.2 × 10^8 yr, with the true age more probably near the lower limit, a value that is consistent with the 1–2 × 10^8 yr age reported by *Curtis and Wasserburg* (1977).

7.5. MODELS FOR REGOLITH FORMATION

7.5.1. Regolith Dynamics

The movement of regolith materials across the lunar surface, either as individual grains or as large slabs, has built up the present lunar surface and is responsible for the layers observed in lunar core samples. Data from these cores make it possible to model regolith dynamics and to determine the rate constants for the different processes responsible for regolith formation and evolution. Some Apollo core samples were collected from considerable slopes or near rilles; at these locations, mass-wasting processes occur more rapidly, and data from these cores are particularly useful in the development of dynamic models for regolith evolution.

The most important parameters for models of regolith development are the mass and velocity distributions of impacting meteoroids, the impact flux rate, and the relation between the mass and velocity of an impacting object and the diameter, depth, and volume of the resulting crater. The present meteoroid fluxes are well known (see section 4.1.3), although significant uncertainties still exist. Cratering mechanics have been studied in detail on Earth and the application of the results to the Moon has been carried out with considerable success (see section 4.1.2). These two datasets—impact flux rates and lunar cratering mechanics—have been used to develop models for regolith development and turnover on the Moon. These models have been very successful. They show general agreement with the measured buildup rates of the regolith and with erosion rates measured on individual lunar rocks, and, on larger scales, they agree with the cratering history of the Moon. Models that have proven particularly appropriate for measurements of regolith development are reviewed in detail by *Langevin and Arnold* (1977). In particular, the models derived from meteoroid flux data by *Gault et al.* (1974), *Arnold* (1975), and *Duraud et al.* (1975) have been the most useful.

The differences between models reflect the choice of different input parameters—meteoroid mass, flux rate, and the depths and diameters of the resulting craters. Other differences arise from different calculational methods. The model of *Gault et al.* (1974) assumes that the number of crater excavations to a given depth is a Poisson distribution that is functionally dependent on the input parameters. This model cannot predict the exposure ages indicated by different lunar soil characteristics. However, the critical factor that it can predict is the probability of turning the regolith over to a given depth as a function of time (see section 4.1.4).

The models of *Arnold* (1975) and *Duraud et al.* (1975) are more random Monte Carlo models. Particle mass and impact location are chosen from their respective distributions with pseudorandom numbers. A "run" consists of a continuous series of such choices until some predetermined endpoint is reached, e.g., the regolith is turned over to a specific depth. The statistical effects on different maturity parameters in the soil are determined by examining many such "runs."

In further work, *Arnold* (1975) developed a model to describe the evolutionary history of a section of lunar regolith, while *Duraud et al.* (1975) developed a model to determine the burial history of individual lunar soil grains. When identical input parameters are used, both models produce remarkably close predictions for specific lunar observations such as track densities and cosmogenic nuclide distributions (*Langevin and Arnold,* 1977) within the regolith. In particular, these models can successfully predict levels of exposure developed in individual grains and can provide estimates of when they became saturated. In their models, *Gault et al.* (1974) predicted the turnover rate for the lunar regolith. These different models have subsequently been tested against the data from the Apollo core samples. *Morris* (1978a) assumed that the measured depths of surface reworked zones was equivalent to the *in*

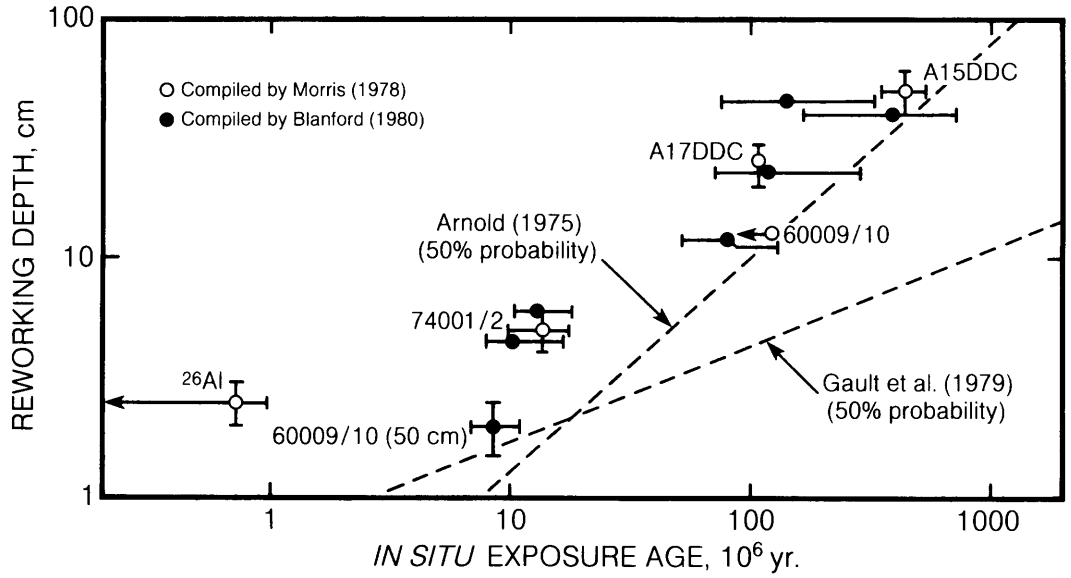

Fig. 7.28. Diagram showing calculated and measured relationships between near-surface exposure ages of lunar soil samples and reworking depths in the regolith layer. Samples represent several landing sites: Apollo 15 (A15 deep drill core), Apollo 16 (core 60009/10), and Apollo 17 (A17 deep drill core; core 74001/2). Horizontal axis shows surface exposure ages, measured with a variety of techniques; vertical axis shows reworking depth as determined from I_s/FeO values and ^{26}Al average profiles. Data are from *Morris* (1978a) and *Arnold* (1975). The experimentally determined points lie on a power-law trend that follows the *Arnold* (1975) model closely.

situ turnover of the cores and compared these depths with measured exposure ages for the cores. These data are shown in Fig. 7.28, together with additional data obtained from track densities. Because the regolith turnover is produced by stochastic (random) meteoroid impacts, the observed ages and depths can be compared with those predicted by different models. From the cores that have been measured so far, it appears that the experimental points agree with the *Arnold* (1975) model for exposure ages longer than 1–2 × 10^7 yr, while the *Gault et al.* (1974) model predicts reworking depths that are too shallow at all times.

7.5.2. Grain-size Distributions

McKay et al. (1974) have developed a steady-state model for the evolution of grain-size distributions in the lunar regolith that is in qualitative agreement with observed grain-size distributions of lunar soils. This model consists of three mechanisms. The first is the continuous pulverization of large particles to make smaller particles. The second mechanism, operating in reverse to the first, is the formation of agglutinates from multiple small particles. If these two mechanisms were the only ones operating, then any lunar soil would reach an equilibrium state in which there were no large particles and all the small particles were comminuted agglutinates. However, this is not the distribution found in lunar soils, and a third mechanism is required, one which continually adds large particles directly from bedrock or from exhumed deposits of coarse material produced earlier from bedrock. This third mechanism consists of occasional large meteoroid impacts that penetrate the deeper layers of the regolith or penetrate the entire regolith, excavating fresh bedrock and scattering the fragments across the surface. It is the inclusion of this third mechanism—occasional large meteoroid impacts—that distinguishes the steady-state model from equilibrium soil models.

A comprehensive steady-state model must also allow for the slow and steady addition of exotic fine-grained material, transported ballistically from distant impacts, directly to the small particle component of the soil. Such a comprehensive model predicts that a definite relationship should exist between the mean grain size of the finest soils and the thickness of the regolith in which they are found. Finer size fractions also begin to appear, and become progressively more important, as the soil matures. Because regolith thickness is related to age, mean grain size of the finest-grained soil will also

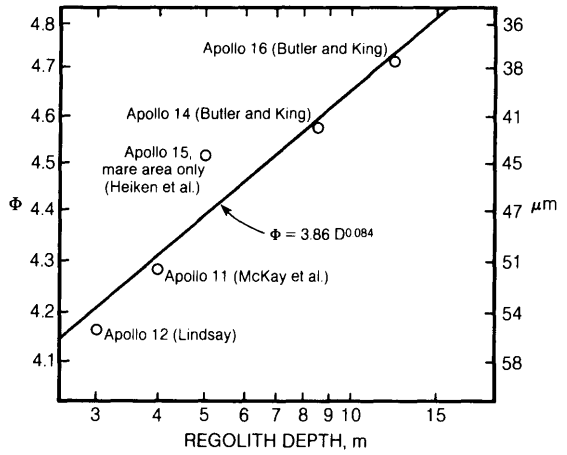

Fig. 7.29. A plot of mean grain size of the most fine-grained soil sample at several Apollo sites as a function of the regolith depth at that site (after *McKay et al.,* 1974), showing a clear relation between the two quantities. Finer-grained soils (higher ϕ values) are associated with thicker, deeper regolith. From *Butler and King* (1974); *Heiken et al.* (1973); *McKay et al.* (1970); and *Lindsay* (1973).

be indirectly related to the age of the site. The actual data for Apollo soil samples shown in Fig. 7.29 demonstrate that the mean grain size of the finest-grained soil samples does, in fact, correlate with regolith thickness.

7.5.3. Differential Comminution

The Moon is randomly bombarded by large and small impacts that fracture lunar rocks, comminute smaller particles, and then redistribute and mix the resulting lunar soils (section 7.3.1). Therefore, it would be reasonable to expect that all lunar rocks and minerals would be crushed, abraded, and eroded at approximately the same rate. The data from Apollo lunar soil samples show a more complex pattern. In particular, the rates of abrasion and erosion are also dependent on the grain sizes of the target material. In addition, we find that different minerals in lunar soils are apparently comminuted at different rates.

In terrestrial sediments, feldspars are broken down into finer sizes much faster and more efficiently than quartz; the explanation given is that the excellent cleavage in feldspars promotes fracturing and facilitates its breakdown relative to quartz, which has very poor cleavage (*Basu,* 1976; *Basu et al.,* 1975). Measurements of the chemical compositions of different size fractions of lunar soils also show a general enrichment of feldspar components in the finer sizes over other minerals (*Devine et al.,* 1982; *Papike et al.,* 1982) (Fig. 7.30). It is likely that the cleavage in feldspars is the cause of this preferential fragmentation in both lunar and terrestrial samples, a conclusion that is supported by experimental shock studies (*Hörz et al.,* 1984).

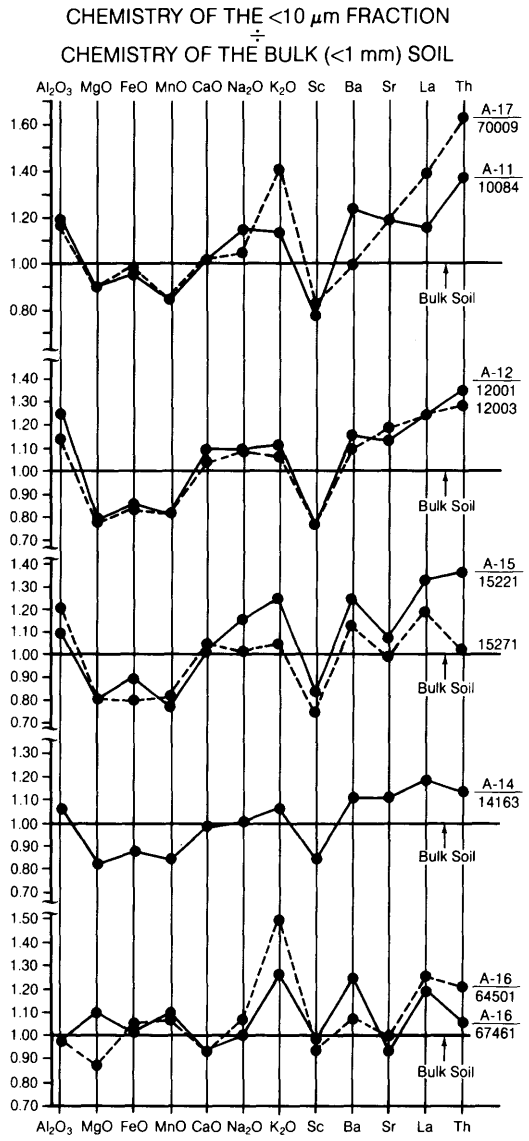

Fig. 7.30. Diagrams showing the ratios of chemical composition of the <10-μm fraction of nine lunar soils to the composition of the bulk soils (*Papike et al.,* 1982). The data show a general enrichment of feldspar components (Al_2O_3 and Na_2O) and rock mesostasis components (K_2O, Ba, Sr, La, and Th; see section 8.4) in the fine-grain-size fraction relative to the bulk soils from the same samples (normalized to 1).

These studies have also demonstrated that minerals that occur as very small grains in the original parent rocks (e.g., mesostasis minerals in mare basalts, or small olivine "beads" in granulitic breccias) are concentrated into the finer soil fractions (e.g., *Laul et al.,* 1981). It is therefore probable that comminution of lunar rocks occurs, at least partly, along grain boundaries, a phenomenon also observed in terrestrial rocks.

In summary, the grain-size distributions of lunar soils are controlled primarily by random meteoroid impacts, but the distribution of individual minerals in different grain-size fractions also reflects other variables like mineral cleavage and original grain sizes.

7.5.4. Comparison of Soil Chemistry With Bedrock Chemistry

Significant insights into the formation of the lunar regolith can be obtained by comparing the chemical compositions of soils from different landing sites (or from geologically distinct areas within a single site) with the compositions of common lunar rocks. These comparisons are one way to evaluate the degrees to which local, regional, and distant sources of different rock types have contributed to the lunar regolith at any single point. The complexity of regolith formation is indicated by the fact that no lunar soil, or any average composition of several soils from any region, is compositionally identical to any single lunar rock type. Average soil compositions from all lunar sample return missions are given in Table 7.15. Compositions of common rocks in the lunar crust are discussed in Chapter 6.

The most common crustal rock type from the Moon, based on sample returns and chemical measurements made from orbit, is anorthositic gabbro, as represented by samples 15455, 60335 and 66095 (*Taylor,* 1982*; Vaniman and Papike,* 1980). The Apollo 16 and Luna 20 landing sites are well within highland areas, and these sites provide our best samples of the premare lunar crust.

The Apollo 16 soils come closest to being similar to anorthositic gabbros. The average Apollo 16 soil is only slightly enriched in Al and Ca, but is substantially depleted in Mg, in comparison with sample 60335, a typical anorthositic gabbro. It appears that some contribution from relatively pure anorthosite to the average Apollo 16 soil is responsible for these differences in major element abundances. Apollo 16 soils are also slightly depleted in the KREEP component relative to sample 60335, and they have a lower abundances of K, La, U, and Th. In contrast to the Apollo 16 soils, the highland soils from the Luna 20 site are even less similar to anorthositic gabbro, or, for that matter, to any other lunar crustal rock.

In contrast, the Apollo 11, Luna 16, and Luna 24 soils have been collected from mare areas far from any exposed highland material. Despite their apparent derivation entirely from mare basalt lavas, the soils from these sites differ significantly from samples of mare basalts returned as large rocks. In general, the soils are considerably enriched in Si relative to high-Ti basalts, depleted in Al relative to high-Al basalts, or enriched in Mg relative to low-Ti basalts. The Luna 24 soils and the Apollo 15 soil 15601 (from the edge of Hadley Rille) are the two most mare-basalt-rich soils from the Moon. Except for substantial Mg enrichment, Luna 24 soils are compositionally closest to the very-low-Ti basalts; they are, however, more enriched in the KREEP component.

The differences between these soils and the dominant local bedrock are explained by the addition to the soil of material from a high-Mg gabbroic rock to account for the Mg enrichment (*Basu et al.,* 1978) and by the concentration of mare basalt mesostasis, which is always enriched in the KREEP component and other large-ion lithophile elements, into the finer soil fractions as a result of differential comminution. The Apollo 15 rille-margin soil (sample 15601) is compositionally similar to the Apollo 15 pigeonite basalt sample 15597, except that the soil is depleted in Si and enriched in Mg. In addition, this soil is relatively enriched in KREEP components such as K and La (Tables 7.16 and 7.17). The addition of fragments of local olivine basalt appears able to account for the differences in Si and Mg; preferential concentration of mesostasis, together with some KREEP basalt clasts, into the finer fractions produces the observed trace element differences.

The examples mentioned above, in which soil compositions can be easily related to a few local bedrock sources, actually represent the few exceptions among returned soil samples. Most other lunar soils are compositionally far removed from known lunar rocks.

7.5.5. Variation of Soil Chemistry Within Sites

Extended traverses by astronauts during the Apollo 15, Apollo 16, and Apollo 17 missions provided a collection of soil samples that is large enough to be used to examine variations of soil composition within single landing sites. These landing sites all share a common geomorphic feature: They are located at the boundary between

TABLE 7.15. Chemical compositions (wt.%) of average soils at lunar landing sites and in selected regions at the Apollo 15, Apollo 16, Apollo 17, Luna 16, Luna 20, and Luna 24 sites.

	11	12	14	15a	15b	15c	15	16a	16b	16c	16	17a	17b	17c	17d	17	L16	L20	L24
SiO_2	42.2	46.3	48.1	46.7	46.6	47.1	46.8	45.0	44.9	45.1	45.0	40.6	45.1	43.5	43.7	43.2	41.7	45.1	43.9
TiO_2	7.8	3.0	1.7	1.7	1.4	1.0	1.4	0.56	0.47	0.60	0.54	8.4	1.7	3.4	3.5	4.2	3.4	0.55	1.3
Al_2O_3	13.6	12.9	17.4	13.2	17.1	13.4	14.6	27.1	28.0	26.8	27.3	12.0	20.7	18.0	17.4	17.1	15.3	22.3	12.5
Cr_2O_3	0.30	0.34	0.23	0.44	0.27	0.37	0.36	0.34	0.54	0.11	0.33	0.45	0.25	0.28	0.32	0.33	0.28	–	0.32
FeO	15.3	15.1	10.4	16.3	11.7	14.9	14.3	5.2	4.7	5.4	5.1	16.7	8.8	10.9	12.2	12.2	16.7	7.0	19.8
MnO	0.20	0.22	0.14	0.21	0.16	0.19	0.19	0.41	0.27	0.22	0.30	0.23	0.12	0.16	0.16	0.17	0.23	0.13	0.25
MgO	7.8	9.3	9.4	10.9	10.5	13.0	11.5	5.8	5.6	5.7	5.7	9.9	9.8	10.7	11.1	10.4	8.8	9.8	9.4
CaO	11.9	10.7	10.7	10.4	11.6	10.3	10.8	15.8	15.7	*15.6*	*15.7*	10.9	12.8	12.12	11.3	11.8	12.5	15.1	12.3
Na_2O	0.47	0.54	0.70	0.38	0.45	0.33	0.39	0.46	0.50	0.43	0.46	0.35	0.42	0.42	0.42	0.40	0.34	0.50	0.31
K_2O	0.16	0.31	0.55	0.23	0.20	0.19	0.21	0.13	0.23	0.14	0.17	0.16	0.16	0.12	0.09	0.13	0.10	0.10	0.04
P_2O_3	0.05	0.4	0.51	0.16	0.19	0.19	0.18	0.13	0.10	0.10	0.11	0.14	0.15	0.09	0.08	0.12	0.12	0.16	0.11
S	0.12	–	–	0.07	0.08	0.04	0.06	0.07	0.05	0.09	0.07	0.12	0.09	0.07	0.09	0.09	0.21	0.08	0.14
Total	99.9	99.6	99.8	100.6	100.2	100.9	100.8	100.9	100.9	100.4	100.8	100.1	100.0	99.8	99.9	100.5	99.7	100.8	100.4
ppm																			
Sc	60	38	23	30	22	24	25.3	9.0	8.0	9.0	8.7	63	17	31	37	37	37	16	34
U	0.5	1.7	1.5	1.3	–	0.9	0.73	0.53	0.45	0.61	0.53	0.29	0.90	0.44	–	0.41	0.25	0.29	0.26
Th	1.9	6.4	6.7	3.8	–	3.0	2.3	1.9	1.4	2.8	2.0	0.53	2.7	2.7	1.5	1.9	0.8	0.85	1.1
La	16	39	70	23	32	24	26.3	11	8	13	10.7	8	15	11	–	8.5	13	5	5

11 Composition of soil 10002 from Apollo 11 site.
12 Average composition of selected soils (12001, 12023, 12030, 12032, 12033, 12037, 12041, 12042, 12044, 12070) from the Apollo 12 site.
14 Average composition of selected soils (14003, 14148, 14149, 14156) from the Apollo 14 site.
15a Average composition of selected mare soils (15012, 15013, 15020, 15030, 15040, 15070, 15080, 15470, 15500, 15530, 15600) from the Apollo 15 site.
15b Average composition of selected Apennine Front soils (15090, 15100, 15210, 15221, 15230, 15250, 15270, 15290) from the Apollo 15 site.
15c Average composition of selected green-glass-rich soils (15300, 15400, 15410, 15403) from the Apollo 15 site.
15 Average composition of Apollo 15 soils.
16a Average composition of Cayley Plain soil (60050, 60500, 61140, 61161, 61180, 61220, 61240, 61500, 62240, 62280) from the Apollo 16 site.
16b Average composition of selected North Ray soils (63320, 63340, 63500, 67460, 67480, 67600, 67700, 67710, 68500, 68820, 69920, 69940) from the Apollo 16 site.
16c Average composition of selected Stone Mountain and South Ray soils (64420, 64500, 64800, 65500, 65700, 66040, 66080) from the Apollo 16 site.
16 Average composition of Apollo 16 soils.
17a Average composition of selected mare soils (70011, 70160, 70180, 71040, 71060, 71500, 72160, 75060, 75080, 79220, 79240) from the Apollo 17 site.
17b Average composition of selected South Massif and light mantle soils (72320, 72440, 72460, 72500, 73120, 73140, 73220, 73280, 74120) from the Apollo 17 site.
17c Average composition of selected North Massif soils (76246, 76260, 76280, 76320, 76500, 77530) from the Apollo 17 site.
17d Average composition of selected Sculptured Hill soils (78220, 78420, 78440, 78460, 78480) from the Apollo 17 site.
17 Average composition of Apollo 1 7 soils.
L16 Average composition of Luna 16 soils (Russian data).
L20 Average composition of Luna 20 soils (Russian data; Sc from *Laul and Papike,* 1980).
L24 Average composition of Luna 24 soils (Russian data).

Data Source: *Baedecker et al.* (1974)*; Barisal et al.* (1972); *Boynton et al.* (1975, 1976a); *Brunfelt et al.* (1972a,b, 1973a,b); *Carron et al.* (1972); *Christian et al.* (1976)*; Compston et al.* (1973)*; Cuttitta et al.* (1971)*; Duncan et al.* (1973, 1975); *Finkelman et al.* (1975)*; Frondel et al.* (1971); *Fruchter et al.* (1974a,b)*; Goles et al.* (1971); *Haskin et al.* (1971, 1973); *Korotev* (1976, 1981, 1982)*; Krähenbühl et al.* (1973); *Laul and Papike* (1980); *Laul and Schmitt* (1973b); *Laul et al.* (1972, 1974)*; Lindstrom et al.* (1972); *LSPET* (1972, 1973a,b); *Mason et al.* (1973); *Masuda et al.* (1972); *Miller et al.* (*1974*)*; Morgan et al.* (1972); *Philpotts et al.* (1972, 1974); *Rhodes et al.* (1974); *Rose et al.* (1972, 1973, 1974, 1975); *Schnetzler and Philpotts* (1971); *Simkin et al.* (1973); *Tarasov et al.* (1977); *Taylor et al.* (1973)*; Vinogradov et al.* (1973)*; Wakita et al.* (1971); *Wänke et al.* (1973; 1974; 1975); *Warren et al.* (1978); *Willis et al.* (1972); *Woodcock and Pillinger* (1978).

TABLE 7.16. Major and minor element abundances (wt.%) in bulk soils and separated size fractions of "reference suite" lunar soils and sample 15601 (*Papike et al.*, 1982; *LSPET,* 1972).

Sample	Size, μm	SiO_2	TiO_2	Al_2O_3	FeO	MgO	CaO	Na_2O	K_2O	MnO	Cr_2O_3	Total
10084,1591	Bulk	41.3	7.5	13.7	15.8	8.0	12.5	0.41	0.14	0.213	0.290	99.8
	>90	41.6	7.4	13.1	16.1	8.0	12.5	0.42	0.14	0.205	0.300	99.9
	20–90	41.0	7.3	12.8	16.2	9.2	12.4	0.38	0.15	0.220	0.305	99.9
	10–20	41.5	7.3	14.6	15.8	7.5	11.4	0.43	0.15	0.200	0.295	99.2
	<10	41.3	7.3	16.3	15.1	7.2	12.7	0.47	0.16	0.180	0.290	101.0
12001.599	Bulk	46.0	2.8	12.5	17.2	10.4	10.9	0.48	0.26	0.220	0.410	101.1
	>90	45.8	2.5	11.8	17.7	11.2	10.0	0.46	0.25	0.219	0.414	100.3
	20–90	45.8	2.7	11.7	17.7	10.7	10.3	0.44	0.22	0.230	0.420	100.2
	10–20	45.7	3.1	13.2	17.2	9.9	10.7	0.50	0.26	0.200	0.460	101.2
	<10	45.0	3.0	15.6	14.8	8.2	12.0	0.53	0.29	0.180	0.410	100.0
12033.464	Bulk	46.9	2.3	14.2	15.4	9.2	11.1	0.67	0.41	0.195	0.387	100.8
	>90	48.0	2.4	13.5	14.5	10.2	10.2	0.71	0.44	0.200	0.360	100.5
	20–90	45.9	2.6	12.5	16.9	9.8	10.6	0.62	0.33	0.220	0.385	99.9
	10–20	46.6	2.5	14.8	15.0	9.7	11.1	0.65	0.39	0.190	0.350	101.2
	<10	47.3	2.6	16.2	13.0	7.2	11.5	0.73	0.44	0.160	0.330	99.5
14163.778	Bulk	47.3	1.6	17.8	10.5	9.6	11.4	0.70	0.55	0.135	0.200	99.8
	>90	48.0	1.6	17.3	10.4	10.7	11.3	0.71	0.58	0.140	0.190	100.9
	20–90	46.2	1.6	17.1	11.1	10.7	11.5	0.68	0.52	0.143	0.205	99.8
	10–20	48.0	1.5	17.5	10.2	9.8	10.9	0.69	0.54	0.135	0.190	99.5
	<10	48.5	1.7	19.0	9.2	8.0	11.3	0.71	0.59	0.115	0.190	99.3
15221,29	Bulk	46.0	1.1	18.0	11.3	10.7	12.3	0.43	0.16	0.154	0.325	100.5
	>90	46.4	1.0	17.5	12.0	11.0	11.7	0.46	0.19	0.159	0.305	100.7
	20–90	46.5	1.1	16.7	12.1	11.4	11.3	0.42	0.16	0.162	0.335	100.2
	10–20	47.0	1.1	18.0	11.4	9.6	11.7	0.42	0.19	0.145	0.318	100.0
	<10	46.5	1.2	19.8	10.2	8.6	12.6	0.50	0.20	0.120	0.305	100.0
15271,27	Bulk	46.0	1.5	16.4	12.8	10.8	11.7	0.49	0.22	0.162	0.350	100.4
	>90	47.0	1.3	15.5	13.2	11.7	10.8	0.50	0.22	0.167	0.370	100.7
	20–90	45.9	1.4	15.3	13.8	11.8	11.0	0.49	0.20	0.175	0.381	100.4
	10–20	45.7	1.4	17.1	12.4	10.0	11.7	0.50	0.20	0.157	0.360	99.5
	<10	46.0	1.5	19.8	10.3	8.7	12.3	0.50	0.23	0.133	0.300	99.8
64501.122	Bulk	45.3	0.37	27.7	4.2	4.9	17.2	0.44	0.10	0.056	0.090	100.3
	>90	45.5	0.45	27.9	4.5	4.4	16.8	0.40	0.090	0.060	0.085	100.2
	20–90	44.8	0.33	27.2	4.3	5.1	16.8	0.43	0.099	0.055	0.090	99.2
	10–20	45.2	0.38	27.9	4.4	5.0	16.1	0.44	0.11	0.060	0.090	99.7
	<10	45.6	0.45	27.4	4.4	4.3	16.1	0.47	0.15	0.060	0.100	99.0
67461,74	Bulk	45.0	0.29	29.2	4.2	3.9	17.6	0.43	0.055	0.055	0.075	100.8
	>90	45.3	0.29	28.7	4.3	3.9	17.2	0.42	0.050	0.060	0.080	100.3
	20–90	44.4	0.40	28.8	4.5	4.6	17.2	0.43	0.055	0.062	0.084	100.5
	10–20	44.3	0.40	29.3	4.4	4.0	17.6	0.42	0.062	0.065	0.087	100.6
	<10	45.1	0.29	28.6	4.3	4.3	16.5	0.43	0.070	0.060	0.088	99.7
72501,15	Bulk	45.2	1.4	20.1	9.50	10.0	12.5	0.44	0.17	0.120	0.230	99.7
	>90	45.9	1.1	20.2	8.80	10.3	13.4	0.51	0.17	0.110	0.220	100.7
	20–90	45.2	1.6	19.4	10.0	11.0	12.9	0.43	0.14	0.120	0.250	101.0
	10–20	45.1	1.6	20.6	9.10	10.4	12.7	0.44	0.16	0.100	0.230	100.4
	<10	—	1.4	20.6	8.60	8.5	12.2	0.43	0.17	0.096	0.230	—

TABLE 7.16. (continued).

Sample	Size, μm	SiO_2	TiO_2	Al_2O_3	FeO	MgO	CaO	Na_2O	K_2O	MnO	Cr_2O_3	Total
76501,48	Bulk	43.4	3.2	18.1	10.8	12.0	12.8	0.38	0.10	0.145	0.270	101.2
	>90	43.7	3.1	18.5	10.3	12.3	12.8	0.38	0.10	0.130	0.260	101.5
	20–90	42.7	3.5	16.7	12.0	12.7	11.4	0.37	0.10	0.150	0.300	99.9
	10–20	41.8	3.4	18.7	11.6	11.1	13.0	0.38	0.10	0.147	0.290	100.5
	<10	41.6	3.2	20.2	10.6	9.8	12.7	0.40	0.12	0.130	0.280	99.0
78221,71	Bulk	43.0	4.2	17.0	12.6	11.0	12.4	0.37	0.10	0.163	0.350	101.1
	>90	42.0	4.1	16.5	12.7	11.9	11.9	0.39	0.10	0.154	0.360	100.1
	20–90	43.4	4.2	16.0	13.7	11.8	11.9	0.37	0.090	0.168	0.360	101.9
	10–20	41.8	4.2	17.3	12.2	10.7	11.9	0.36	0.10	0.160	0.325	99.5
	<10	43.9	3.9	19.0	11.9	9.3	12.4	0.40	0.12	0.135	0.320	101.4
Luna 16	Bulk	—	3.5	15.5	16.5	8.1	11.8	0.38	0.11	0.230	0.300	—
21000,5	>90	—	3.4	15.5	16.4	8.1	12.4	0.41	0.12	0.230	0.300	—
	20–90	—	3.2	14.0	17.6	9.0	11.4	0.37	0.10	0.220	0.323	—
	10–20	—	3.8	14.0	16.6	8.5	11.4	0.36	0.11	0.219	0.320	—
	<10	—	3.0	16.7	13.0	6.6	11.5	0.40	0.13	0.170	0.280	—
Luna 20	Bulk	—	0.48	23.5	7.27	9.7	14.1	0.35	0.068	0.100	0.180	—
22001,35	>90	—	0.43	21.2	6.68	8.8	13.7	0.34	0.066	0.090	0.170	—
	20–90	—	0.50	22.8	8.00	9.6	14.4	0.32	0.063	0.120	0.210	—
	10–20	—	0.46	20.5	8.00	9.5	12.3	0.34	0.065	0.107	0.210	—
	<10	—	0.50	25.0	6.25	7.2	14.9	0.36	0.078	0.070	0.170	—
Luna 24	Bulk	—	1.0	11.7	20.2	9.7	11.1	0.27	0.027	0.270	0.467	—
24999,6	>90	—	0.97	10.6	20.5	10.8	10.7	0.23	0.017	0.280	0.410	—
	20–90	—	1.1	11.4	20.8	10.3	10.8	0.25	0.024	0.290	0.450	—
	10–20	—	1.3	11.7	19.5	9.0	10.8	0.30	0.040	0.229	0.510	—
	<10	—	1.0	14.7	13.8	8.0	10.7	0.37	0.066	0.162	0.400	—
Apollo 15 15601	Bulk	45.05	1.98	10.2	19.8	10.9	9.9	0.29	0.10	0.26	0.56	—

the bottom of a hill and the edge of a plain. At the Apollo 15 and Apollo 17 sites, the plains consist of mare basalt flows; at the Apollo 16 site, the plain consists mainly of fragmental highland rocks. The hills at all these sites are composed of highland material that may have been ejected from the interiors of large impact basins (*Head,* 1976b, 1977).

Apollo 17. At the Apollo 17 landing site, strong contrasts are observed between soils from the mare plain and from the adjoining South Massif light mantle deposit (analyses 17a and 17b in Table 7.15). Soils from the plain were derived largely from mare basalts. The massif soils were derived mostly from highland material, and are enriched in the feldspar components CaO and Al_2O_3. These differences indicate that the soil compositions are controlled mostly by local bedrock compositions; the sharp contrast in albedo between these two adjacent areas also supports this conclusion. Small differences in soil compositions between the South Massif and the North Massif suggest that the South Massif is a little more anorthositic (Ca- and Al-rich) than the North Massif, the latter being more enriched in gabbroic components Mg and Fe. It is interesting to note that a model soil composition, produced by mixing together equal quantities of soil from all of the four distinct geomorphic areas of the Apollo 17 site, is nearly identical to that of the soil sampled in the Sculptured Hills area (see Fig. 10.28).

Apollo 15. Variations in soil compositions are also seen in the different geomorphic areas at the Apollo 15 site. The relatively flat, bay-like area below the Apennine Front and adjacent to Hadley Rille is apparently composed of thin mare basalt lava flows that range in composition from higher SiO_2 (quartz-normative) to lower SiO_2 (olivine-normative). Some pyroclastic deposits and KREEP basalt flows are also intercalated with the basalt flows (*Spudis and Ryder,*

TABLE 7.17. Trace element abundances (parts per million) in bulk soils and separated size fractions of "reference suite" lunar soils and sample 15601 (*Papike et al.,* 1982; *Brunfelt et al.,* 1972a).

Sample	Size, μm	Sc	V	Co	Ba	Sr	La	Ce	Nd	Sm	Eu	Tb	Dy	Ho	Tm	Yb	Lu	Hf	Ta	Th	U	Ni*
10084,1591	Bulk	60.2	70	28.0	170	160	15.8	43	37	11.4	1.60	2.9	17	4.1	1.6	10.0	1.39	9.00	1.25	1.90	0.5	200
	>90	64.7	70	30.5	160	160	15.4	44	36	11.8	1.65	3.0	18	4.3	1.6	10.3	1.47	8.90	1.20	2.00	0.5	230
	20–90	66.4	80	28.4	150	160	14.9	42	36	11.9	1.60	3.0	18	4.3	1.6	10.6	1.53	8.95	1.20	1.90	0.5	190
	10–20	55.3	70	30.3	180	180	15.4	44	37	11.4	1.70	2.9	18	4.2	1.5	10.0	1.43	9.32	1.30	2.00	0.5	290
	<10	46.9	70	37.4	210	190	18.3	52	40	12.8	1.95	2.9	18	4.2	1.5	10.1	1.43	9.60	1.40	2.60	0.7	450
12001,599	Bulk	40.2	110	42.5	430	140	35.6	85	57	17.3	1.85	3.7	22	5.0	1.8	13.0	1.85	11.8	1.50	5.40	—	190
	>90	42.0	120	43.0	420	130	34.7	87	57	16.7	1.85	3.8	22	4.8	2.0	12.6	1.80	11.8	1.60	5.70	1.7	150
	20–90	42.0	120	45.2	380	120	31.1	78	54	15.2	1.70	3.4	20	4.8	1.9	11.9	1.70	11.6	1.50	5.10	1.4	210
	10–20	38.0	110	46.2	410	130	36.3	95	63	17.5	1.95	3.5	21	5.0	2.1	13.0	1.85	13.3	1.65	6.40	1.7	400
	<10	31.0	100	41.0	500	160	44.6	112	75	21.4	2.15	4.3	26	6.2	2.3	14.5	2.05	12.8	1.75	7.30	2.0	600
12033,464	Bulk	36.4	100	34.3	600	160	50.0	133	85	22.8	2.45	4.9	30	7.2	2.6	17.3	2.45	16.6	2.20	8.50	2.4	130
	>90	34.6	100	31.3	670	160	60.7	150	95	27.7	2.60	5.6	34	7.8	3.2	20.8	2.96	21.2	2.60	10.2	2.6	110
	20–90	40.7	100	39.5	530	150	43.6	112	74	20.5	2.20	4.3	26	6.5	2.3	16.2	2.40	17.0	2.10	7.50	2.2	190
	10–20	34.5	100	32.3	540	170	43.0	120	76	19.0	2.30	4.4	25	6.4	2.5	15.5	2.20	17.0	2.10	8.40	2.1	220
	<10	28.2	90	32.0	660	190	62.4	170	105	28.4	2.70	5.7	33	8.0	3.0	19.2	2.70	15.2	2.30	10.8	2.7	600
14163,778	Bulk	21.7	45	33.0	800	170	66.7	170	100	29.1	2.45	5.9	36	8.6	3.2	21.2	3.00	22.5	2.90	13.3	3.5	350
	>90	21.1	35	32.5	800	180	73.0	185	110	30.2	2.40	6.3	40	9.4	3.6	23.4	3.20	23.5	2.90	14.7	3.5	380
	20–90	23.5	*50*	*35.5*	730	160	60.6	154	95	25.2	2.30	5.4	35	8.6	3.2	20.5	2.90	22.0	2.80	12.4	3.1	380
	10–20	21.3	45	30.5	780	160	63.4	160	103	26.4	2.30	5.5	36	8.6	3.2	20.2	2.85	22.0	2.90	12.4	3.3	480
	<10	18.5	40	31.0	890	190	79.1	200	120	33.7	2.65	6.5	41	10	3.6	22.4	3.16	20.2	3.10	15.2	4.0	690
15221,29	Bulk	21.2	80	41.0	240	120	20.5	54	36	9.70	1.30	2.0	12	2.9	1.1	6.90	0.97	6.70	0.93	3.00	—	360
	>90	22.7	70	34.5	250	140	22.6	58	40	10.8	1.50	2.1	13	3.1	1.2	8.10	1.15	7.50	0.96	3.30	1.0	220
	20–90	22.7	85	37.0	210	120	20.0	50	32	9.56	1.20	2.0	12	2.9	1.1	7.10	1.00	6.60	0.90	3.10	0.9	220
	10–20	20.8	70	35.5	250	130	22.1	59	36	10.7	1.40	2.2	13	3.2	1.2	7.60	1.10	7.60	1.00	3.75	1.0	290
	<10	17.8	75	36.0	300	130	27.2	69	44	12.5	1.60	2.6	15	3.7	1.2	8.20	1.15	7.60	1.10	4.10	1.3	640
15271,27	Bulk	24.3	80	40.5	300	130	25.8	70	45	12.0	1.50	2.6	15	3.9	1.4	8.54	1.20	8.60	1.20	4.60	1.2	230
	>90	26.1	85	39.0	280	130	27.1	70	44	12.6	1.60	2.7	15	3.9	1.3	9.00	1.27	9.00	1.10	4.30	1.3	200
	20–90	26.5	80	41.0	280	130	25.7	66	43	12.2	1.50	2.6	15	3.9	1.4	9.00	1.27	9.30	1.20	4.10	1.1	200
	10–20	23.4	80	39.0	280	130	25.9	70	46	12.3	1.50	2.5	15	3.9	1.3	8.75	1.25	9.40	1.20	4.30	1.2	370
	<10	18.3	70	36.4	340	130	31.0	82	54	14.4	1.70	2.7	16	3.9	1.4	9.20	1.30	8.20	1.30	4.72	1.2	700
64501,122	Bulk	8.0	20	19.5	130	170	10.8	28	19	4.79	1.05	1.0	6.0	1.4	0.55	3.40	0.49	3.30	0.45	1.85	0.4	300
	>90	8.9	20	21.0	120	160	10.6	27	18	4.70	1.10	1.0	6.0	1.4	0.60	3.60	0.51	3.50	0.43	1.70	0.5	340
	20–90	7.8	15	20.1	120	160	10.8	27	18	4.70	1.10	1.0	6.4	1.5	0.56	3.50	0.50	3.50	0.45	1.80	0.5	320
	10–20	8.2	20	17.9	130	160	11.5	30	20	5.20	1.05	1.1	6.5	1.6	0.60	3.90	0.55	3.80	0.47	1.85	0.5	400
	<10	7.6	20	22.5	140	170	13.6	34	22	5.83	1.15	1.2	7.5	1.8	0.65	4.00	0.54	4.00	0.54	2.25	0.55	850

TABLE 7.17. (continued).

Sample	Size, μm	Sc	V	Co	Ba	Sr	La	Ce	Nd	Sm	Eu	Tb	Dy	Ho	Tm	Yb	Lu	Hf	Ta	Th	U	Ni*
67461,74	Bulk	7.8	20	9.0	60	170	4.67	12	7.2	2.00	1.00	0.45	2.8	—	0.25	1.60	0.22	1.60	0.24	0.83	—	80
	>90	8.4	20	10	60	160	4.40	11	7.0	2.00	0.95	0.43	2.9	—	0.24	1.55	0.21	1.30	0.20	0.82	—	100
	20–90	8.1	20	14	70	170	4.78	12	7.7	2.17	0.98	0.47	3.0	—	0.27	1.73	0.26	1.50	0.24	0.81	—	170
	10–20	8.1	20	9.2	70	170	4.85	12	8.3	2.20	0.98	0.44	3.0	—	0.28	1.76	0.25	1.70	0.22	0.83	—	200
	<10	7.7	15	9.5	75	160	5.60	15	10	2.44	1.00	0.56	3.2	—	0.33	1.80	0.26	1.95	0.25	0.89	—	540
72501,15	Bulk	20.0	45	33.0	210	160	16.2	46	29	8.00	1.30	1.6	10.0	—	0.84	5.90	0.82	6.00	0.90	3.00	1.0	260
	>90	18.6	45	27.0	230	180	18.6	49	30	8.75	1.40	1.7	11.7	—	0.98	6.50	0.93	6.50	0.90	3.50	1.0	240
	20–90	21.5	50	31.0	210	170	15.1	40	27	7.70	1.25	1.6	10.7	—	0.84	6.00	0.90	6.40	0.85	3.00	1.0	260
	10–20	19.4	50	28.7	210	180	15.5	42	26	7.63	1.30	1.6	10.5	—	0.89	5.70	0.80	6.00	0.80	2.80	0.8	340
	<10	17.2	45	30.0	210	190	17.5	46	30	8.10	1.30	1.6	10.5	—	0.86	5.70	0.79	5.60	0.95	3.20	0.9	700
76501,48	Bulk	28.0	65	30.4	120	160	8.30	23	16	5.30	1.20	1.2	8.3	—	0.71	4.60	0.66	4.20	0.70	1.60	0.4	190
	>90	27.7	50	32.6	130	160	8.30	22	17	5.30	1.20	1.2	8.0	—	0.70	4.40	0.64	4.20	0.72	1.50	0.4	220
	20–90	32.5	70	32.5	120	160	8.20	23	16	5.40	1.25	1.3	8.2	—	0.71	4.70	0.72	4.60	0.80	1.60	0.4	220
	10–20	28.9	60	31.0	120	160	8.80	26	18	5.75	1.25	1.3	8.3	—	0.69	4.60	0.66	4.80	0.80	1.75	0.4	300
	<10	24.5	60	32.0	150	190	10.4	29	20	6.30	1.35	1.4	8.6	—	0.71	4.70	0.68	4.70	0.80	2.00	0.5	6.00
78221,71	Bulk	36.3	70	40.0	120	160	8.10	24	16	5.46	1.25	1.3	8.4	—	0.72	4.70	0.70	4.70	0.86	1.60	0.4	200
	>90	39.8	70	37.0	140	160	8.00	23	17	5.55	1.25	1.3	8.7	—	0.71	4.90	0.73	4.60	0.85	1.40	0.4	250
	20–90	39.5	75	35.0	110	160	8.30	24	18	5.75	1.30	1.3	8.5	—	0.74	5.10	0.75	4.90	0.85	1.40	0.4	230
	10–20	33.2	75	34.5	120	160	8.90	26	18	5.80	1.30	1.3	9.1	—	0.75	4.90	0.74	5.10	1.00	1.60	0.4	350
	<10	29.3	65	36.5	170	170	11.4	30	22	6.90	1.50	1.5	10.0	—	0.81	5.40	0.79	5.00	0.93	1.85	0.4	600
Luna 16	Bulk	52.0	80	29.6	180	260	11.6	33	26	8.25	2.15	1.7	11	—	0.90	5.70	0.80	7.04	0.50	1.39	0.4	200
21000,5	>90	52.0	85	29.4	170	270	12.5	35	27	8.70	2.30	1.7	11	—	0.85	5.80	0.80	7.50	0.53	1.33	0.4	190
	20–90	58.0	85	28.9	180	220	11.0	33	24	7.80	2.10	1.6	11	—	0.80	5.40	0.76	7.00	0.51	1.25	0.4	600
	10–20	50.5	80	30.7	300	220	11.1	31	26	7.95	1.90	1.6	11	—	0.86	5.50	0.81	6.90	0.49	1.27	0.4	1000
	<10	35.0	60	36.6	330	290	11.7	32	25	7.30	2.10	1.5	10	—	0.75	4.70	0.73	6.30	0.55	1.52	0.4	2700
Luna 20	>125	15.4	40	31.6	100	130	7.20	17	12	3.20	0.90	0.65	4.2	—	0.37	2.55	0.35	2.30	0.28	1.32	—	300
22001,35	90–125	15.2	35	26.2	80	120	6.50	16	10	2.80	0.82	0.61	4.3	—	0.36	2.45	0.34	2.00	0.23	1.20	—	300
	20–90	18.6	50	26.0	80	120	6.60	17	10	2.80	0.85	0.62	4.4	—	0.38	2.45	0.33	2.15	0.28	1.20	—	390
	10–20	16.9	40	31.7	80	110	6.30	15	11	2.70	0.85	0.62	4.5	—	0.40	2.40	0.35	2.50	0.31	0.90	—	1000
	<10	12.3	40	30.7	130	130	7.60	19	12	3.30	0.92	0.66	4.6	—	0.37	2.40	0.34	2.40	0.38	1.45	—	1000
Luna 24	Bulk	44.0	150	47.0	40	80	2.40	6.1	5.0	1.70	0.59	0.43	2.7	—	—	1.75	0.27	1.20	0.17	0.40	—	110
24999,6	>90	43.5	150	50.0	30	70	1.90	4.9	4	1.30	0.55	0.3	2.2	—	—	1.40	0.22	1.00	0.11	0.16	—	140
	20–90	43.7	140	50.0	40	80	2.75	7.3	6.0	1.90	0.62	0.5	3.0	—	—	2.00	0.29	1.30	0.18	0.38	—	170
	10–20	37.2	130	50.5	80	80	3.40	9.0	6.0	2.20	0.70	0.53	3.2	—	—	2.10	0.32	1.70	0.30	0.50	—	1500
	<10	24.0	90	36.1	100	80	5.30	13	10	2.70	0.80	0.60	3.8	—	0.36	2.10	0.30	2.00	0.28	0.91	—	1700
Apollo 15 15601	Bulk	35.1	200	48.9	135	—	11.3	29	—	6.3	1.01	1.33	9.7	—	—	5.2	0.9	4.9	0.60	1.52	0.46	170

* The Ni values are suspect of contamination from the Rh-plated Ni sieves.

* The Ni values are suspect of contamination from the Rh-plated Ni sieves.

1985; Figs. 10.21 and 10.22). The average soil compositions from this embayment are unlike that of any single rock type; instead they are intermediate between the compositions of the three different basalt types.

The average composition of the soils from the Apennine Front, including those ejected from Elbow Crater, is distinctly different from that of the embayment soils. Significant differences also exist on the Apennine Front itself. The average composition of the soils near Spur Crater, which are rich in green glass deposits, are clearly distinct from other Apennine Front soils. Spur Crater soils are significantly more magnesian than average Apollo 15 soils because of the abundance of the high-Mg green glasses.

It appears that there has been more mixing of fragments from the local bedrock into the soil over larger areas at the Apollo 15 site than at the Apollo 17 site. Albedo and other remotely sensed properties measured at the Apollo 15 site do not clearly define geologic units, in sharp contrast to the Apollo 17 site, where specific units could be readily distinguished. This result suggests that the boundaries between surficial units at the Apollo 15 site are more gradational than at the Apollo 17 site, implying a higher degree of mixing and transport of surface materials. In addition, compositional variations among soils from different areas of the Apollo 15 site are also less pronounced than at the Apollo 1 7 site.

Apollo 16. In comparison with the Apollo 15 and Apollo 17 sites, the Apollo 16 site is remarkably uniform. At this location there are only small variations in albedo, other remotely sensed properties, and the compositions of large rocks. The important geomorphic features are the hills north and south of the Cayley Plain, on which the lunar module landed (see Fig. 10.25). The average compositions of soils collected from the bases of these two hills and from the plains between them are remarkably similar. Only minor differences exist between the soils collected near Smoky Mountain, in the north, and those collected from Stone Mountain, in the south. The northern soils are slightly less magnesian, more enriched in Al and Cr, and somewhat depleted in U, Th, and La, although K is more abundant in the northern soils. The average composition of soils from the Cayley Plain, between the two hills, is intermediate between those of the northern and southern soils. However, the differences between the averages are small, and firm conclusions regarding mixing cannot be made.

The bedrock at the Apollo 16 site is composed of anorthositic gabbros and anorthosites, both of which are found in a highly shattered (cataclastic) state. The largest rock samples are generally crystalline breccias. It is likely that these breccias, which are themselves mixtures of several rock types (see sections 6.3 and 6.4), control the bulk of soil compositions at the Apollo 16 site and account for the apparent overall uniformity. A similar situation may exist at all highland areas of the Moon in which similar breccias are probably the dominant rock types.

Local control of regolith chemistry. The chemical variations observed between different soil samples at the three landing sites suggest that the primary factors controlling soil composition are the compositions of the local bedrock and the proportions of different bedrock types in a given soil sample. If soil compositions were completely controlled by the regional compositions of rock types, the soils within a single landing site would be uniform, a situation that is not observed.

7.5.6. Variation of Soil Chemistry Between Sites

Because the average soil compositions are primarily controlled by local bedrock, the variations of soil composition from site to site should reflect the variation of the average bedrock compositions at each site. If this is correct, then there are significant differences in lunar bedrock compositions, not only between maria and highland regions, but at different areas within these regions.

Both the Apollo 16 and Luna 20 sites are in similar-appearing highland regions, but the average composition of Luna 20 soils is much more mafic than those at the Apollo 16 site (Table 7.15). The Luna 20 site is located in a highland region relatively close to Mare Fecunditatis, and it is possible that there has been an appreciable contribution of material from the mare to the Luna 20 site. However, this explanation seems unlikely; the boundary between mare and highlands in this region is sharp, as indicated by both topography and albedo changes, implying that there has been little lateral migration of surface material. It is more likely that the composition of Luna 20 soils reflects the addition of an unknown mafic highland rock present near the site itself.

The Apollo 11, Apollo 12, Luna 16, and Luna 24 missions all landed on areas of mare basalt flows fairly far away from any highlands; despite this, the soil compositions from these missions are quite distinct from each other. The Apollo 11 soils are rich in Ti, Luna 16 soils have the highest Al of sampled mare soils, and Luna 24 soils are enriched in Fe. Apollo 11 soils have the highest abundance of Sc; Apollo 12 soils are significantly enriched in K, U, Th, and La; Luna 16 and Luna 24 soils are depleted in U, Th, and La. These variations and related differences have also been observed with Earth-based

telescopic spectral studies and in measurements of gamma-ray and X-ray intensities made from lunar orbit during the later Apollo missions. In addition, the average compositions of mare soils from the Apollo 15 and Apollo 17 sites each have their own distinctive character.

The chemical data from lunar soils therefore suggest that the nine different regions of the Moon from which we have soil samples are composed of significantly different rock types. These rocks have been shattered, pulverized, differentially comminuted, and mixed to produce soils with a wide range of different compositions. The soils therefore reflect the local bedrock. Even though small amounts of exotic and distant materials are found in the soils from all missions, usually in the finer grain-size fractions, these occur in such small amounts that bulk soil compositions are not significantly affected.

7.6. REGOLITH BRECCIAS

Ancient regolith. Ballistic ejection from impact craters, together with gravitational creep, tend to emplace newer soils on top of older soils, burying them. However, even deeply buried soils may subsequently be ejected by larger meteoroid impacts and reexposed at the lunar surface. The irradiation histories deduced from discrete soil layers in some regolith cores reveal that such processes of burial and reexposure have, in fact, been operative at the surface of the Moon. It is therefore theoretically possible that some shallow cores can actually penetrate and sample layers of very old (i.e., >4.0 b.y.) regolith, which has been excavated and reexposed at or near the lunar surface. However, a more definite source of samples of such ancient regolith has already been provided in the form of a group of samples called *regolith breccias.*

Characteristics of regolith breccias. Regolith breccias are polymict breccias that contain rock, mineral, and glass fragments in a glassy matrix (see also section 6.4.8). The presence of glass fragments and agglutinates within these breccias shows clearly that they have formed from earlier regolith deposits (*Stöffler et al.,* 1980).

Regolith breccias are abundant among the samples returned by the Apollo 11 astronauts, and early studies showed that they were formed from the local regolith. There was considerable early debate about the process that had indurated the originally loose regolith particles into a more or less coherent rock. Most investigators (e.g., *King et al.,* 1970; *Quaide and Bunch,* 1970) concluded that the breccias were *shock-lithified,* i.e., compacted and indurated by the action of shock waves passing through the regolith, generated by nearby meteoroid impacts. *McKay et al.* (1970) and *Duke et al.* (1970b) disagreed and said that the breccias were more analogous to hot welded deposits of volcanic ash. In particular, *McKay et al.* (1970) stated that the breccias were too porous and the materials in them not shocked enough to be consistent with shock lithification.

However, subsequent experimental studies have shown that the lunar regolith can be shock-lithified at pressures as low as 170 kbar (*Schaal and Hörz,* 1980; *Simon et al.,* 1986b). This result reflects the fact that the lunar soil is porous, and the pores collapse rapidly during passage of the compressive phase of the shock wave. During this collapse, the fine soil particles are efficiently melted by the resulting frictional heat. The small-scale melts then quickly cool to glass, bonding the unmelted soil particles to form a coherent rock. The materials used in shock-wave experiments did not retain any of their original porosity. It is therefore possible that some regolith breccias, which still retain considerable porosity, have formed at even lower shock pressures. This possibility has yet to be confirmed experimentally.

In a survey of Apollo 11 and Apollo 12 regolith breccias, *Chao et al.* (1971) distinguished four groups on the basis of texture: (1) porous and unshocked, (2) shock-compressed but still porous, (3) glass-welded, and (4) thermally metamorphosed and recrystallized. The coherence of these samples varies from extremely friable (crumbly) to very coherent. These characteristics reflect not only the intensity of the events that formed the breccias, but also their postformation histories. For example, porous breccias were probably formed at low shock pressure without suffering any later impacts, whereas the more compressed or welded breccias probably formed by more intense shock waves (closer to the impact) or were shocked again by later impacts.

These regolith breccias are important because they represent samples of old regolith that have been protected from the processes of maturation and mixing since the breccia formed. Some of the breccias are ancient, having formed between 500 and 1500 m.y. ago. Over these long periods of time, further maturation and mixing of the original regolith will produce significant changes in the composition and properties between the regolith and the ancient material preserved in these breccias. Even over long periods of time, these differences are subtle, and detailed petrologic and chemical data are needed to identify them. Such data already exist for soils (*Papike et al.,* 1982), and similar data have recently been collected for some regolith breccias, using the members of the regolith breccia reference suite selected by *Fruland* (1983).

Results for Apollo 11 regolith breccias (*Simon et al.,* 1984) show that they were formed locally; their compositions can be modeled closely by using appropriate proportions of local bedrock and soils. However, the breccias contain different populations of glass and plagioclase feldspar than the present-day soils, and they also have a higher ratio of high-K basalt to low-K basaltic components than do the soils. Although the exposed soil has been open to the addition of exotic materials much longer than have the breccias, both the present-day soil and the ancient breccias have similar amounts of highland components, indicating that little or no addition of highland material to the Apollo 11 site has occurred since the formation of the breccias.

By contrast, only five of the eleven Apollo 12 regolith breccias studied (*Simon et al.,* 1985) could be modeled by using the compositions of present-day Apollo 12 soils. One breccia (sample 12034) that could not be modeled was extremely KREEP-rich and clearly originated in a very different source regolith. Two other breccia samples were formed from anorthositic soils representing either a source exotic to the Apollo 12 site or perhaps the local premare regolith, present before eruption of the mare basalt lavas.

The Apollo 15 site is geologically diverse, with a highland-mare contact to the south and the deep Hadley Rille to the west. There are gradients with distance in the compositions of the regolith in both directions from the highland-mare contact (*Basu and McKay,* 1979). Mare components become more abundant toward the mare, and highland components increase toward the highlands. The Apollo 15 regolith breccias appear to have formed from local materials at the site (*Bogard et al.,* 1985; *Korotev,* 1985; *Simon et al.,* 1986a), and they can therefore provide information on local regolith dynamics and evolution.

Simon et al. (1986a) showed that most of the breccias collected at the Apollo 15 site had not traveled far from where they were formed. Except for an anomalously KREEPy breccia (sample 15205) and one (sample 15306) with less green volcanic glass than the corresponding soil, each breccia is compositionally similar to the regolith at the spot (station) where it was collected. Comparison of the rock and mineral components of breccias and soils from the same station yields insights into regolith evolution over the whole site. For example, breccias collected at the edge of Hadley Rille contain slightly higher highland components than the soil there. This effect can be explained by the location; there is a continuous loss of regolith particles by gravitational creep into the rille, and the lost material is steadily replaced by material excavated from the mare bedrock under the thin regolith. Thus, any basalt particles lost into Hadley Rille are efficiently replaced by local mare material, but highland fragments are not, because the sources of highland material are more distant. As time passed, the regolith became progressively richer in mare basalt components, while the breccias stayed the same, and the regolith has evolved to a point where the difference is detectable.

On the other hand, soils from the highland stations at the Apollo 15 site are slightly richer in highland components than are the corresponding regolith breccias. This observation can also be explained by the morphology of the site. The highland samples were collected at the base of the Apennine Front, a mountain of highland rock that rises above the mare plain. With time, loose material from higher up on the mountain creeps or rolls down to collect at the base, enriching the soils there in highland materials while the breccias, which were formed much earlier, do not evolve. The fact that we can observe and explain such contrasts between breccias and soils demonstrates that both the geology and morphology of the Apollo 15 site has remained essentially the same since the mare basalts were erupted there more than 3×10^9 yr ago.

A multidisciplinary study of Apollo 16 regolith breccias that included petrography, chemistry, texture analysis, and attempts at age-dating the individual breccia components has been completed by *McKay et al.* (1986). They found, as did *Simon et al.* (1988), that the breccias are generally similar to the soils, except that agglutinate contents are higher in the soils. Although the Apollo 16 regolith breccias were apparently formed locally, their compositions do not correlate closely with the compositions of soils collected at the same stations.

McKay et al. (1986) disaggregated two breccias, measured surface irradiation parameters, and found them to be very low, indicating that they had been buried at least a few meters deep in the regolith since they formed. They also found relatively high $^{40}Ar/^{36}Ar$ ratios in most of the breccias, indicating that the materials making up the breccias may have been exposed and irradiated at the lunar surface as early as 4×10^9 yr ago. *McKay et al.* (1986) concluded that the Apollo 16 breccias contain ancient regolith that was only briefly exposed at the surface and is unlike any of the sampled Apollo 16 soils.

Finally, a characteristic of all regolith breccias studied thus far is a very low content of fused soil components (agglutinates and fragments of older regolith breccias) compared to present lunar soils. There are two possible explanations for this situation. Either the breccias were formed from an extremely immature regolith (unlike any present-day

regolith that was sampled) that contained very little fused soil, or agglutinates were present in the source material and were destroyed in the breccia-forming process. Because intact agglutinates and glass beads are observed in the Apollo 11 breccias, implying that they can survive moderate shock, *Simon et al.* (1984) preferred an origin from immature regolith. However, experimental studies (*Simon et al.,* 1986b) have shown that agglutinates are easily destroyed by shock, although they can survive mild shock (<200 kbar). *Simon et al.* (1986a) then suggested that formation of regolith breccias from an immature regolith source can be inferred only for the unshocked, porous regolith breccias. Agglutinates originally present in more intensely shock-compressed (or higher-grade) regolith breccias would probably be destroyed, and the absence of agglutinates in such breccias cannot be used as evidence for an immature source. Nonetheless, the virtual absence of agglutinates in unshocked regolith breccias is consistent with the idea that they are very ancient rocks that formed at a time of much more intense meteoroid bombardment, ~4 b.y. ago (*McKay et al.,* 1986). At that time, when both large and small impacts were frequent, agglutinates should have been rare due to the youth of the regolith, the higher turnover rates, and shorter exposure times. The results of *McKay et al.* (1986) suggest such an origin for Apollo 16 regolith breccias. Many other types of breccias seem to have formed at about that time as well (see section 6.4).

7.7. THE RECORD OF SOLAR HISTORY PRESERVED IN THE LUNAR REGOLITH

The Moon has virtually no atmosphere or magnetic field, and a relatively quiet and passive surface. Because of these features, the Moon has little ability to deflect or attenuate the energetic solar particles that constantly bombard it. Many studies have attempted to examine these particles or the products of their impact into the lunar regolith in order to unravel the history of solar radiation. This topic is of considerable importance for the near-term and long-term history of solar activity and has direct implications for climate, atmosphere, and life on Earth.

7.7.1. A Summary of Historical Results

In order to read the "fossil" evidence of solar particles in the lunar regolith, it is necessary to know (1) the timespan over which the regolith sample studied was exposed at the lunar surface and (2) the antiquity of the sample, i.e., the interval or intervals in history during which the sample was exposed. It is possible to generate models for these parameters that suit the "average" regolith (section 7.5.1), but specific soil samples must be studied carefully to unravel their actual exposure history (section 7.4.2). Although quiet, the lunar surface is impact gardened—mixed and overturned—on a timescale that is brief (Fig. 7.28) relative to the age of the sun (4.7 b.y.). Ideally, the soil presently at the lunar surface is the most readily studied, because it might be assumed to have been in place for a measurable timespan leading up to the present. It is common, however, for the regolith at the lunar surface to have been recycled and mixed, including some fraction of material that has been at the lunar surface more than once. Thus it is critical to examine several types of solar exposure measures with differing effects to help unravel the regolith sample's history.

Materials in the top centimeter of the lunar soil are churned back into the deeper regolith with such regularity that they seldom provide exposure records extending back in time more than 1 m.y., and almost never more than 10 m.y. Large rocks in the regolith at the lunar surface can provide a more durable surface, with practical in-place exposure ages up to ~50 m.y. (*Walker,* 1980).

The effects of energetic particles from the sun on the lunar surface are related mainly to bombardment energy. Solar-wind particles are typically ionized atoms (mostly H, He, C, N) with energies of ~1000 electron volts per nuclear particle (i.e., ~1 keV/amu; see section 3.11.1). This energy is sufficient to implant these particles several hundred angstroms (about 10^{-4} mm) into the surfaces of exposed mineral grains. The energies of particles accelerated by solar flares range from <1 MeV/amu to >100 MeV/amu, and these particles penetrate several millimeters to several centimeters to produce nuclear reactions with some elements (e.g., conversion of Si, Fe, and ^{27}A1 to ^{26}A1 or ^{21}Ne, and conversion of Fe to ^{53}Mn or ^{54}Mn). These particles also produce lattice damage tracks and trapped-electron anomalies in crystals.

Despite the problems in obtaining lunar samples with decipherable surface exposure histories, the effort expended to date has shown that, within a factor of about 2 or 3, the solar-wind composition has remained constant over most of the lifetime of the sun (*Pepin,* 1980). This result is consistent with current astronomical theories in which the sun, slightly less than 5 b.y. old, is regarded as a main-sequence star about halfway through a long stable period that began shortly after its formation and that should last for about another 5 b.y.

Studies of lunar samples have also been able to examine different solar processes on a number of different timescales. First-order stability in the sun is

indicated by the presence of a solar wind at least 4.2 b.y. ago; solar-wind elements from this era have been identified in meteorites (*Crozaz,* 1980; *Goswami et al.,* 1980). However, there is evidence that both the intensity and the composition of the solar wind have changed with time.

The evidence for relative solar stability should not be read to imply that the sun has not changed at all over the last 4 b.y. The most striking example of possible change is an apparent systematic increase in the ratio $^{15}N/^{14}N$ over this timespan (*Kerridge,* 1975, 1989). Although this change is not readily explained by theories of solar activity, it has been equally difficult to explain away the variation by other causes. If caused by the internal operations of the sun, the significance of this timewise change is still unknown.

At the time of the Apollo missions, it was hoped that vertical core samples throughout the regolith might be sufficient to provide a readily datable stratigraphy, from which a well-constrained record of solar activity might be reconstructed. This ideal was not realized because of the complex nature of lunar regolith processes and the difficulty of distinguishing between the *antiquity* of an exposed sample (*when* it was exposed) and its *maturity* (*how long* it was exposed) (*Kerridge,* 1980). However, based on what we now know, it may be possible to seek other situations in which regolith samples may be collected with well-known duration and timing of exposure. For example, it should be possible to collect regoliths that were developed on one mare lava flow and then covered by another, allowing both the age and duration of the regolith exposure to be precisely obtained by dating the lava flows above and below.

7.7.2. Solar-Wind History

The sun has been generating solar wind for most of its lifetime. Samples of ancient solar wind are found in the oldest solar-system materials available for analysis—meteorites whose individual components were assembled more than 4.2 b.y. ago (*Crozaz,* 1980; *Goswami et al.,* 1980). These studies suggest that this ancient solar wind was not greatly different from the modern solar wind in intensity or composition.

Lunar samples provide a shorter record of ancient solar wind than do meteorites because of the complex dynamics of the lunar surface. In particular, the erosion of exposed lunar rock fragments, which takes place at a rate of several millimeters per million years, removes the surface layers containing solar wind and limits the solar-wind record in exposed samples to less than 1 m.y. However, buried lunar materials preserve samples of more ancient solar wind. The deep (3-m) cores contain single grains that accumulated solar wind about 1 b.y. ago, while soil breccias contain solar wind from up to 3.5 b.y. ago.

The suite of solar-wind elements available for analysis is limited to the volatile elements (e.g., H, He, Ne, Ar, Kr, Xe, C, and N) because lunar materials have very low volatile contents, and the solar-wind contributions can easily be recognized. However, these elements can be measured to establish the character of the solar wind over a considerable fraction of the sun's lifetime.

Analyses of lunar samples have established that the solar wind has been generally constant (within a factor of 2) over at least the last 2.5 b.y. (*Pepin,* 1980). However, significant changes in specific characteristics have been detected between ancient and modern solar winds. In the area of physical changes, analyses of solar-wind Xe (*Geiss,* 1973; *Kerridge,* 1989) suggested that the flux was higher (2–3×) in the ancient solar wind. This conclusion is model-dependent and not definitely established, but it is supported by independent measurements of solar-wind N (*Clayton and Thiemans,* 1980; *Kerridge,* 1980). In addition, a more energetic solar wind in the past has been proposed to explain the erosion and rounding of small mineral grains in the lunar soil (*Borg et al.,* 1980).

The earliest studies of returned lunar samples provided evidence that some compositional characteristics of ancient and modern solar winds were significantly different. An early conclusion was that the relative amount of Ar had decreased with time (*Geiss,* 1973). Despite a general constancy in the ratios of isotopes of Ar, Kr, and Xe over time, a significant decrease in the ratio $^{4}He/^{3}He$ was noted (*Eberhardt et al.,* 1972; *Kerridge,* 1980; *Becker and Pepin,* 1989); the change amounted to a decrease of 23% over the age of the regolith. There is also evidence for a roughly 50% decrease in the proportions of He and Xe, relative to N or Kr (*Kerridge,* 1980; *Becker and Pepin,* 1989). A possible decrease in the ratio $^{22}Ne/^{20}Ne$ over the same time was also indicated, but is less definite (*Pepin,* 1980; *Becker and Pepin,* 1989).

The strongest and most definite change in solar wind composition with time is a pronounced *increase* in the $^{15}N/^{14}N$ ratio with time (*Kerridge,* 1975, 1989; *Clayton and Thiemens,* 1980). Careful isotopic measurements of the N extracted from recently exposed soils and from a series of old regolith breccias, which trapped solar wind as much as 3.5 b.y. ago, show an increase in the $^{15}N/^{14}N$ ratio of about 50% or about 15% per billion years. This result, which has been reinforced by more recent measurements, is still not explained (*Kerridge,* 1989).

A variety of lunar-related mechanisms have been proposed: meteoroid contamination, infall of interstellar material, and N outgassing from the Moon. For various reasons none of these is satisfactory. A solar mechanism seems necessary to explain the change, though its nature is not clear at this time (*Kerridge,* 1989).

7.7.3. Solar-Flare History

Evidence for the existence of solar-flare activity more than 4 b.y. ago is present as particle tracks in grains of chondritic meteorites (*Crozaz,* 1980; *Goswami et al.,* 1980). Solar-flare effects in lunar rocks and soil are relatively shallow (less than a few centimeters), and the erosion of exposed lunar rocks limits the available solar-flare record to about 10^7 yr. However, because of the continual stirring of the regolith, individual grains in deep lunar cores may provide solar-flare records from as much as 10^9 yr ago.

Within these time limits, the record of solar-flare behavior is approximately constant, with no deviations $\gtrsim 3\times$ noted in the distant past. There is no evidence that the average intensity of solar flares was higher in the past 10^7 yr. A maximum intensity for past solar flares may be no more than 10^{10} particles/cm^2 per flare (Lingenfelter and Hudson, 1980), but it possible that larger flares could have occurred.

Several specific studies have provided other indicators of long-term constancy. The overall solar proton flux, as indicated by the radioactive elements ^{26}A1 and ^{53}Mn produced in lunar samples, has been constant over the last 1–10 m.y. and is similar to the modern flux (*Reedy,* 1980; *Russ and Emerson,* 1980). The enrichment in the ratio of VVH (atomic number, Z >30) to VH (Z = 20–28) atoms, observed at particle energies of less than 20 MeV, is present in both ancient and modern solar-flare particles. The ratio Fe/H in flare particles appears to have been constant over the last 2 m.y. (*Zinner,* 1980), and is still about 20× the solar ratio (*Crozaz,* 1980; *Goswami et al.,* 1980).

However, some lunar sample studies have provided indications that modern solar-flare activity may be different from that in the past. Studies of particle tracks developed in the glass linings of microcraters on lunar rocks suggest that the flux of solar flare particles was higher about 20,000 yr ago (*Zook,* 1980), but these estimates are both model-dependent and controversial. A higher flux over the last 10^4–10^5 yr is also suggested by ^{81}Kr and ^{14}C activities (*Reedy,* 1980). However, *Fireman* (1980) has argued that the latter effect arises from ^{14}C carried to the Moon in the solar wind and that the record from ^{39}Ar and ^{3}H activities shows constancy in both the ancient and modern solar wind.

7.7.4. Galactic-Cosmic-Ray History

The history of galactic cosmic rays (GCR) preserved in lunar materials has been explored by two main methods and over two different timescales. Single grains rich in GCR-produced particle tracks have been recovered from deep lunar regolith cores; these grains preserve records of exposure to GCR during the last 10^8–10^9 yr. The levels of GCR-produced radionuclides in most lunar rocks or soil provide younger records of GCR behavior over the last 10^6–10^8 yr.

The records so far deciphered show that the flux and composition of GCR have been constant (within about a factor of 2) and similar to the present flux, over all the timescales studied. The ratio of VVH/ VH particles has been constant at about $(1.3 \pm 0.6) \times 10^{-3}$ for the last 10^8–10^9 yr (*Bhandari and Padia,* 1974a,b).

Studies of the GCR-produced radionuclides developed in exposed lunar rocks indicate that the same constancy has existed on shorter timescales (*Crozaz,* 1980). Rocks with simple exposure histories indicate constancy over exposure ages of 2 m.y. to 50 m.y. (*Walker and Yuhas,* 1973; *Yuhas and Walker,* 1973). Other samples show a similar constancy over periods from 60 yr to about 10^4 yr (*Fireman,* 1980).

Studies of both lunar samples and recently fallen meteorites have detected the modulation in GCR flux that is produced by variations in the sun's magnetic field during the 11-yr solar cycle (*Reedy,* 1987). Activities of such GCR-produced radionuclides as ^{54}Mn, ^{46}Sc, and ^{22}Na in these samples vary by about a factor of 2, and the timing of these variations is closely correlated with solar activity and the strength of the sun's magnetic field.